USGS
science for a changing world

هيئة المساحة الجيولوجية السعودية
SAUDI GEOLOGICAL SURVEY

Eruptive History Within the Vicinity of Al Madīnah in Northern Harrat Rahat, Kingdom of Saudi Arabia

Chapter C of
Active Volcanism on the Arabian Shield—Geology, Volcanology, and Geophysics of Northern Harrat Rahat and Vicinity, Kingdom of Saudi Arabia

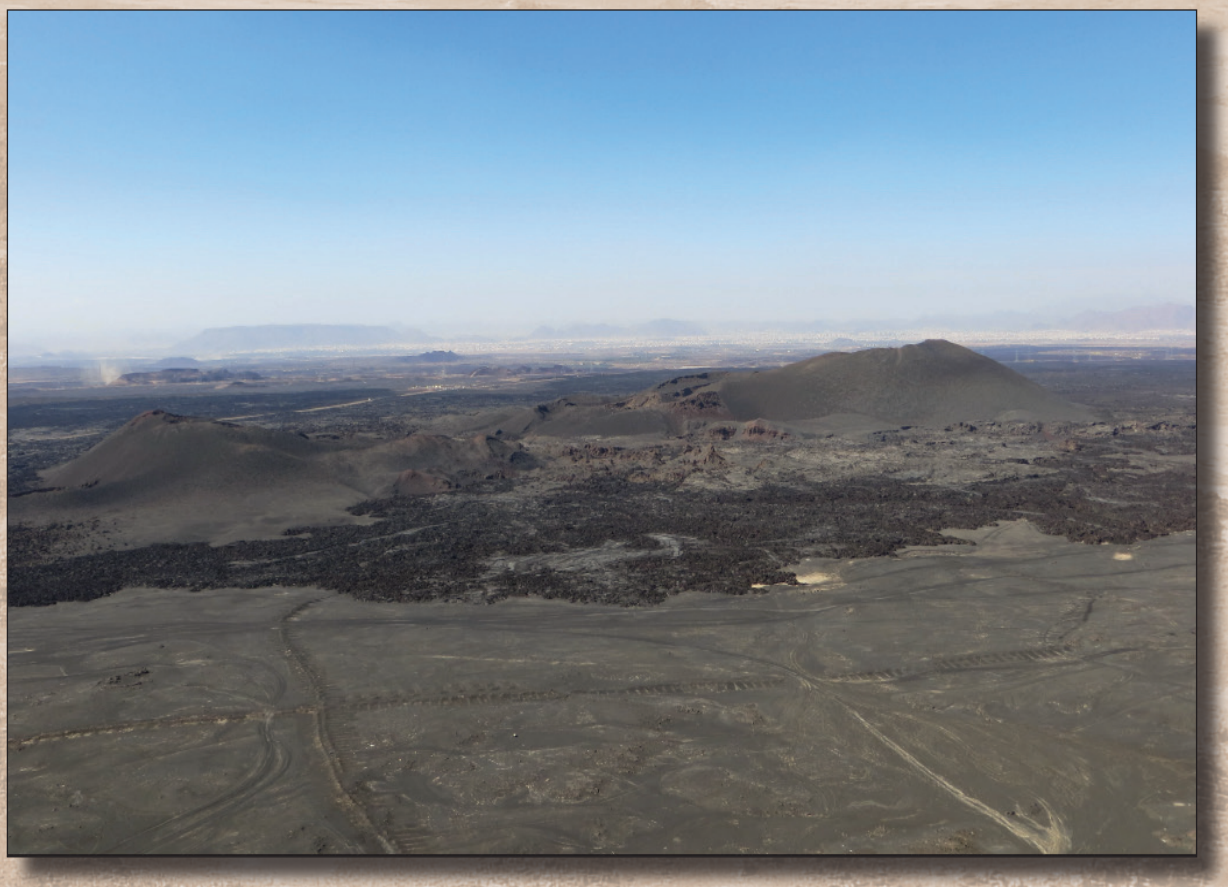

U.S. Geological Survey Professional Paper 1862
Saudi Geological Survey Special Report SGS–SP–2021–1

U.S. Department of the Interior
U.S. Geological Survey

Cover. Photograph looking northwest with Al Madīnah in the background showing the 1256 C.E. basalt of Al Labah scoria cone vent complex and lava flows and older mafic scoria cones and lavas to the west. U.S. Geological Survey photograph by Hannah Dietterich in 2016. Background image shows northern Harrat Rahat lava flows, maars, and lava domes. U.S. Geological Survey photograph by Andrew Calvert, January 25, 2012.

Eruptive History Within the Vicinity of Al Madīnah in Northern Harrat Rahat, Kingdom of Saudi Arabia

By Drew T. Downs, Mark E. Stelten, Duane E. Champion, Hannah R. Dietterich, Khalid Hassan, and Jamal Shawali

Chapter C of

Active Volcanism on the Arabian Shield—Geology, Volcanology, and Geophysics of Northern Harrat Rahat and Vicinity, Kingdom of Saudi Arabia

Edited by Thomas W. Sisson, Andrew T. Calvert, and Walter D. Mooney

U.S. Geological Survey Professional Paper 1862
Saudi Geological Survey Special Report SGS–SP–2021–1

U.S. Department of the Interior
U.S. Geological Survey

U.S. Geological Survey, Reston, Virginia: 2023

Suggested citation:
Downs, D.T., Stelten, M.E., Champion, D.E., Dietterich, H.R., Hassan, K., and Shawali, J., 2023, Eruptive history within the vicinity of Al Madīnah in northern Harrat Rahat, Kingdom of Saudi Arabia, chap. C *of* Sisson, T.W., Calvert, A.T., and Mooney, W.D., eds., Active volcanism on the Arabian Shield—Geology, volcanology, and geophysics of northern Harrat Rahat and vicinity, Kingdom of Saudi Arabia: U.S. Geological Survey Professional Paper 1862 [also released as Saudi Geological Survey Special Report SGS–SP–2021–1], 41 p., https://doi.org/10.3133/pp1862C.

Associated data for this publication:
Downs, D.T., 2019, Major and trace-element chemical analyses of rocks from the northern Harrat Rahat volcanic field and surrounding area, Kingdom of Saudi Arabia: U.S. Geological Survey data release, https://doi.org/10.5066/P91HL91C.

ISSN 1044-9612 (print)
ISSN 2330-7102 (online)

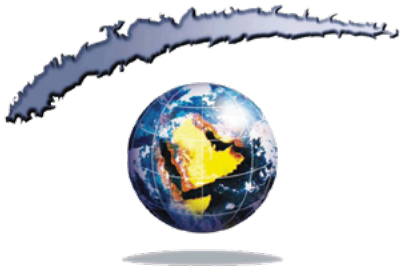

هيئة المساحة الجيولوجية السعودية
SAUDI GEOLOGICAL SURVEY

Ministry of Industry and Mineral Resources
BANDAR BIN IBRAHIM BIN ABDULLAH AL-KHORAYEF, Minister and SGS Chairman

Saudi Geological Survey
Abdullah bin Mufter Al-Shamrani, Chief Executive Officer

Saudi Geological Survey, Jiddah, Kingdom of Saudi Arabia: 2023

Contents

Figures

Tables

Conversion Factors

International System of Units to U.S. customary units

Multiply	By	To obtain
	Length	
centimeter (cm)	0.3937	inch (in.)
millimeter (mm)	0.03937	inch (in.)
meter (m)	3.281	foot (ft)
kilometer (km)	0.6214	mile (mi)
kilometer (km)	0.5400	mile, nautical (nmi)
meter (m)	1.094	yard (yd)
	Area	
square kilometer (km^2)	247.1	acre
square kilometer (km^2)	0.3861	square mile (mi^2)
	Volume	
cubic kilometer (km^3)	0.2399	cubic mile (mi^3)
	Density	
kilogram per cubic meter (kg/m^3)	0.06242	pound per cubic foot (lb/ft^3)
gram per cubic centimeter (g/cm^3)	62.4220	pound per cubic foot (lb/ft^3)

Temperature in degrees Celsius (°C) may be converted to degrees Fahrenheit (°F) as

$$°F = (1.8 \times °C) + 32.$$

Abbreviations

C.E.	Common Era
DRE	dense rock equivalent
ICP-MS	inductively coupled plasma mass spectrometry
ICP-OES	inductively coupled plasma optical emission spectrometry
ka	kilo-annum
k.y.	thousand years
lidar	light detection and ranging
Ma	mega-annum
mg	milligram
Mg#	Mg number
mm/k.y.	millimeter per thousand years
µm	micrometer
ppm	part per million
PRIME	Purdue Rare Isotope Measurement Laboratory
XRF	X-ray fluorescence
±	plus or minus

Active Volcanism on the Arabian Shield
Edited by T.W. Sisson, A.T. Calvert, and W.D. Mooney
U.S. Geological Survey Professional Paper 1862
Saudi Geological Survey Special Report SGS–SP–2021–1

Chapter C

Eruptive History Within the Vicinity of Al Madīnah in Northern Harrat Rahat, Kingdom of Saudi Arabia

By Drew T. Downs,[1] Mark E. Stelten,[1] Duane E. Champion,[2] Hannah R. Dietterich,[1] Khalid Hassan,[3] and Jamal Shawali[3]

Abstract

The northernmost part of the Harrat Rahat volcanic field contains early Pleistocene to Holocene mafic eruptive products within the vicinity of the city of Al Madīnah, Kingdom of Saudi Arabia. A detailed geologic investigation into the eruptive history of a 570 square kilometer (km^2) area covering Al Madīnah and the surrounding area has yielded 33 mapped Quaternary volcanic units consisting of lava flows, scoria cones, and shield volcanoes. These eruptive products consist of continental, intraplate alkalic and minor transitional basalts, hawaiites, and a single mugearite that were emplaced from at least 1,014±14 thousand years ago (ka) to a single Holocene eruption in 1256 C.E. Lava flows are generally 10 to 15 kilometers (km) long (but can reach 23 km long), 1 to 3 km wide, and at least 10 meters thick. Most of the mapped units erupted episodically between 400 and 340 ka and 180 and 100 ka. Despite small individual volumes (less than 1 cubic kilometers dense rock equivalent), each unit represents eruption of a distinct magma batch that was strongly influenced by clinopyroxene, olivine, and plagioclase fractionation. Some of these units are interpreted to have undergone magma mixing pre- and (or) syneruptively. Integrating eruption ages, geochemistry, and paleomagnetic data yields evidence that some eruptions were temporally and (or) spatially clustered. Aligned scoria cones and elongate vent edifices were constructed atop fissure vent systems that reflect the local stress field, which controls dike ascent through the middle and upper crust.

Introduction

Small-volume mafic volcanoes less than 1 cubic kilometer (km^3) are the most prevalent continental volcanic landform on Earth. These volcanic landforms commonly form larger volcanic fields that have been documented in association with subduction zones, rift systems, hot spots, and intraplate settings (de Silva and Lindsay, 2015; Valentine and Connor, 2015). More than 200 volcanic fields are considered active since the start of the Holocene (Siebert and others, 2010). Eruptions are commonly spatiotemporally clustered with tectonism and (or) preexisting structures that exert strong influences on vent locations (Condit and Connor, 1996; Muffler and others, 2011; Le Corvec and others, 2013; Deligne and others, 2016). The spatial, temporal, and geochemical evolution of several small-volume mafic volcanic fields have been studied in considerable detail (Kuntz and others, 1986; Conway and others, 1997; Shaw and others, 2003; Valentine and Perry, 2007; Duncan and Al-Amri, 2013; Deligne and others, 2016; Duncan and others, 2016). However, most small-volume mafic volcanic fields have yet to be extensively investigated. Thorough examination of mafic volcanic fields is useful for characterizing eruptive styles, volumes, durations, and for determining whether volcanic activity is episodic in nature.

The western Arabia Plate encompasses more than 15 continental, intraplate volcanic fields that stretch more than 3,000 kilometers (km) from the Gulf of Aden to the Mediterranean Sea (figs. 1*A–B*). These volcanic fields compose one of the largest subaerial alkalic volcanic provinces on Earth, covering an area of about 180,000 square kilometers (km^2; Coleman and others, 1983). Historical activity has been recorded, including at least 21 eruptions proposed over the past 1,500 years, the last of which occurred in 1937 C.E. near Dhamar, Yemen (Ambraseys and others, 2005; Siebert and others, 2010). Eruptions have also occurred within the Red Sea rift as recently as 2013, however, most proposed Holocene eruptions remain unconfirmed and uninvestigated. As a result, the timing, composition, and magmatic processes that control and influence activity within these late Cenozoic volcanic fields are topics of interest (Shaw and others, 2003; Moufti and others, 2012, 2013; Duncan and Al-Amri, 2013; Murcia and others, 2015, 2017; Abdelwahed and others, 2016; Duncan and others, 2016; Konrad and others, 2016).

Many of the volcanic fields on the Arabia Plate are in sparsely populated areas but one of the Holocene eruptions occurred within the northernmost part of the Harrat Rahat volcanic field (fig. 2) in the vicinity of the city of Al Madīnah al Munawwarah (referred to hereafter as Al Madīnah; fig. 3). This city sits atop, and through time has been expanding over, mafic eruptive products that consist of lava flows, scoria cones, and shield volcanoes. Few individual eruptions from

[1]U.S. Geological Survey.
[2]U.S. Geological Survey, now deceased.
[3]Saudi Geological Survey.

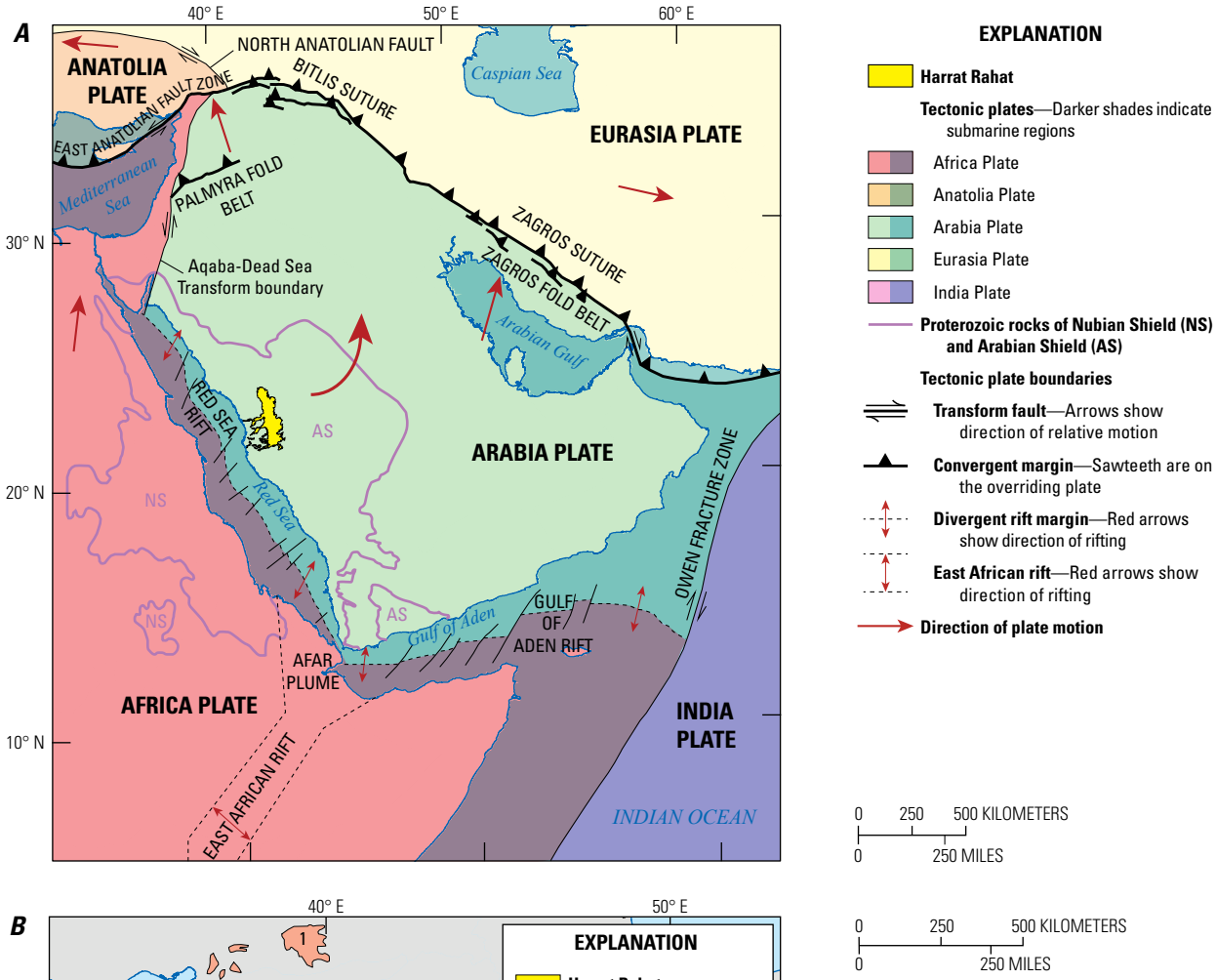

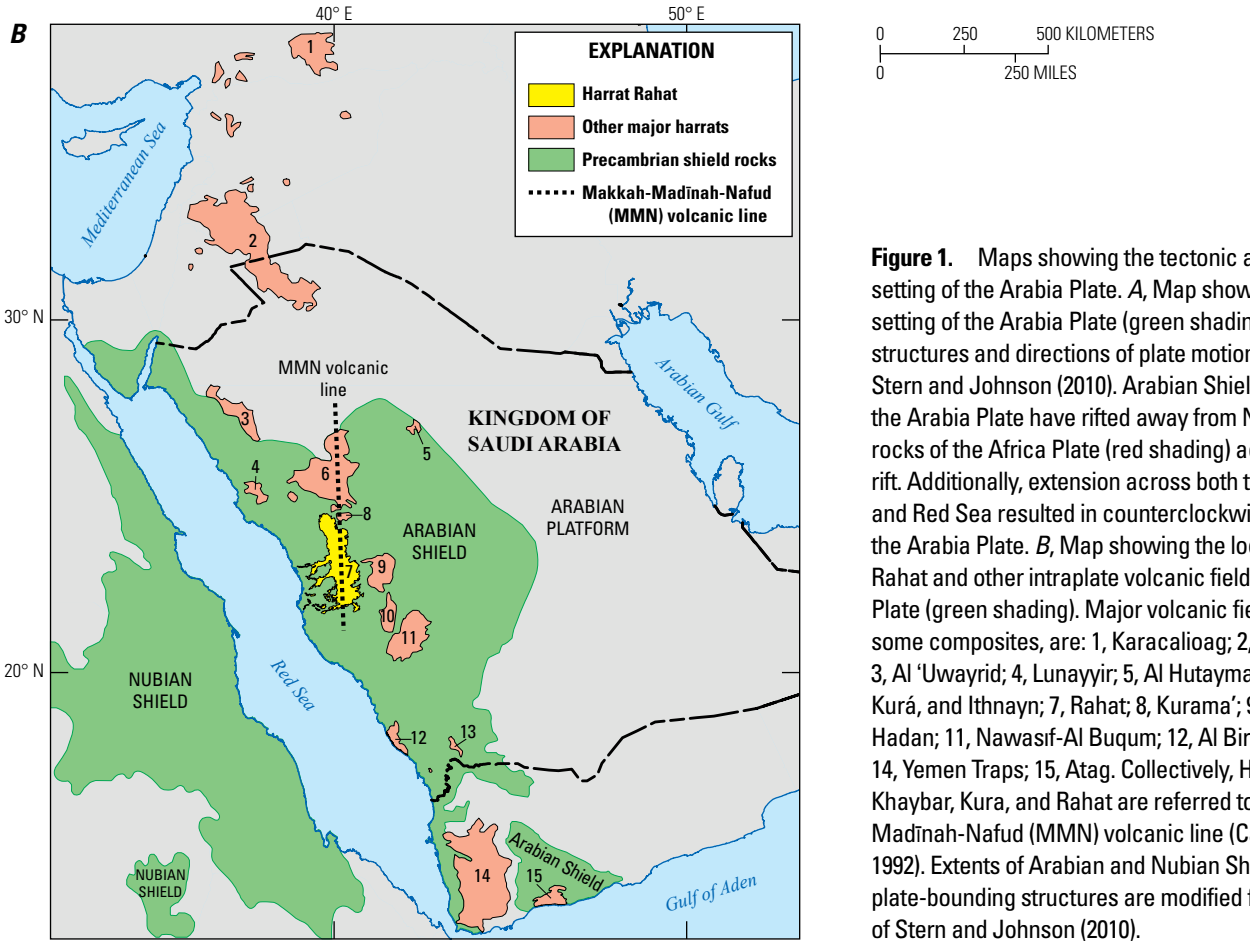

Figure 1. Maps showing the tectonic and volcanic setting of the Arabia Plate. *A*, Map showing the tectonic setting of the Arabia Plate (green shading). Bounding structures and directions of plate motion are compiled by Stern and Johnson (2010). Arabian Shield (AS) rocks of the Arabia Plate have rifted away from Nubian Shield (NS) rocks of the Africa Plate (red shading) across the Red Sea rift. Additionally, extension across both the Gulf of Aden and Red Sea resulted in counterclockwise rotation of the Arabia Plate. *B*, Map showing the locations of Harrat Rahat and other intraplate volcanic fields of the Arabia Plate (green shading). Major volcanic fields (harrats), some composites, are: 1, Karacalioag; 2, Ash Shama; 3, Al 'Uwayrid; 4, Lunayyir; 5, Al Hutaymah; 6, Khaybar, Kurá, and Ithnayn; 7, Rahat; 8, Kurama'; 9, Al Kishb; 10, Hadan; 11, Nawasıf-Al Buqum; 12, Al Birak; 13, As Sirat; 14, Yemen Traps; 15, Atag. Collectively, Harrats Ithnayn, Khaybar, Kura, and Rahat are referred to as the Makkah-Madīnah-Nafud (MMN) volcanic line (Camp and Roobol, 1992). Extents of Arabian and Nubian Shield rocks and plate-bounding structures are modified from compilation of Stern and Johnson (2010).

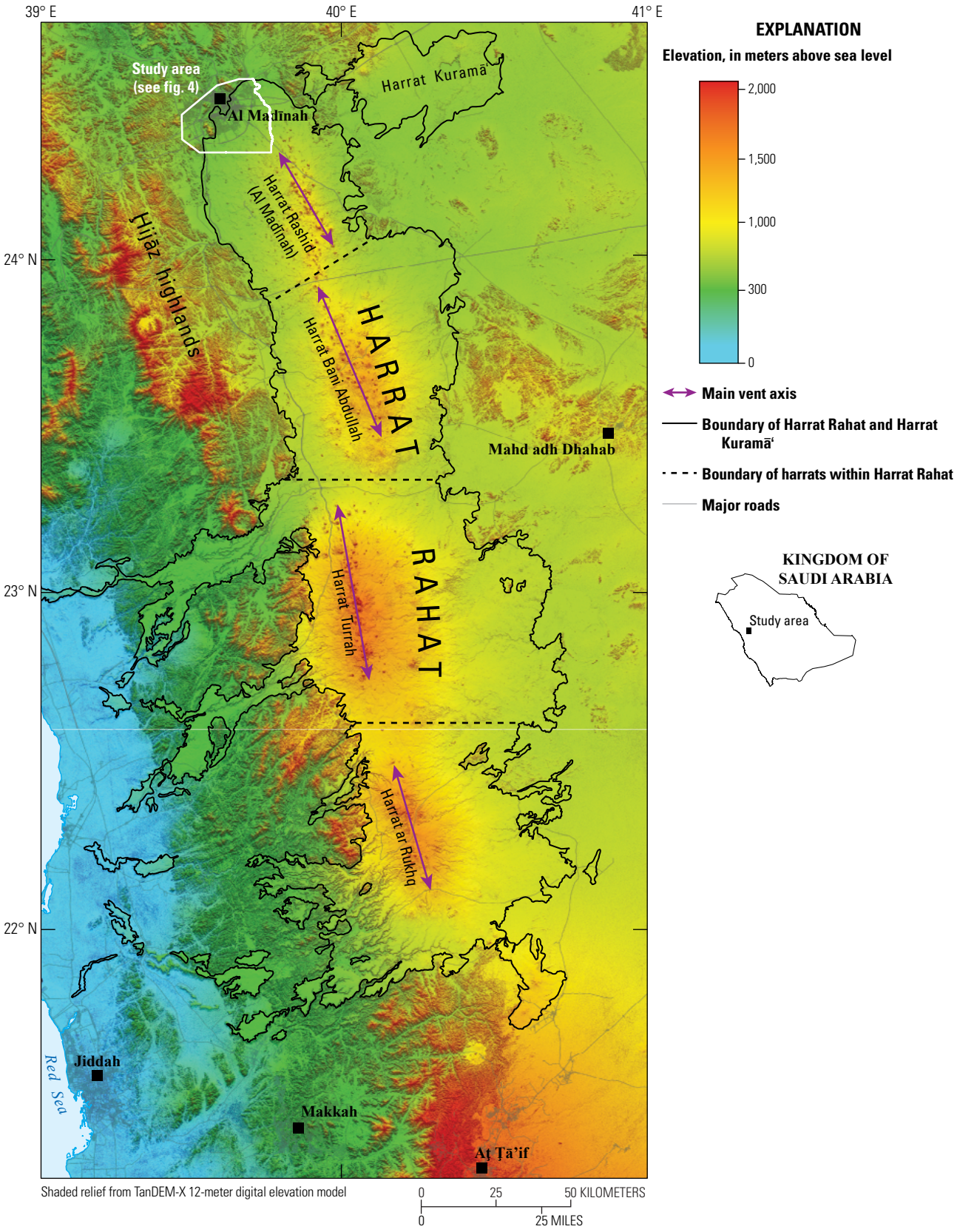

Figure 2. Color shaded-relief map of the Harrat Rahat volcanic field, which is a composite of the (listed from south to north) Harrat ar Rukhq, Harrat Turrah, Harrat Bani Abdullah, and Harrat Rashid (also called Harrat al Madīnah) volcanic fields, each of which has a separate main vent axis. Although the northernmost part of Harrat Rahat can be called either Harrat Rashid or Harrat Al Madīnah, we refer to it as northern Harrat Rahat. Outlines of the harrats are from Camp and others (1987). The shaded-relief base map is from a 12-meter resolution TanDEM-X digital elevation model acquired from German Aerospace Center in 2017.

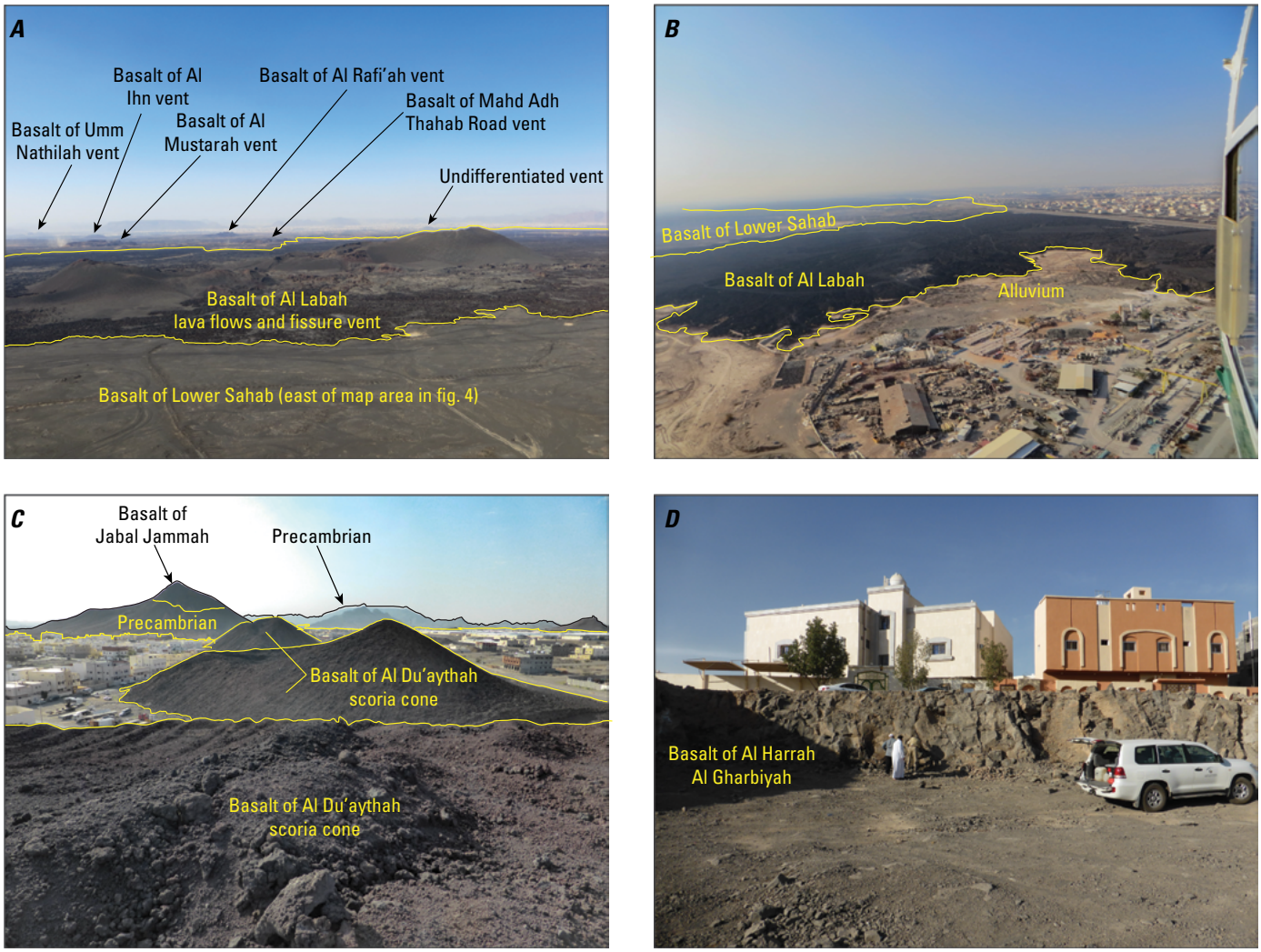

Figure 3. Photographs of scoria cone and lava flows exposed within the northernmost part of Harrat Rahat. *A*, Photograph looking northwest with Al Madīnah in the background showing the 1256 C.E. basalt of Al Labah scoria cone vent complex and lava flows and older mafic scoria cones and lavas to the west. Photograph by Hannah Dietterich in 2016. *B*, Photograph looking south, near the distal end of the basalt of Al Labah, illustrating expansion of the city over young lava flows. Photograph by Hannah Dietterich in 2016. *C*, Photograph looking south at three of the four scoria cones of the basalt of Al Du'aythah within the western suburbs of Al Madīnah. Photograph by Andrew Calvert in 2014. *D*, Typical exposure of a dense basaltic lava flow (basalt of Al Harrah Al Gharbiyah) within the western part of Al Madīnah. Photograph by Drew Downs in 2015. See table 1 and figures 4 and 5 for unit locations and descriptions.

Harrat Rahat have been studied in detail, with emphasis on the youngest appearing eruptions within the northernmost confines of the volcanic field (Camp and others, 1987; Murcia and others, 2015, 2017; Dietterich and others, 2018). Most other studies have considered the volcanic field in its entirety and have focused on magmatic processes (Camp and Roobol, 1989; Moufti and others, 2012, 2013; Stelten and others, 2018; Sisson and others, 2023; Salters and others, 2023). More recent investigations have undertaken a systematic study of eruptive strata from individual volcanoes and volcanic centers within the northern quarter of Harrat Rahat (Downs and others, 2019; Stelten and others, 2020). Piecing together the geologic history is fundamental for (1) understanding the overall spatial, temporal, and compositional evolution of the volcanic field and (2) determining the timescales of magmatic processes in the mantle and crust.

This chapter expands on the research of Downs and others (2018) and examines the field relations, petrography, geochemistry, paleomagnetism, and geochronology used to define distinct, mappable mafic volcanic units within the vicinity of Al Madīnah in the northernmost part of Harrat Rahat. The results are used to understand the timing, composition, and eruptive processes of mafic volcanism that have been obscured, in part, through anthropogenic processes of urbanization.

Geological Setting

Harrat Rahat is 50 to 75 km wide by 300 km long, covers an area of 20,000 km^2, has a volume of 2,000 km^3, and encompasses more than 900 volcanic vents (Coleman and others, 1983; Camp and Roobol, 1989, 1991; Runge and others, 2014). It is a composite of the four smaller volcanic fields of Harrat ar Rukhq, Harrat Turrah, Harrat Bani Abdullah, and Harrat Rashid (fig. 2). Harrat Rahat is elongate in the north-south direction and is situated within the western part the Arabia Plate in the center of a series of northward-striking volcanic fields (fig. 1). These include the volcanic fields of Harrats Khaybar, Kurá, and Ithnayn that are located more than 50 km to the north along a feature termed the Makkah-Madīnah-Nafud volcanic line (Camp and Roobol, 1992). Clustering of vents along a north-south lineament in northern Harrat Rahat constructed a topographic crest that stands 100 to 400 meters (m) above the adjacent Precambrian basement. Most of the exposed lava flows were emplaced either to the east or west from this main vent axis (fig. 2). The northern end of Harrat Rahat is an exception, where lava flows are emplaced to the northeast, north, and northwest of the main vent axis into low-lying areas in part occupied by Al Madīnah. Volcanism is proposed to have initiated at least 10 million years ago (Ma) in Harrat Rahat and the most recent eruption occurring in 1256 C.E. just to the southeast of Al Madīnah (Al-Samhūdī, 1488).

Camp and Roobol (1991) presented a 1:250,000 scale geologic map highlighting the volcanic units of Harrat Rahat. Their mapping was done through a combination of fieldwork, examining and interpreting aerial images, geochemistry, and compiling K-Ar eruption ages. In total, Camp and Roobol (1989) estimated the entirety of Harrat Rahat to consist of 62 percent transitional basalt, 21 percent alkalic basalt, 13 percent hawaiite, and 4 percent more evolved compositions of mugearite, benmoreite, and trachyte by volume (compositional nomenclature from Le Bas and others [1986], with transitional and alkalic basalts distinguished by Irvine and Baragar [1971]). Transitional basalts dominated early volcanism, some of which flowed west to the Red Sea coastal plain, along with minor volumes of alkalic basalts. These early transitional basalts are now preserved mainly as deeply eroded lava flows. Alkalic basalts replaced transitional basalts as the dominant eruptive products during the Pliocene and have been contemporaneous with minor volumes of evolved eruptive products (such as hawaiite, mugearite, benmoreite, and trachyte) since the middle Pleistocene. Basalt, hawaiite, and mugearite magmas predominantly erupted in Hawaiian and Strombolian styles and created scoria cones and lava flows, with some lava flows reaching as far as 23 km away. Maar craters and fine-grained tuff rings indicate phreatomagmatic activity (Camp and Roobol, 1989, 1991; Murcia and others, 2015, 2017) but these eruption styles appear to be restricted to the high-standing main vent axis that is at least 10 km south of Al Madīnah. Air-fall-tephra deposits are rarely preserved, which is likely the result of their small volumes, and the combination of eolian and fluvial processes in the dry, unvegetated environment. The only well-preserved air-fall-tephra deposit is a near-vent (extends 5 km from its source vent) deposit created by fire fountaining during the 1256 C.E. eruption (Kawabata and others, 2015). Benmoreite and trachyte magmas tended to erupt as Peléan domes and spines before occasionally collapsing and generating small-volume pyroclastic-flow deposits that consist of poorly inflated juvenile clasts (Camp and Roobol, 1989; Stelten and others, 2018, 2020; Downs and others, 2019, 2023). Benmoreites and trachytes make their first appearances farther than 10 km south of the map displayed in figure 4 and these deposits are not discussed further in this chapter (see Stelten and others, 2018, 2020, 2023; Downs and others, 2019, 2023; Robinson and Downs, 2023).

Geology of the Northernmost Part of Harrat Rahat

Late Cenozoic volcanic rocks of Harrat Rahat were divided into the Shawahit (10–2.5 Ma), Hammah (2.5– 1.7 Ma), and Madinah basalts (1.7 Ma to present) by Camp and Roobol (1989, 1991). The Madinah basalts were further subdivided into seven Quaternary subunits (Qm_1 through Qm_7) based on their degree of erosion, and the size and abundance of loess-filled depressions. Eight K-Ar ages, and archeological and historical evidence (for Qm_6 and Qm_7, respectively) from northern Harrat Rahat provided time estimates for the Qm_1 through Qm_7 subunits (Camp and Roobol, 1989). Moufti and others (2013) provided 25 $^{40}Ar/^{39}Ar$ ages, which were used to redefine these subunits as lasting from 10.31 Ma to the present. However, each of their subunits overlap temporally and both the K-Ar and $^{40}Ar/^{39}Ar$ eruption ages are commonly contradictory with the stratigraphic superposition for adjacent units. Only one of the Moufti and others (2013) $^{40}Ar/^{39}Ar$ eruption ages is from a lava flow that is mapped in figure 4. Their age is 270±60 thousand years ago (ka) for the unit mapped here as the hawaiite of Al Anahi 3 (unit names are from Downs and others [2019] and Robinson and Downs [2023]). Thus, a lack of eruption ages for mafic volcanic rocks within the vicinity of Al Madīnah, and inconsistencies between published radiometric ages and stratigraphic superposition, highlighted a need for reliable age and geologic constraints throughout the northernmost part of Harrat Rahat. Downs and others (2018) presented 19 eruption ages for the 33 mapped units in a 570 km^2 area in the northwesternmost part of the Harrat Rahat volcanic field, which includes the city of Al Madīnah (figs. 4–5). Stelten and others (2018, 2020) and Downs and others (2019) present eruption ages for the Matan volcanic center and the entire northern part of Harrat Rahat.

Volcanic landforms present throughout the map area of figure 4 are dominated by the rough surfaces of lava flows and their associated scoria cones and (or) shield volcanoes (figs. 3*A–D*). Scoria cones and shield volcanoes have been correlated with their lava flows where possible, however this is not possible for all vents because of scoria-cone collapse and (or) burial by younger lava flows. Most cones are steep-sided and rise more than 100 m above their surrounding lava flows, although some of the smallest volume eruptions produced scoria cones that are only a few tens of meters high. Many eruptions created scoria cones that have nested craters,

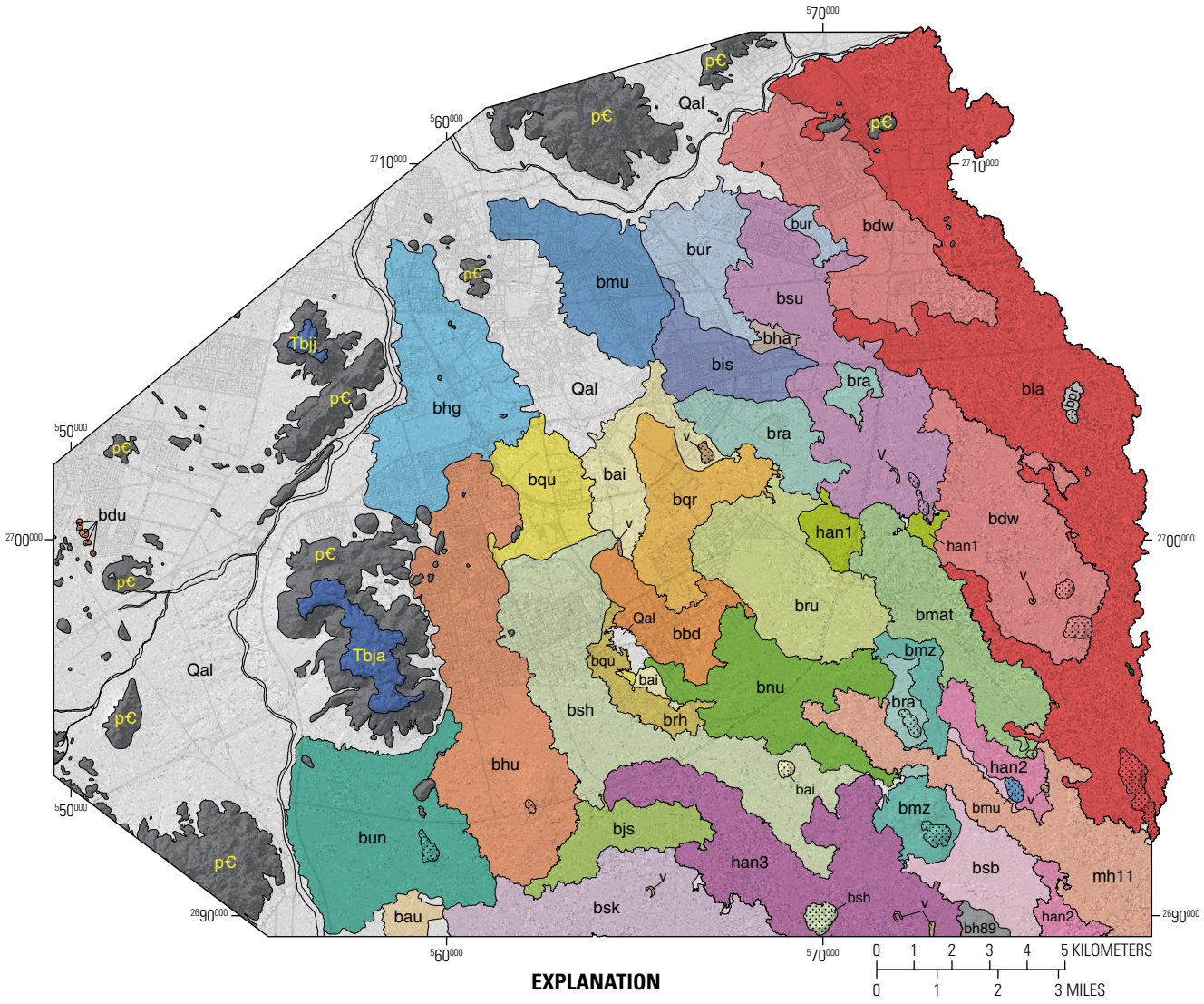

Figure 4. Geologic map of mafic lava flows and scoria cones (stippled pattern) within the vicinity of Al Madīnah. The base map is a 0.5-meter-resolution shaded relief constructed from light detection and ranging (lidar) topography. Roads are marked in light gray. See figure 5 for the correlation of map units by age. Quaternary volcanic strata are present farther east and south of the map area (fig. 2) but are not shown here (see Downs and others [2019] and Robinson and Downs [2023] for the full geologic map).

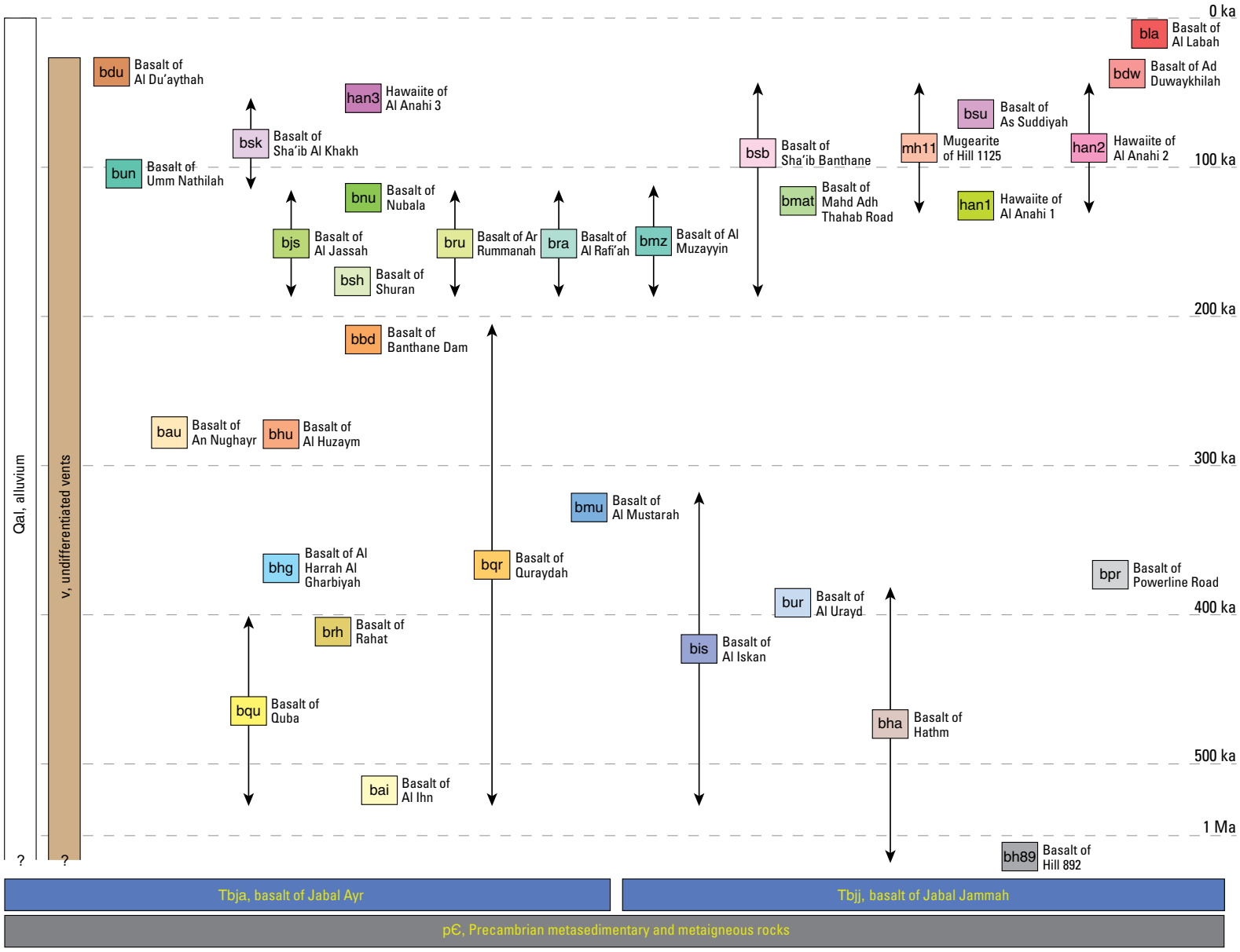

Figure 5. Correlation of map units by age in northernmost Harrat Rahat near Al Madīnah. Units are arranged by their absolute or approximate age. Age ranges shown by black arrows are constrained stratigraphically and (or) paleomagnetically such that arrows denote the constrained range over which these short-duration (weeks to at most months) eruptions occurred. ka, thousand years ago; Ma, million years ago.

or clusters of north-northwest aligned craters and (or) cones. Aligned craters and cones resulted from fissure eruptions, such as the 2.25-km-long fissure that created seven north-northwest aligned scoria cones during the 1256 C.E. eruption of the basalt of Al Labah (figs. 3*A*, 4). Other examples of elongate scoria cone complexes interpreted as products of fissure eruptions are evident on figure 4, such as for the basalts of Al Du'aythah, Ad Duwaykhilah, As Suddiyah, and Umm Nathilah. These scoria cones also typically contain breaches where lava drained and rafted cone material. Rafted cone material has been identified farther than 1 km from their vents in a few places. Vents typically consist of vesicular, vitric bombs, lapilli, and agglutinate spatter. Because of the unconsolidated nature of the scoria cones, many of the older (older than 100 ka) cones are heavily eroded, exposing deeply oxidized syneruptive reddish-brown scoria and lapilli. Only the youngest scoria cones retain a black, vitric uneroded appearance. Lava flows within the northernmost part of Harrat Rahat can be thicker than 10 m, and consist of near-vent pāhoehoe, broad 'a'ā channels with levees, and transitional morphologies (figs. 3*A–B*, *D*). Shield volcanoes are rare within northern Harrat Rahat, and only two are present near Al Madīnah as the vents for the basalts of Al Huzaym and Hill 892. These shield volcanoes have gentle slopes of only a few degrees and can measure as much as 4 km in diameter with interior craters of 1 km diameter.

Most volcanic rocks near Al Madīnah are alkalic basalts accompanied by minor volumes of transitional basalts, hawaiites, and a single mugearite flow (table 1, fig. 6*A*) (note, alkalic and transitional rocks are reclassified from previous publications based on CIPW normative nepheline or traces of hypersthene as by Sisson and others [2023]). Additionally, there is both petrographic and geochemical evidence for mixing of distinctive basaltic magmas pre- and (or) syneruptively for several eruptions (Camp and others, 1987). All Harrat Rahat mafic lavas and scoriae have broadly similar petrographic characteristics and mineral assemblages. Individual eruptive units range from aphyric to containing olivine (± chromian spinels) ± plagioclase phenocrysts, and olivine + plagioclase + pyroxene + Fe-Ti oxide + glass-bearing groundmass. In most samples, zoned olivine phenocrysts constitute 1 to 10 volume percent of the vesicle-free rock, are typically 1 to 5 millimeters (mm) in diameter (with rare phenocrysts greater than 20 mm), and have a variety of colors (dark to pale green, honey yellow, and varying degrees of iddingsite alteration) and textures (from resorbed to corroded and skeletal) (figs. 7*A–D*). Plagioclase phenocrysts show a similar array of characteristics, constituting less than 1 to 5 volume percent of samples. Plagioclase phenocrysts can achieve grain sizes greater than 50 mm in diameter, but most are less than 10 mm in diameter and many are euhedral to resorbed with overgrowth rims (figs. 7*A–D*). Pyroxene phenocrysts are almost unknown within mafic units. Calcic clinopyroxene is almost exclusively confined to interstitial spaces within the groundmass, and neither hypersthene nor pigeonite have been indentified even in transitional samples. Equant to sub-equant Fe-Ti oxides (from 10 to 100 micrometers [µm] in diameter) are ubiquitous throughout the groundmass of Harrat Rahat's mafic through intermediate eruptive products. Volcanic rocks with more evolved compositions (low MgO alkalic basalt, hawaiite, and mugearite) contain trace amounts of apatite and rarely amphibole. At least eight units (basalts of Al Labah, Ad Duwaykhilah, Hill 892, Al Huzaym, Mahd Adh Thahab Road, Al Rafi'ah, Quraydah, and Al Mustarah) contain dark greenish-brown chromian spinels hosted in olivine phenocrysts (figs. 7*B–D*), of which some have more Fe-Ti oxide-rich rims.

Shield volcanoes in the Al Madīnah area consist of relatively alkali-poor alkalic basalts, in some cases accompanied by transitional basalts, both with a coarse-grained, diktytaxitic groundmass, although some are holocrystalline with seriate textures (fig. 7*A*). Weakly alkalic and transitional basalts range from aphyric to phenocryst rich. Olivine is commonly the only phenocryst phase, constituting 5 to 10 percent of samples, with skeletal, corroded, and (or) euhedral textures, and colors ranging from shades of green to honey yellow or heavily altered to iddingsite. Groundmass plagioclase laths are ubiquitous, but plagioclase phenocrysts are sparse.

Physical characteristics for individual eruptive units vary. Table 1 summarizes the estimated area, volume, and flow length from vent for each unit. Because of extensive anthropogenic modification of vents and lava flows around Al Madīnah, erupted volumes were calculated using a uniform lava flow thickness of 10 m (although some may be as thick as 15 m). This is consistent with field observations in the less disturbed parts of Harrat Rahat to the south of Al Madīnah. Most of the older lava flows are exposed discontinuously because of younger lava flows partly covering them. As such, their limits have been conservatively reconstructed where possible. Minimum estimates of scoria cone volumes were made by drawing multiple cross sections to assess average cone heights and multiplying by cone area. These cones are typically strongly elongate in the northwest direction and many have undergone breaches or collapse, precluding the use of simple geometry to calculate the volume of each cone. Additionally, scoria cones (except for the basalt of Al Du'aythah) constitute less than or equal to 1 percent of the total dense rock equivalent (DRE) volume of eruptions, where exposures provide reliable constraints on vent and lava flow area and volume estimates. Lava flow DRE volumes were calculated using a lava density equal to that of a basaltic magma of 2,500 kilograms per cubic meter (kg/ m^3) (Crosweller and others, 2012) and a scoria cone of 1,500 kg/ m^3 (McGetchin and others, 1974).

Individual eruptive products range in area from the four small-volume scoria cones of the basalt of Al Du'aythah at 0.1 km^2 to the extensive lava flows of the hawaiite of Al Anahi 3 at 69 km^2. As expected, these also have the smallest and largest estimated DRE volumes at 0.002 and 0.7 km^3, respectively. Overall, individual mapped eruptive units cover an average area of 21 km^2 and emplaced an average DRE volume of 0.2 km^3. Since most older lava flows are buried beneath younger lava flows to the point that

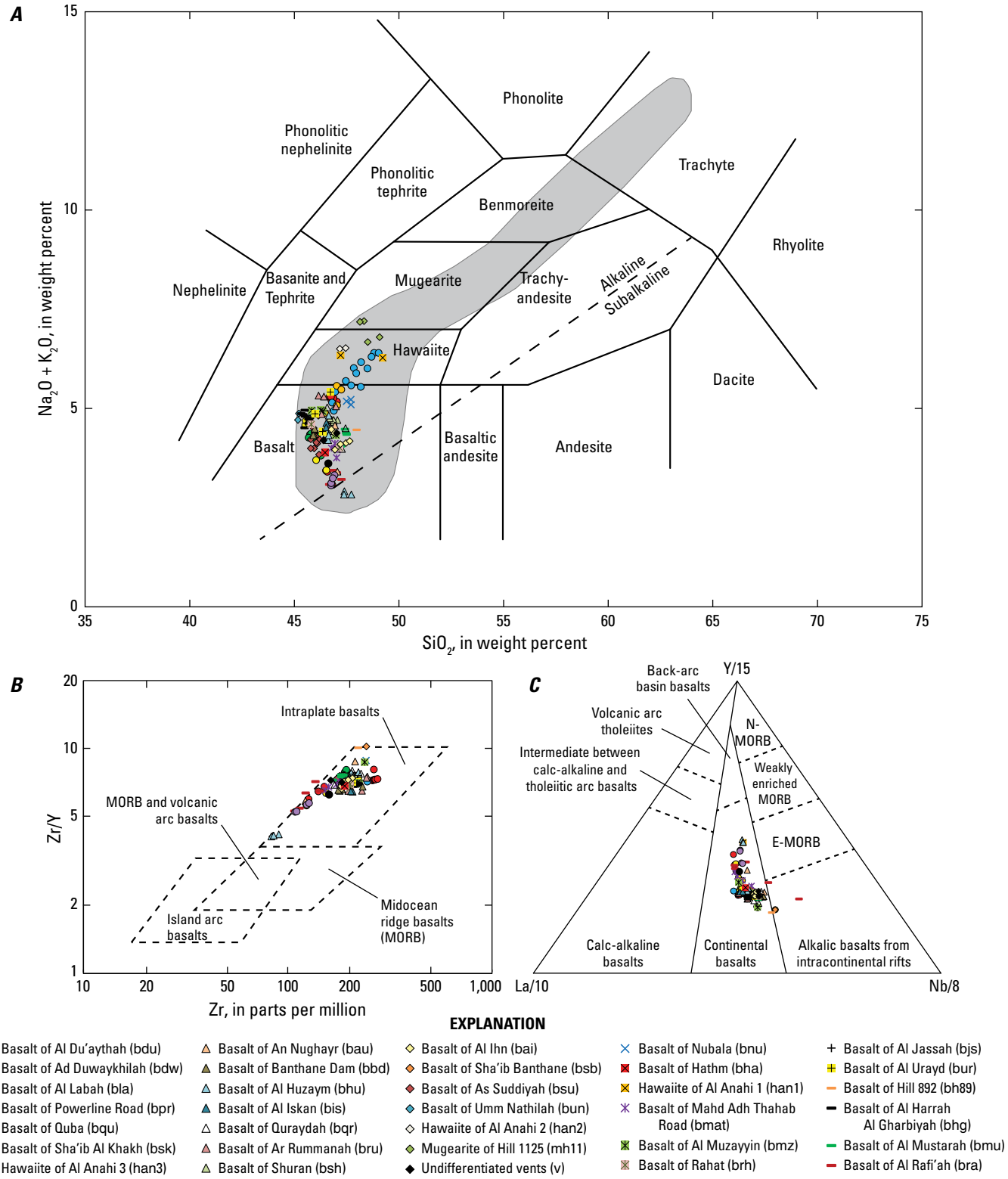

Figure 6. Compositional classification plots for northernmost Harrat Rahat volcanic rocks. All unit names and symbols from Downs and others (2019) and Robinson and Downs (2023). *A*, Total alkali versus silica plot (as defined by Cox and others, 1979) with the alkaline and subalkaline fields from Macdonald and Katsura (1964). The gray field represents the range in composition of volcanic rocks as determined by Camp and Roobol (1989). *B*, Tectonic discrimination plot of Pearce and Norry (1979) illustrating the intraplate nature of basalts containing 6 or more weight percent MgO. *C*, Tectonic discrimination plot of Cabanis and Lecolle (1989) indicating continental basaltic processes with a few plotting in the alkalic basalts from intracontinental rift field for basalts containing 6 or more weight percent MgO. See Downs and others (2018) and Downs (2019) for whole-rock chemical compositions. E-MORB, enriched midocean ridge basalt; N-MORB, normal midocean ridge basalt.

Table 1. Physical and petrographic characteristics of Quaternary volcanic rocks from the northernmost Harrat Rahat.

[Glomerocrysts are crystal clots consisting of both plagioclase and olivine phenocrysts. Several units consist of multiple lobes of lava flowing in divergent directions. The flow length is the longest lobe of lava relative to its vent. All unit names from Downs and others (2019); rock types are reclassified from those of Downs and others (2018) based on CIPW normative nepheline (alkalic) or traces of normative hypersthene (transitional) as by Sisson and others (2023). DRE, dense rock equivalent; km, kilometer; km^2, square kilometer; km^3, cubic kilometer; mm, millimeter; %, percent]

Unit	Area, in km^2	DRE volume, in km^3	Flow length, in km	Composition	Phenocrysts assemblage
Basalt of Al Labah (bla)	60.7	0.5	22.8	Alkalic basalt	<1% olivine (+spinel) to 5 mm, <1% plagioclase to 2 mm
Basalt of Al Du'aythah (bdu)	0.1	0.002	0.2	Alkalic basalt	1–5% olivine to 1–3 mm, 1–15% plagioclase to 2–10 mm
Basalt of Ad Duwaykhilah (bdw)	48.6	0.5	16.5	Alkalic basalt	<1% olivine (+spinel) to 2 mm, ≤1% plagioclase to 8 mm
Hawaiite of Al Anahi 3 (han3)	68.7	0.7	20.6	Hawaiite and alkalic basalt	<1% olivine to ≤1–4 mm, 5–10% plagioclase to 2–10 mm
Mugearite of Hill 1125 (mh11)	45.6	0.5	19.3	Mugearite and hawaiite	≤1% olivine to 1 mm, <<1% plagioclase
Hawaiite of Al Anahi 2 (han2)	25.4	0.3	12.4	Hawaiite	1% olivine to 2–5 mm, <1% plagioclase to 4 mm
Basalt of Sha'ib Banthane (bsb)	11.1	0.1	8.0	Alkalic basalt	1% olivine to 1–4 mm, <<1% plagioclase to 15 mm
Basalt of Sha'ib Al Khakh (bsk)	53.6	0.5	16.6	Alkalic basalt	2–3% olivine to <1 mm, <<1% plagioclase to 3–4 mm
Basalt of As Suddiyah (bsu)	26.8	0.3	9.5	Alkalic basalt	<1–4% olivine to 1–5 mm (clots to 10 mm), 2% plagioclase to 6–10 mm
Basalt of Umm Nathilah (bun)	19.7	0.2	4.5	Alkalic basalt	1–3% olivine to 2–3 mm (clots to 5–7 mm), 1–2% plagioclase to 10 mm
Basalt of Nubala (bnu)	12.6	0.1	7.5	Alkalic basalt	<1% olivine to 1 mm, 2% plagioclase to 5–9 mm (glomerocrysts present)
Basalt of Mahd Adh Thahab Road (bmat)	13.9	0.1	7.7	Alkalic basalt	2–5% olivine (+spinel) to 2–10 mm, <1% plagioclase to 2–10 mm
Basalt of Al Muzayyin (bmz)	6.9	0.07	6.2	Alkalic basalt	1–2% olivine to 2–4 mm, <1% plagioclase to 5 mm
Hawaiite of Al Anahi 1 (han1)	30.5	0.3	19.2	Hawaiite	3% olivine to 1 mm, 1% plagioclase to 5 mm
Basalt of Al Rafi'ah (bra)	23.5	0.2	11.9	Alkalic basalt	1–10% olivine (+spinel) to 1–3 mm (clots to 5–10 mm), <1% plagioclase to 3–10 mm
Basalt of Al Jassah (bjs)	5.5	0.05	5.5	Alkalic basalt	<1% olivine to 1 mm, <1% plagioclase to <1 mm
Basalt of Ar Rummanah (bru)	14.2	0.1	5.7	Alkalic basalt	1% olivine to 2–4 mm, 1% plagioclase to 3–10 mm
Basalt of Shuran (bsh)	30.8	0.3	14.7	Alkalic basalt	1% olivine to 1–8 mm, 1–2% plagioclase to 10–30 mm (glomerocrysts present)
Basalt of Banthane Dam (bbd)	6.3	0.06	4.5	Alkalic basalt	1–2% olivine to 1–4 mm, 1–2% plagioclase to 10 mm (glomerocrysts present)
Basalt of Quraydah (bqr)	9.0	0.09	5.4	Alkalic basalt	1–3% olivine (+spinel) to 1–3 mm, 1–3% plagioclase to 10 mm
Basalt of Al Huzaym (bhu)	26.1	0.3	9.6	Alkalic and transitional basalt	4–15% olivine (+spinel) to 2–7 mm, <<1% plagioclase
Basalt of An Nughayr (bau)	4.4	0.05	3.2	Alkalic basalt	10% olivine (+spinel) to 7 mm, <<1% plagioclase to 50 mm
Basalt of Al Mustarah (bmu)	31.4	0.3	21.4	Alkalic basalt	1–10% olivine (+spinel) to 1–8 mm, 2–5% plagioclase to 3–20 mm
Basalt of Al Iskan (bis)	6.4	0.06	4.4	Alkalic basalt	2–4% olivine to 1–4 mm, <1% plagioclase to 5 mm
Basalt of Powerline Road (bpr)	0.4	0.004	0.9	Alkalic basalt	3–4% olivine to 1–2 mm, 3–5% plagioclase to 2–3 mm
Basalt of Al Harrah Al Gharbiyah (bhg)	17.9	0.2	7.3	Alkalic basalt	<1–2% olivine to 3–5 mm, ≤1% plagioclase to 5–10 mm
Basalt of Al Urayd (bur)	14.0	0.1	5.6	Alkalic basalt	<<1% olivine to 1 mm, 1–3% plagioclase to 10 mm
Basalt of Hathm (bha)	0.7	0.007	1.2	Alkalic basalt	1–2% olivine to 1 mm, <<1% plagioclase to 1 mm (glomerocrysts present)
Basalt of Rahat (brh)	3.2	0.03	1.6	Alkalic basalt	<1–2% olivine to 1–3 mm, 1–2% plagioclase to 5 mm
Basalt of Quba (bqu)	13.7	0.1	8.3	Alkalic basalt	2–4% olivine to 5–7 mm (clots), <1% plagioclase to 5–15 mm
Basalt of Al Ihn (bai)	38.3	0.4	11.7	Alkalic basalt	1–5% olivine to 1–2 mm, <1% plagioclase to 1 mm
Basalt of Hill 892 (bh89)	1.9	0.02	1.5	Alkalic basalt	2–3% olivine (+spinel) to 4–5 mm, 1% plagioclase to 1 mm
Undifferentiated vents (v)	0.6	0.01	---	Alkalic basalt	Variable, aphyric to 1–2% olivine to 1 mm, 1–8% plagioclase to 1–10 mm

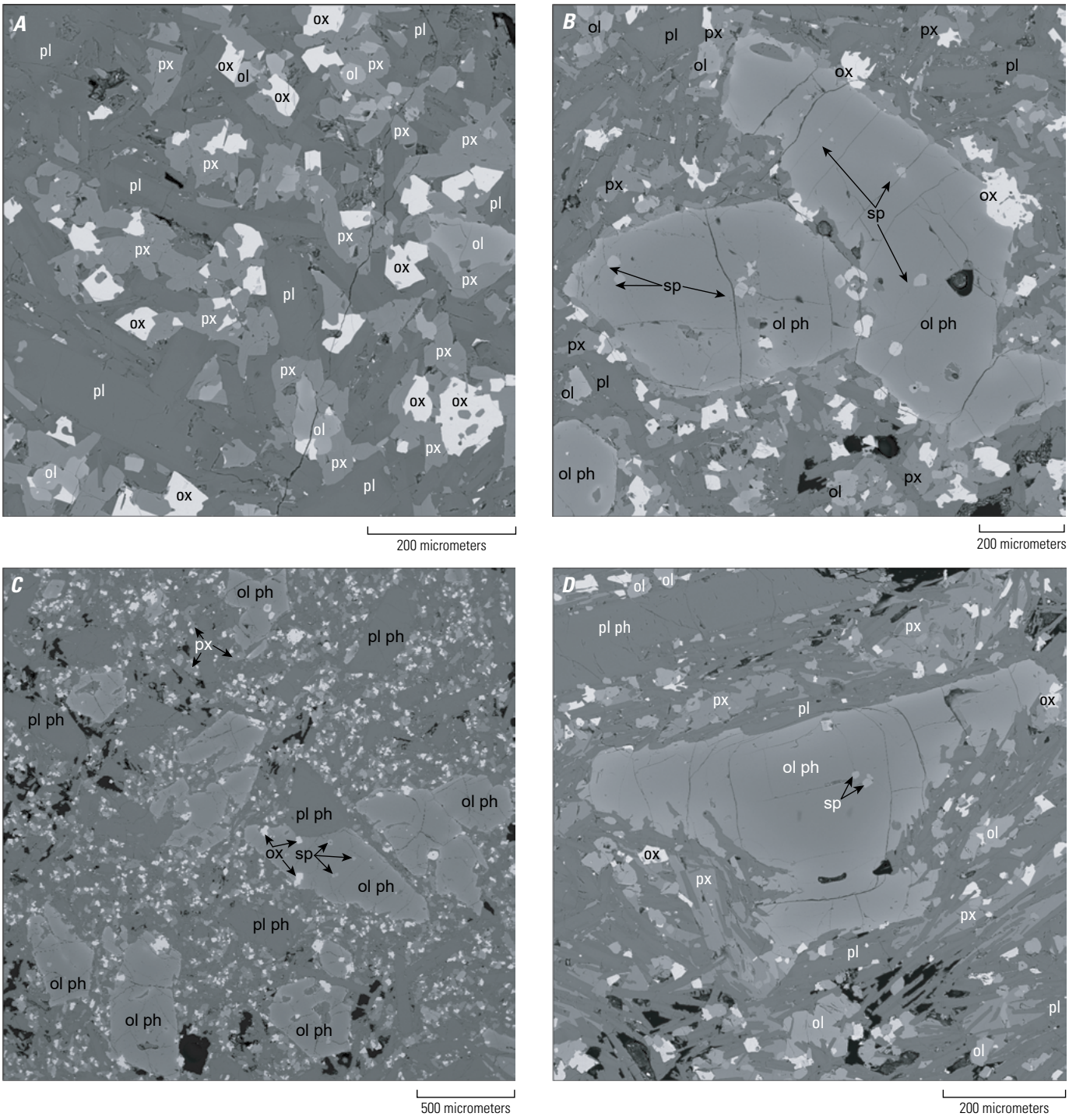

Figure 7. Scanning electron microscope backscatter images of representative textures and mineral assemblages of northern Harrat Rahat mafic volcanic rocks. *A*, Groundmass containing plagioclase, pyroxene, olivine, and Fe-Ti oxides from the basalt of Al Huzaym. *B*, Olivine phenocrysts hosting chromian spinels in a groundmass of plagioclase, olivine, pyroxene, and Fe-Ti oxides from the basalt of Al Huzaym. *C*, Vent sample from the basalt of Al Huzaym with plagioclase and olivine phenocrysts (hosting chromian spinels) in a groundmass of plagioclase, olivine, pyroxene, and Fe-Ti oxides. *D*, Olivine phenocryst with skeletal margins containing chromian spinels in a groundmass of plagioclase, olivine, pyroxene, and Fe-Ti oxides from the basalt of Quraydah. Abbreviations: ol, olivine; ox, Fe-Ti oxide; pl, plagioclase; ph, phenocryst; px, pyroxene; sp, chromian spinel.

reconstructing their total areas and volumes is difficult, the youngest units are used to give the most robust estimate of the total area and volumes of individual units. Using the 13 youngest eruptions (younger than 200 ka) that have vents tied to lava flows gives a higher average area of 34 km^2 and average DRE volume of 0.3 km^3. Lava flow lengths vary from slightly more than 20 km, with the basalt of Al Labah reaching about 23 km, to the short, stubby lava flows of the basalt of Al Du'aythah that are only 115 and 200 m long. Lava flow complexes from the same 13 eruptions yield an average lava flow length of 13.5 km. This estimate only considers the length of the longest lobe of lava from its vent, although some units contain multiple lobes of lava flowing down more than one channel. For example, the hawaiite of Al Anahi 3 has a lobe of lava that reaches 20.6 km northwest of its vent, but also one that reaches 14.3 km west-northwest, and a third that reaches 15 km west-southwest. These two more southerly lava flows are not shown on figure 4 as they are beyond the southern limit of the map area (see Downs and others [2019] and Robinson and Downs [2023] for their full lava flow extents).

Methods

Discrimination of Map Units

Individual eruptive units presented in this chapter were mapped in the field through a combination of outcrop-scale and hand-specimen petrography and observing lava flow contacts and stratigraphic superposition. Around Al Madīnah, these efforts were supported using 0.5-m-resolution light detection and ranging (lidar) and satellite photogrammetric digital topographic bases. Differences in phenocryst abundances, sizes, and habits, as well as groundmass are noticeable among most adjacent units (table 1). Thin-section petrography, geochemistry, paleomagnetic studies, and eruption ages via $^{40}Ar/^{39}Ar$ radiometric and ^{36}Cl cosmogenic surface-exposure dating techniques were obtained to confirm and further refine field observations. Integrating these observations and results allowed for the discrimination of 33 distinct mafic volcanic units ranging from older than 1 Ma to as young as 1256 C.E., each interpreted to have been produced by a distinct eruption (figs. 4–5).

The geologic map for this area from Downs and others (2018) uses some unit names that have been revised by Downs and others (2019), and this chapter follows the nomenclature of the latter for all unit names. Previous names were kept where possible for units, such as in the case of the basalt of Al Du'aythah (Murcia and others, 2015), whereas unit names assigned by Downs and others (2019) are based on geographic landforms, city districts, or other distinguishing features. To a first order, unit names were assigned based on source vent geographic landform names (in other words, scoria cones, shield volcanoes, craters, and domes). Some previously named scoria cones (such as Al Anahi) of similar composition are spatially clustered, in which case the previously assigned name was used and a numeric identifier was added with one being the oldest (for example, hawaiites of Al Anahi 1, Al Anahi 2, and Al Anahi 3 for the three scoria cones near Al Anahi). Where a source vent could not be assigned to a unit owing to its burial and (or) destruction, a unit name was assigned based on some other proximal distinguishing geomorphic feature (such as a mountain, hill, or wadi) or the city district (such as Shuran and Quba) where the unit is predominantly exposed.

To aid in mapping, unaltered juvenile lava and scoria were collected for major-oxide and trace-element chemical analyses by X-ray fluorescence (XRF) spectrometry and inductively coupled plasma mass spectrometry (ICP-MS) at the GeoAnalytical Laboratory at Washington State University in Pullman, Washington, using the methods of Knaack and others (1994) and Johnson and others (1999). Detailed XRF and ICP-MS methods are discussed by Downs and others (2018) and all whole-rock geochemical compositions are provided by Downs (2019).

Geochronology

$^{40}Ar/^{39}Ar$ Radiometric Dating

Samples for $^{40}Ar/^{39}Ar$ dating were collected from 16 basaltic eruptive units exposed within the map area shown in figure 4. Dense samples with a crystalline groundmass were chosen for analysis. Each sample was crushed in a roller mill, ultrasonicated, and sieved to 250 to 355 μm size. Approximately 150 milligrams (mg) of fresh groundmass was separated from phenocrysts using a Frantz LB-1 Magnetic Barrier Laboratory Separator, and carefully handpicked under a binocular microscope. Groundmass separates were packaged in copper foil, bracketed by packets of Bodie Hills sanidine monitor minerals (9.7946±0.0033 Ma; Fleck and others, 2019), encapsulated in quartz vials that were wrapped in 0.5 mm thick cadmium foil to shield samples from thermal neutrons during irradiation, and irradiated for 1 hour in the central thimble of the U.S. Geological Survey TRIGA reactor in Denver, Colorado (Dalrymple and others, 1981) at a power level of 1 megawatt. The reactor vessel was rotated continuously and oscillated vertically during irradiation to minimize vertical and lateral neutron flux gradients.

Argon isotope analyses were conducted at the U.S. Geological Survey Menlo Park facility using a MAP216 single-collector mass spectrometer with a Baur-Signer ion source and a Johnston MM1 electron multiplier. Argon was extracted from fluence monitors in a single heating step (that is, total fusion) using a New Wave CO_2 laser, whereas argon from groundmass separates of unknown age were extracted in 7 to 15 discrete temperature steps (typically spanning the temperature range of 550 to 1,400 degrees Celsius [°C]) using a molybdenum shielded custom-resistance furnace with a molybdenum crucible. Extracted argon was exposed to a 4-ampere tungsten filament, 125 kelvin cold finger, and two SAES St-175 getters (one operated at 300 °C and one at room temperature) to remove active gases. Prior to measurement of argon isotopes, samples were degassed at 500 °C to reduce the levels of undesirable gases (water, nitrogen, and

hydrocarbons as measured by a Granville-Phillips Series 835 vacuum quality monitor). Ages were calculated using the decay constants of Steiger and Jäger (1977). Uncertainties in $^{40}Ar/^{39}Ar$ ages are reported at the one-sigma level unless otherwise noted and include propagated uncertainties in counting statistics and J values.

Instrumental mass discrimination was calculated by repeated measurement of atmospheric argon. Initially, mass discrimination was calculated assuming atmospheric $^{40}Ar/^{36}Ar = 295.5\pm0.5$ (Steiger and Jäger, 1977). In July 2016, the Menlo Park facility began calculating mass discrimination assuming atmospheric $^{40}Ar/^{36}Ar = 298.56\pm0.31$ (Lee and others, 2006). The change in the assumed atmospheric $^{40}Ar/^{36}Ar$ does not result in a bias in ages between the two irradiations because both monitors and unknowns from each irradiation were calculated in the same manner.

^{36}Cl Cosmogenic Surface-Exposure Dating

Samples for ^{36}Cl cosmogenic surface-exposure dating were collected using a hammer and chisel from three mafic units exposed within the map area shown in figure 4. Samples were collected from areas on the lava flow that were high-standing relative to the surrounding topography to minimize shielding effects. Each sample was trimmed such that only the upper 4 centimeters (cm) of material was collected and the surface dip for samples was negligible (less than 5°). Shielding factors for each sample location were calculated from the inclination of the visible horizon at 30° increments of azimuth (Goose and Phillips, 2001). In all cases, the angle to the horizon was less than or equal to 6° in every direction but shielding factors were still calculated for the sake of completeness. Erosion rates are estimated to be low (less than or equal to 1 millimeter per thousand years [mm/k.y.]) based on the preservation of small-scale (smaller than 1 cm), irregular surface features on each lava flow. Given the uncertainty in erosion rate for each sample site, a conservative rate of 1±1 mm/k.y. was used for the calculations.

Chemical separation and analysis of samples took place at the Purdue Rare Isotope Measurement (PRIME) Laboratory at Purdue University in West Lafayette, Indiana. Samples were chemically dissolved, spiked with a ^{35}Cl enriched tracer (Desilets and others, 2006) and analyzed via accelerator mass spectrometry. Each sample was analyzed for major-oxide abundances via wavelength dispersive XRF and trace-element abundances via inductively coupled plasma optical emission spectrometry (ICP-OES) and ICP-MS at the U.S. Geological Survey in Denver, Colorado (Taggart, 2002), which are presented by Downs and others (2018). Trace elements of importance for the calculation of ^{36}Cl cosmogenic surface-exposure ages include U and Th that can produce thermal neutrons during alpha decay, and B, Li, Sm, and Gd, which have large thermal neutron absorption cross sections, and therefore reduce the production of ^{36}Cl from ^{35}Cl. Of these elements, all were above detection limits except B and Li. Given the detection limit for B and Li was 10 parts per million (ppm), the concentrations of B and Li in each sample were assumed to be 5±5 ppm during calculations.

Cosmogenic surface-exposure ages were calculated using the online CRONUScalc ^{36}Cl Exposure Age Calculator v. 2.0 (Cosmic-Ray Produced Nuclide Systematics on Earth Project), which uses a MATLAB-based code that is described in Marrero and others (2016). Ages were calculated using the Lal and Stone time-independent scaling model (Lal, 1991; Stone, 2000). Marrero and others (2016) provide a detailed discussion of production rates for various production pathways, details of scaling models, and other parameters used in the calculation of ^{36}Cl cosmogenic surface-exposure ages.

Paleomagnetism

Paleomagnetic secular variations were measured for mafic lava flows and scoria cones within the northernmost part of Harrat Rahat to correlate individual units (table 2) independent of field, petrographic, and geochemical interpretations. Additionally, paleomagnetic analyses helped to unravel discrete temporal groupings that could not otherwise be divided based on the precision of modern dating techniques.

Paleomagnetic samples were collected, processed, and interpreted using the methods of McElhinny (1973). Eight cores of 10 cm length were collected at each field sampling site using a handheld, gasoline powered, water cooled, modified chainsaw motor with a 2.5 cm diamond coring drill, and cores were oriented by sun compass. A 2.5-cm-long specimen from each core was measured using an automated cryogenic magnetometer and then subjected to alternating-field demagnetization to remove secondary components of magnetization. An isothermal component from nearby lightning strikes was the most frequent source of secondary magnetization. The characteristic direction of remanent magnetization for each site was calculated using Fisher statistics on data from (1) line fits of data on vector component diagrams, (2) plane fits on equal-area diagrams, and (3) mixtures of lines and planes data. Table 2 presents site mean directions of magnetization for each group, including 95 percent confidence limits.

Obtaining accurate paleomagnetic samples from the youngest (younger than 100 ka) Harrat Rahat mafic lava flows is difficult because their surfaces tend to be rubbly and uneroded. However, older units have undergone enough erosion that in-place blocks and deeply incised drainage channels into lava flow interiors could be easily sampled. Drilling in road cuts and drainage channels where erosion has penetrated the interior of a lava flow was ideal but eroded surfaces composed of large blocks regarded as having undergone minimal movement since cooling below their Curie temperature were also successful. Lava flow margins were avoided during drilling to reduce the risk of sampling from blocks that have undergone post-magnetization rotation. It is impossible to preclude minor rotations, and accordingly, dispersion of directions is observed for some groups. This is particularly apparent in the youngest, rubbly lava flows, and scoria cones where agglutinate spatter was generally the only candidate for drilling. Potential signs of post-cooling rotation include larger 95 percent confidence values after alternating-field treatment and scattered inclination and declination pairs.

Table 2. Paleomagnetic analyses of Quaternary volcanic rocks from northernmost Harrat Rahat.

[All unit names from Downs and others (2019) and Robinson and Downs (2023). Easting and northing are in the World Geodetic System of 1984 using the Universal Transverse Mercator zone 37 north coordinate system. N/No is the number of cores used compared to the number originally taken. Treatment is the nature of the demagnetization procedure, where Li indicates lines, Pl indicates planes, and Mx indicates a mixture of lines and planes data. Inclination and declination are in degrees. α95 is the radius of the 95-percent confidence limit about the mean direction. k is the estimate of the Fisher precision parameter. R is the length of the resultant vector. Pole lat. (°N) in degrees north and Pole long. (°E) in degrees east are the coordinates of the virtual geomagnetic pole calculated from the mean direction. Inclination and declination values in parentheses were not used in determining group mean values]

Sample	Easting	Northing	N/No	Treatment	Inclination	Declination	α95	k	R	Pole lat. (°N)	Pole long. (°E)
Basalt of Al Labah (bla)											
R14DC033	575865	2694831	8/8	Li	30.2°	11.3°	3.5°	256	7.9727	76.7°	165.2°
R14DC034	578710	2692212	8/8	Li	31.2°	9.9°	1.2°	1977	7.9965	78.1°	166.9°
R14DC049	573396	2707253	8/8	Li	30.2°	9.1°	1.9°	855	7.9918	78.1°	172.1°
Mean	**576047**	**2698719**	**3/3**		**30.5°**	**10.1°**	**1.7°**	**5227**	**2.9996**	**77.6°**	**168.0°**
Basalt of Al Du'aythah (bdu)											
R15DC012	550438	2700242	8/8	Li	51.0°	12.9°	3.2°	307	7.9772	76.5°	93.9°
R15DC013	550305	2700519	8/8	Mx	50.1°	14.5°	2.9°	381	7.9816	75.6°	99.5°
R15DC014	550562	2699734	8/8	Li	44.4°	12.1°	2.4°	518	7.9865	78.9°	118.2°
Mean	**550387**	**2700375**	**2/3**		**50.6°**	**13.7°**	**3.0°**	**7121**	**2.9999**	**76.1°**	**96.9°**
Basalt of Ad Duwaykhilah (bdw)											
R15DC037	570525	2708047	8/9	Li	41.1°	14.7°	2.1°	713	7.9902	76.6°	130.7°
R16DC018	572970	2703453	7/8	Li	40.2°	11.8°	2.0°	893	6.9933	79.1°	135.4°
R16DC021	573563	2700533	7/8	Li	36.9°	11.2°	4.0°	233	6.9742	79.0°	147.9°
Mean	**571963**	**2704234**	**3/3**		**39.4°**	**12.5°**	**4.0°**	**943**	**2.9979**	**78.3°**	**137.6°**
Hawaiite of Al Anahi 3 (han3)											
R14DC011	582195	2684226	7/8	Li	16.7°	16.2°	3.5°	292	6.9794	67.9°	172.6°
R14DC042	566121	2694062	8/8	Li	16.8°	14.4°	2.9°	363	7.9807	69.1°	176.2°
Mean	**574071**	**2688743**	**2/2**		**16.8°**	**15.3°**	**3.8°**	**4406**	**1.9998**	**68.5°**	**174.3°**
Mugearite of Hill 1125 (mh11)											
R15DC028	585871	2685809	8/8	Mx	22.1°	355.4°	2.6°	477	7.9853	76.5°	239.5°
R15DC030	583975	2687049	8/8	Mx	23.9°	358.0°	3.1°	344	7.9797	78.1°	229.3°
Mean	**584238**	**2685478**	**2/2**		**23.0°**	**356.7°**	**6.5°**	**1464**	**1.9993**	**77.3°**	**234.7°**
R16DC035	573194	2693544	6/8	Mx	34.4°	358.7°	7.7°	89	5.9436	84.4°	232.5°
R16DC037	576429	2691800	4/8	Mx	29.9°	3.5°	4.2°	637	3.9953	81.1°	197.5°
Mean	**575069**	**2692070**	**2/2**		**32.2°**	**1.2°**	**13.3°**	**357**	**1.9972**	**83.0°**	**210.6°**
Basalt of Sha'ib Banthane (bsb)											
R16DC032	573197	2691108	8/8	Mx	30.9°	349.3°	3.6°	275	7.9746	77.4°	274.3°
Basalt of Sha'ib Al Khakh (bsk)											
R17DC014	573836	2685243	5/8	Pl	22.5°	0.7°	29.7°	4	---	77.4°	216.6°
R14DC038	566343	2687852	5/9	Mx	21.9°	346.6°	3.3°	629	4.9936	71.9°	266.5°
R15DC042	562935	2689896	7/8	Li	21.4°	356.8°	2.1°	849	6.9929	76.5°	233.0°
R16DC046	566684	2684576	8/8	Mx	26.6°	355.4°	2.1°	700	7.99	78.9°	243.5°
Mean	**564944**	**2687591**	**3/4**		**23.4°**	**352.9°**	**8.9°**	**192**	**2.9896**	**76.2°**	**249.9°**
Basalt of As Suddiyah (bsu)											
R15JR006	568576	2706564	6/8	Mx	42.3°	351.4°	8.8°	61	5.9183	82.2°	311.4°
R15DC024	570137	2704579	8/8	Li	41.4°	354.1°	1.6°	1268	7.9945	84.5°	304.0°
R15DC036	571542	2703268	8/8	Li	36.8°	356.4°	2.4°	542	7.9871	84.8°	260.8°
R16DC005	569657	2705186	8/8	Mx	42.7°	355.6°	2.4°	557	7.9874	86.0°	315.0°
R16DC019	572458	2702642	7/8	Li	40.5°	355.5°	2.9°	428	6.986	85.7°	293.0°
R16DC020	572444	2701247	8/8	Mx	39.5°	354.5°	2.1°	721	7.9903	84.6°	289.0°
Mean	**570949**	**2704229**	**6/6**		**40.5°**	**354.6°**	**2.1°**	**1011**	**5.9951**	**84.9°**	**296.1°**
Basalt of Umm Nathilah (bun)											
R16DC001	559356	2693977	6/8	Mx	58.5°	349.9°	3.0°	553	5.991	72.9°	12.1°
R16DC002	556180	2694385	8/8	Li	57.5°	346.2°	2.4°	516	7.9864	71.9°	2.5°

Table 2. Paleomagnetic analyses of Quaternary volcanic rocks from northernmost Harrat Rahat.—Continued

Sample	Easting	Northing	N/No	Treatment	Inclination	Declination	α95	k	R	Pole lat. (°N)	Pole long. (°E)
Basalt of Nubala (bnu)											
R14DC043	567841	2695078	6/8	Mx	33.5°	357.7°	3.5°	371	5.9865	83.6°	239.6°
R14DC044	569589	2696482	8/8	Mx	39.0°	352.1°	3.3°	302	7.9768	82.4°	293.4°
R16DC028	569568	2694511	8/8	Mx	31.9°	359.2°	2.3°	598	7.9883	82.9°	225.9°
Mean	**568965**	**2695361**	**3/3**		**34.8°**	**356.5°**	**7.3°**	**285**	**2.993**	**83.9°**	**252.8°**
Basalt of Mahd Adh Thahab Road (bmat)											
R15DC033	571932	2698443	8/8	Li	44.0°	354.1°	2.1°	693	7.9899	84.5°	325.4°
R15DC035	570988	2700630	7/8	Li	45.7°	359.8°	3.3°	334	6.9821	87.3°	35.9°
R16DC038	575127	2694340	8/8	Mx	41.2°	351.4°	3.2°	329	7.9787	82.1°	306.3°
R16DC040	575082	2695226	8/8	Li	45.7°	358.1°	2.4°	544	7.9871	86.8°	8.2°
Mean	**573011**	**2697596**	**4/4**		**44.2°**	**355.8°**	**3.9°**	**545**	**3.9945**	**85.9°**	**332.4°**
Basalt of Al Muzayyin (bmz)											
R16DC031	572574	2691913	8/8	Mx	46.9°	9.7°	3.3°	288	7.9757	80.5°	104.2°
R16DC033	572752	2696730	8/8	Mx	46.8°	9.1°	3.0°	362	7.9806	81.1°	103.7°
Mean	**572622**	**2694272**	**2/2**		**46.9°**	**9.4°**	**0.9°**	**73584**	**1.9999**	**80.8°**	**103.9°**
Hawaiite of Al Anahi 1 (han1)											
R15DC052	569857	2699705	7/8	Li	50.2°	341.6°	1.8°	1184	6.9949	72.4°	335.6°
Basalt of Al Rafi'ah (bra)											
R15JR007	567505	2703791	7/8	Mx	44.9°	356.5°	2.9°	386	7.9818	86.2°	343.2°
R16DC008	571020	2704307	7/8	Li	46.4°	353.7°	5.7°	114	6.9473	83.5°	341.0°
R16DC034	572342	2695521	8/8	Mx	37.2°	359.2°	2.4°	653	7.9893	86.3°	231.5°
Mean	**569952**	**2700902**	**3/3**		**42.9°**	**356.6°**	**8.1°**	**231**	**2.9913**	**86.9°**	**319.0°**
Basalt of Al Jassah (bjs)											
R14DC041[a]	564322	2692725	8/8	Mx	48.5°	331.8°	3.3°	318	7.978	64.4°	327.4°
Basalt of Ar Rummanah (bru)											
R15DC034[a]	570341	2698235	8/8	Mx	46.7°	329.2°	3.6°	270	7.9741	62.2°	323.8°
R16DC012	568530	2701371	6/8	Mx	49.0°	336.3°	4.2°	324	5.9846	68.3°	329.5°
R16DC015[a]	567440	2700458	8/9	Mx	43.0°	331.9°	2.0°	1004	7.993	64.5°	316.9°
Mean	**568944**	**2699790**	**3/3**		**46.3°**	**332.4°**	**5.9°**	**435**	**2.9954**	**65.0°**	**323.0°**
Basalt of Shuran (bsh)											
R16DC044	570199	2690007	7/8	Mx	45.6°	4.7°	2.3°	824	6.9927	85.0°	95.9°
R15DC008[a]	563255	2697637	8/8	Mx	22.4°	26.4°	2.0°	880	7.992	61.9°	151.9°
R15DC031[a]	564337	2698395	7/8	Li	22.7°	26.1°	3.2°	349	6.9828	62.3°	151.9°
R16DC027	567367	2694489	9/9	Mx	28.9°	19.4°	4.8°	125	8.9362	69.7°	152.2°
R16DC030[a]	569765	2691589	6/8	Mx	28.7°	31.5°	10.7°	56	5.9104	59.1°	140.8°
R16DC029[a]	570473	2693973	7/8	Li	17.9°	22.7°	2.8°	468	6.9872	63.6°	160.9°
Mean	**566937**	**2695351**	**5/6**		**24.2°**	**25.2°**	**5.9°**	**171**	**4.9767**	**63.5°**	**151.3°**
Basalt of Banthane Dam (bbd)											
R16DC014	564534	2699492	7/8	Mx	26.5°	357.7°	3.7°	322	6.9814	79.4°	231.8°
R16DC016	566916	2697587	7/8	Mx	25.8°	9.1°	3.2°	423	6.9858	76.2°	179.5°
R16DC017	564592	2697942	5/8	Mx	27.8°	10.1°	2.8°	768	4.9948	76.5°	173.2°
Mean	**564897**	**2697777**	**2/3**		**26.8°**	**9.6°**	**4.8°**	**2738**	**2.9996**	**76.4°**	**176.4°**
Basalt of Quraydah (bqr)											
R15DC032	566169	2699079	7/8	Li	44.3°	356.8°	2.0°	945	6.9937	86.7°	338.8°
R16DC011	565968	2702953	7/8	Mx	46.4°	352.7°	3.0°	405	6.9852	82.7°	337.7°
R16DC010[a]	565120	2702241	6/8	Mx	68.5°	50.4°	9.6°	70	5.9284	43.2°	80.5°
R16DC013	565399	2698986	7/8	Mx	84.3°	60.4	13.1°	25	6.7612	29.6°	50.9°
Mean	**565998**	**2700883**	**2/4**		**45.4°**	**354.8°**	**7.8°**	**1033**	**1.999**	**84.7°**	**338.2°**
Basalt of Al Huzaym (bhu)											
R15DC007	561046	2699532	8/8	Mx	44.8°	18.6°	1.9°	943	7.9926	73.1°	118.9°

Table 2. Paleomagnetic analyses of Quaternary volcanic rocks from northernmost Harrat Rahat.—Continued

Sample	Easting	Northing	N/No	Treatment	Inclination	Declination	α95	k	R	Pole lat. (°N)	Pole long. (°E)
Basalt of Al Huzaym (bhu)—Continued											
R15DC009	561258	2692845	8/8	Li	44.7°	25.0°	3.3°	281	7.9751	67.4°	119.3°
R15DC010[a]	560948	2694261	8/8	Li	45.9°	25.7°	2.8°	391	7.9821	66.8°	116.8°
R15DC011	561334	2696455	7/8	Li	44.0°	24.9°	2.0°	927	6.9935	67.4°	120.8°
R15DC015[a]	561697	2701406	8/8	Mx	43.3°	26.0°	3.2°	314	7.9777	66.4°	122.2°
Mean	**561253**	**2696432**	**5/5**		**44.6°**	**24.1°**	**2.3°**	**1146**	**4.9965**	**68.2°**	**119.6°**
Basalt of An Nughayr (bau)											
R16DC042	559400	2688518	6/8	Pl	47.0°	23.2°	5.3°	116	---	68.9°	113.9°
Basalt of Al Mustarah (bmu)											
R15JR004	562948	2707224	8/8	Mx	47.9°	350.6°	1.2°	2272	7.9969	80.5°	339.8°
R15JR005	566034	2706142	7/8	Mx	46.3°	357.1°	4.9°	164	6.9633	85.9°	0.7°
R16DC039	575041	2693421	8/8	Mx	48.6°	347.1°	2.7°	432	7.9838	77.4°	336.9°
Mean	**567919**	**2701999**	**3/3**		**47.7°**	**351.7°**	**5.5°**	**499**	**2.996**	**81.4°**	**341.7°**
Basalt of Al Iskan (bis)											
R16DC007	568786	2705059	8/8	Mx	43.9°	351.9°	2.3°	619	7.9887	82.6°	321.0°
Basalt of Powerline Road (bpr)											
R16DC050	576587	2703937	8/8	Li	53.7°	353.5°	1.7°	1102	7.9937	78.7°	11.2°
Basalt of Al Harrah Al Gharbiyah (bhg)											
R15DC001	559091	2706421	8/8	Mx	(44.7°)	(352.3°)	2.6°	540	7.987	82.8°	326.2°
R15DC002	558440	2706972	8/8	Li	54.7°	342.3°	1.2°	2303	7.997	71.3°	348.6°
R15DC003	560889	2702974	7/8	Mx	55.3°	352.0°	1.9°	1105	6.9946	76.7°	10.3°
R15DC004	560873	2704392	8/8	Mx	54.8°	343.5°	2.4°	558	7.9874	72.1°	350.8°
R15DC005	561890	2703676	8/8	Mx	53.3°	348.2°	2.3°	583	7.988	76.1°	354.8°
R15DC006	559564	2704895	8/8	Mx	58.0°	346.7°	3.2°	322	7.9782	71.9°	4.3°
R15DC051	558390	2701912	7/8	Li	56.2°	349.7°	1.4°	1936	6.9969	74.8°	6.4°
Mean	**559800**	**2704177**	**6/7**		**55.4°**	**347.1°**	**2.2°**	**943**	**5.9947**	**74.0°**	**358.5°**
Basalt of Al Urayd (bur)											
R15JR001	565619	2708178	8/8	Mx	36.0°	352.1°	1.9°	855	7.9918	81.4°	279.5°
R15JR002	566984	2706701	8/8	Mx	37.2°	356.4°	2.5°	511	7.9863	85.0°	262.4°
R15JR003	567036	2708594	8/8	Pl	41.3°	351.7°	16.0°	10	---	82.4°	305.5°
Mean	**566879**	**2707531**	**3/3**		**38.2°**	**353.4°**	**5.3°**	**550**	**2.9964**	**83.2°**	**284.5°**
Basalt of Hathm (bha)											
R16DC006	568968	2705160	7/8	Mx	61.5°	5.9°	2.0°	1067	6.9944	71.2°	53.2°
Basalt of Rahat (brh)											
R16DC022[a]	566460	2695448	7/8	Mx	−13.8°	56.7°	5.9°	123	6.9511	26.5°	151.7°
R16DC025[a]	564475	2696956	8/8	Mx	1.1°	351.4°	2.9°	393	7.9822	64.8°	240.2°
Basalt of Quba (bqu)											
R15DC016	563795	2701659	8/8	Mx	55.6°	17.6°	1.4°	1640	7.9957	70.9°	87.8°
R16DC023	565016	2696294	8/8	Mx	55.9°	12.3°	4.4°	180	7.9612	74.0°	78.0°
Mean	**564386**	**2698661**	**2/2**		**55.8°**	**15.0°**	**6.5°**	**1462**	**1.9993**	**72.5°**	**83.3°**
Basalt of Al Ihn (bai)											
R16DC026	568913	2693710	8/8	Mx	43.4°	350.8°	1.6°	1271	7.9945	81.6°	318.1°
R16DC009	564302	2701639	8/8	Mx	39.8°	349.3°	1.5°	1350	7.9948	80.0°	301.4°
R16DC024	565066	2696361	6/8	Mx	39.7°	352.2°	6.6°	118	5.9577	82.6°	296.8°
Mean	**565912**	**2697560**	**3/3**		**41.0°**	**350.8°**	**3.6°**	**1159**	**2.9983**	**81.5°**	**305.3°**
Basalt of Hill 892 (bh89)											
R16DC036[a]	574379	2690029	8/8	Mx	−57.1°	217.1°	6.4°	85	7.9178	−55.8°	277.8°
Undifferentiated vents (v)											
R16DC003	564614	2699736	6/8	Mx	−35.0°	176.6°	7.7°	107	5.9534	−84.0°	72.0°
R16DC004	566741	2702481	9/9	Mx	45.9°	2.0°	3.6°	234	8.9658	86.6°	71.4°

[a]Indicates excursional analyses.

Results

Geochemistry Interpretation

Major-oxide and trace-element whole-rock compositions employed here are available in Downs and others (2018) and Downs (2019) and are consistent with previously published values of mafic volcanic rocks from Harrat Rahat (Camp and others, 1987; Camp and Roobol, 1989; Murcia and others, 2015, 2017; Dietterich and others, 2018; Stelten and others, 2018). Volcanic rocks within the vicinity of Al Madīnah are dominated by alkalic basalts, and include minor transitional basalts, hawaiites, and one mugearite flow (fig. 6*A*). Basalts with 6 or more weight percent MgO plot within the intraplate field of Pearce and Norry (1979) and continental field of Cabanis and Lecolle (1989) but a few samples plot within the intracontinental rift field of the latter (figs. 6*B–C*). The main purpose of the geochemistry in this chapter was to identify differences among adjacent lava flows to distinguish separate units. Unit chemistries are typically distinct and represent discrete magma batches or more rarely are the result of two magma batches mixing (such as the basalts of Al Labah, Ad Duwaykhilah, Al Huzaym, and An Nughayr).

The whole-rock variations used to distinguish individual units are shown in figure 8. Mapped units range from 45.17 to 49.22 weight percent SiO_2 and 3.66 to 11.47 weight percent MgO (Mg-number [Mg#] values of 35 to 66). Transitional basalts have the most primitive compositions, with MgO values of 8.48 to 11.47 weight percent (Mg# values of 59 to 66). Incompatible major oxides, such as TiO_2, K_2O, and P_2O_5, are especially useful for correlating units as these are not retained within early crystallizing phenocryst phases and their abundances vary considerably over the limited range of SiO_2. For example, K_2O varies by a factor of more than 6 from 0.28 to 1.80 weight percent, P_2O_5 varies by a factor of 13 from 0.14 to 1.82 weight percent, and TiO_2 varies by a factor of 3 from 1.26 to 3.68 weight percent.

Individual eruptive units generally plot in an array indicating concurrent clinopyroxene, olivine, and plagioclase fractionation, along with crystallization of trace phases that can include chromian spinels, Fe-Ti oxides, and (or) apatite depending on the degree of magma evolution. It is common for compositions from each unit to cluster together (fig. 8). The number of mapped units and analyses yield unavoidable overlap, especially for units that have undergone magma mixing. Yet, the combination of geochemistry, petrography, field mapping, and stratigraphic superposition of adjacent units supports the accuracy of mapped contacts. Plotting K_2O/TiO_2 and K_2O/P_2O_5 versus MgO or SiO_2 (analogous to P/K versus Ti/K in fig. 8) yield groupings that aid in distinguishing eruptive units. These elements are not perfectly incompatible over the compositional range discussed here but other incompatible element ratios (Zr/Nb in fig. 8) support map units not being cogenetic, despite some units having experienced pre- and (or) syneruptive magma mixing (basalts of Al Labah, Ad Duwaykhilah, Al Huzaym, and An Nughayr).

Developing a petrogenetic model is not the focus of this study but a few generalizations are made here. Geochemical variations are strongly influenced by the fractionation, crystallization, and accumulation of phenocryst and trace mineral phases. Decreasing Sc and CaO/Al_2O_3 coincide with decreasing MgO, which supports fractionation of a Mg-rich clinopyroxene phase (David and others, 2000; Smith and others, 2008). A lack of clinopyroxene phenocrysts within Harrat Rahat mafic eruptive products indicates that the phenocrysts crystallized and separated at depth, probably near the base of the crust. Similar scenarios of clinopyroxene fractionation have been interpreted at other mafic volcanic fields (for example, Shaw and others, 2003; Smith and others, 2008; McGee and others, 2013; Murcia and others, 2017). Decreasing SiO_2 coincides with decreasing MgO (until MgO falls below 6.5 weight percent), which supports clinopyroxene fractionation stopping after MgO drops below 6.5 weight percent. At this point SiO_2 increases (fig. 8) as olivine and plagioclase become the primary fractionating phases because of either a reduction in pressure or the presence of an amphibole phase. Olivine ± chromian spinel accumulation is indicated in some basalts by high abundances of Ni (129 to 313 ppm) and Cr (144 to 640 ppm), whereas more evolved compositions show variable accumulation of plagioclase from enrichment of Ba and Sr. Chromian spinels within olivine phenocrysts are limited to high-MgO alkalic and transitional basalts. Many chromian spinels have Fe-Ti oxide rims or have been completely transformed to Fe-Ti oxides, especially where situated near olivine rims and (or) fractures in host phenocrysts. Fractionation of Fe-Ti oxides also initiates after MgO drops below 6.5 weight percent, at which point TiO_2 decreases. Apatite crystallization begins in some low MgO alkalic basalts and is present in most hawaiite and mugearite compositions, which is evident below 6.5 weight percent MgO where P_2O_5 increases dramatically.

Geochronology Interpretation

Samples from 16 units were dated by the $^{40}Ar/^{39}Ar$ technique and three by the ^{36}Cl cosmogenic surface-exposure technique. Details for these experiments are outlined in tables 3 and 4, and the $^{40}Ar/^{39}Ar$ age spectra are presented in appendix 1. The $^{40}Ar/^{39}Ar$ eruption ages all conform to the observed stratigraphic position of units as mapped in the field. These ages are described below from the oldest in the early and middle Pleistocene to the youngest Holocene eruption. Tertiary volcanic rocks (Tertiary basalts of Jabal Ayr and Jabal Jammah) that erupted at about 13 Ma (Downs and others, 2019) cap some of the Proterozoic mountains surrounding Al Madīnah as erosional remnants (fig. 4), but these are not discussed further in this chapter.

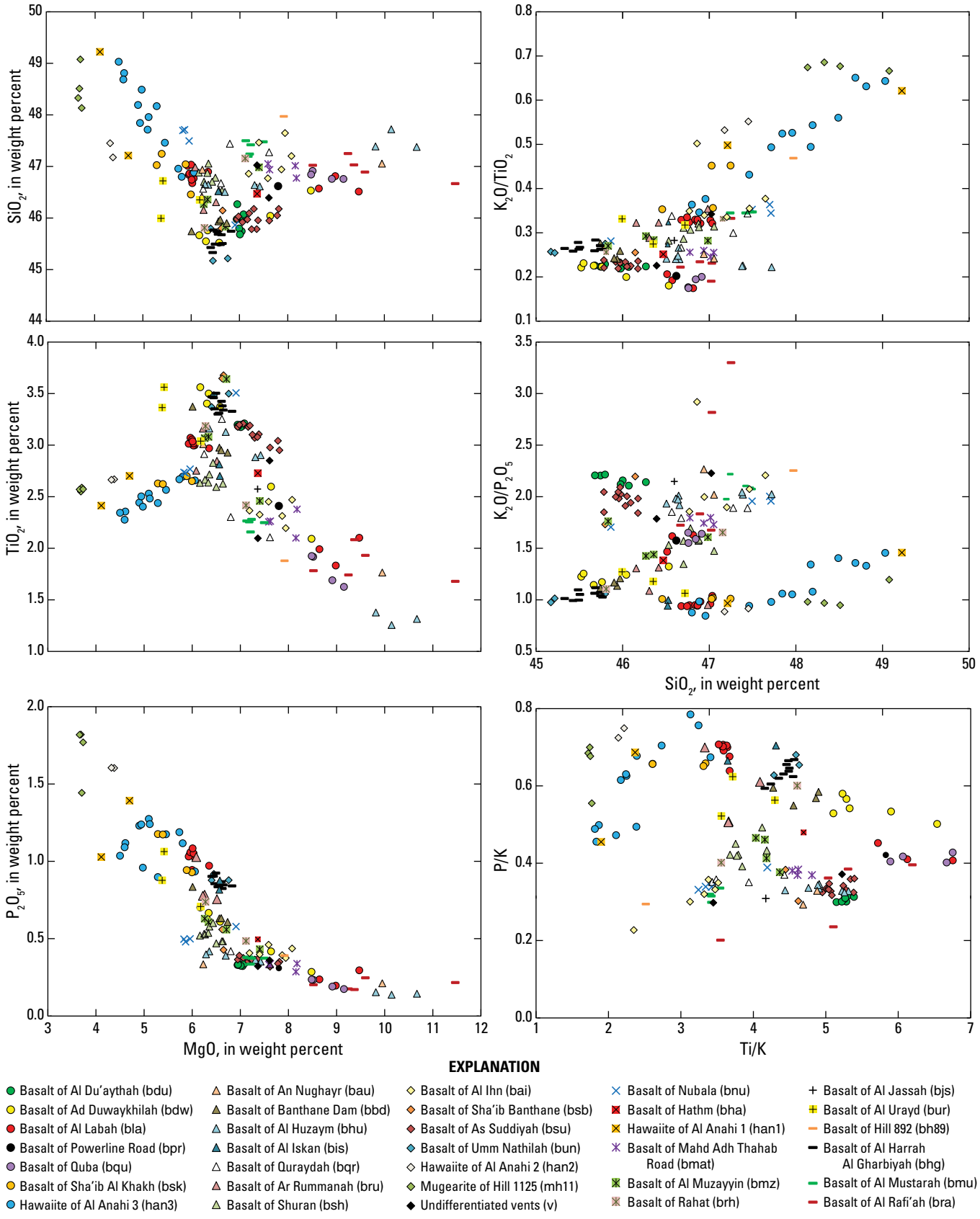

Figure 8 (pages 18–19). Plots of selected whole-rock major oxides, trace elements, Pearce ratios, and incompatible-element ratios. Whole-rock chemical compositions are presented by Downs and others (2018) and Downs (2019). All unit names and symbols from Downs and others (2019) and Robinson and Downs (2023).

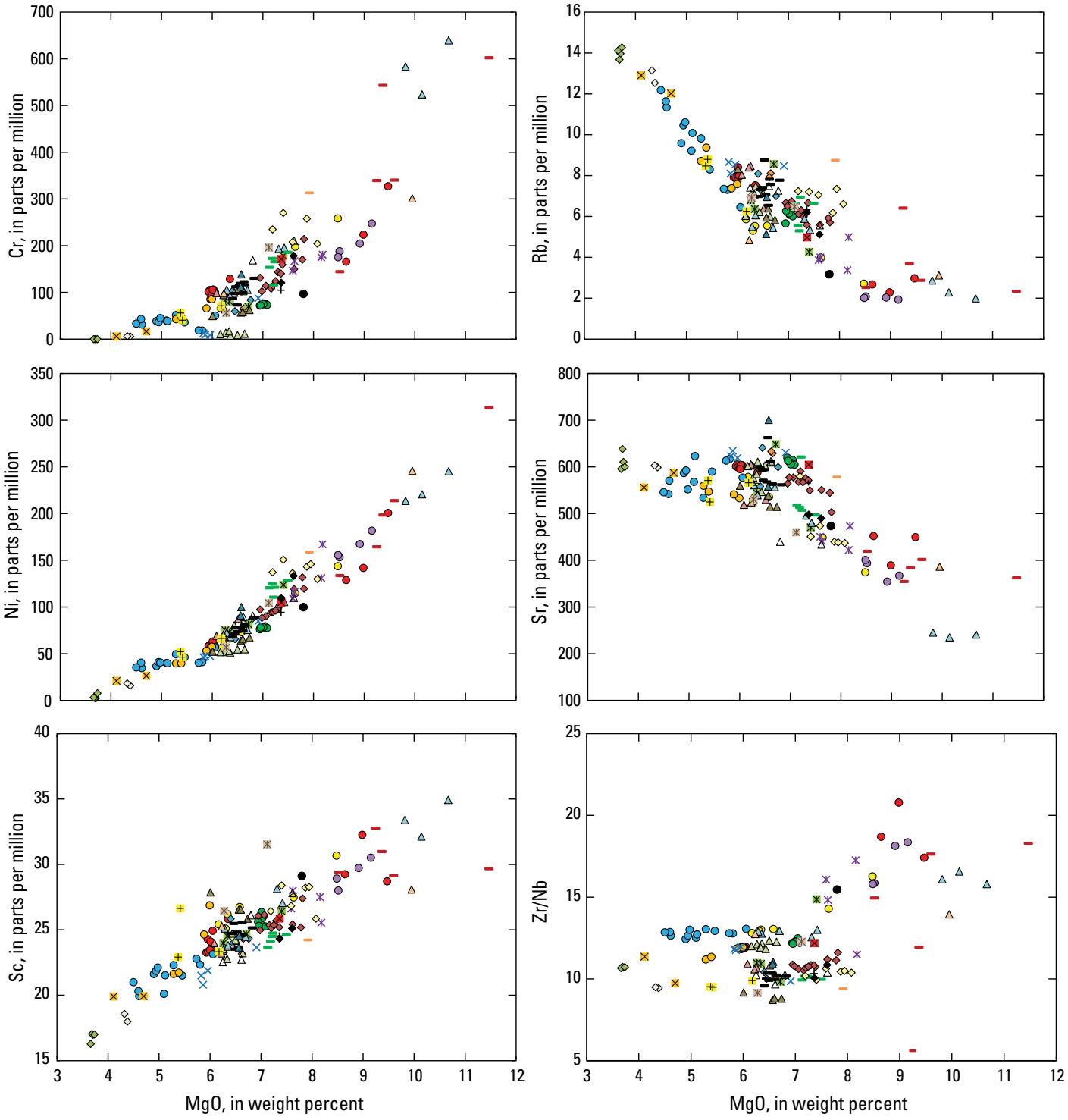

Figure 8 (pages 18–19).—Continued

Table 3. $^{40}Ar/^{39}Ar$ age determinations of Quaternary volcanic rocks from northernmost Harrat Rahat.

[Samples were irradiated at the U.S. Geological Survey TRIGA reactor using 9.7946±0.0033 million-year-old Bodie Hills sanidine as a neutron flux monitor. All samples are groundmass separates. Plateau ages are preferred except where noted. Weighted mean ages are preferred where applicable. Instrumental mass discrimination was calculated by repeated measurement of atmospheric argon. Initially, mass discrimination was calculated assuming atmospheric $^{40}Ar/^{36}Ar$ = 295.5±0.5 (Steiger and Jäger, 1977). In July 2016, the Menlo Park argon laboratory began calculating mass discrimination assuming atmospheric $^{40}Ar/^{36}Ar$ = 298.56±0.31 (Lee and others, 2006). The change in the assumed $^{40}Ar/^{36}Ar$ of atmospheric argon does not result in a bias in ages between the two irradiations, because both monitors and unknowns from each irradiation were calculated in the same manner. Easting and northing coordinates are in the World Geodetic System of 1984 using the Universal Transverse Mercator zone 37 north system. $^{40}Ar/^{36}Ar_i$, $^{40}Ar/^{36}Ar$ isochron intercept. Abbreviations: T, temperature; °C, degree Celsius; ka, kilo-annum; MSWD, mean square of weighted deviates; %, percent]

Sample number	Unit	Easting	Northing	^{39}Ar, in % (T range, in °C)	Plateau		Isochron			Total gas age±1σ (ka)
					Age±1σ (ka)	MSWD	Age±1σ (ka)	MSWD	$^{40}Ar/^{36}Ar_i$±1σ	
R15JR010	Basalt of As Suddiyah	571544	2703271	79 (550–950)	86.8±7.6	1.7	84.2±22.9	2.2	296.0±6.0[a]	112.6±7.5
R16DD200	Basalt of As Suddiyah	569641	2705169	99 (550–1,275)	84.3±8.6	1.4	69.2±13.8	1.3	300.6±1.6[b]	91.0±8.5
Weighted mean	Basalt of As Suddiyah				85.7±5.7					
R15TS155	Basalt of Nubala	569546	2694630	99 (550–1,250)	131.2±8.3	1.5	137.2±13.6	1.6	294.9±0.9[a]	125.3±7.9
R14AC101	Hawaiite of Al Anahi 1	569852	2699714	78 (550–1,000)	139.0±5.4	1.5	143.3±19.5	1.7	294.2±5.1[a]	131.9±5.1
R16DD216	Basalt of Banthane Dam	566681	2697072	62 (550–1,125)	223.4±8.6	0.2	220.4±42.4	0.3	299.0±6.0[b]	253.8±7.4
R15MS039	Basalt of Al Mustarah	564637	2708368	100 (550–1,375)	344.7±4.8	1.0	338.5±6.1	0.7	297.0±0.9[a]	348.4±6.3
R15MS037	Basalt of Al Harrah Al Gharbiyah	561322	2703723	75 (750–1,225)	382.5±5.8	1.2	372.5±19.7	1.3	297.0±2.9[a]	362.5±4.7
R16DD222	Basalt of Rahat	566408	2695456	100 (550–1,400)	411.5±5.9	0.9	409.9±20.8	1.0	298.7±2.9[b]	412.8±6.3
R15TS161	Basalt of Hill 892	574371	2689742	58 (900–1,200)	1,014±14	0.3	988±42	0.2	299.9±2.1[b]	1,018.3±11.7

[a]Mass discrimination was calculated assuming atmospheric $^{40}Ar/^{36}Ar$ = 295.5±0.5 (Steiger and Jäger, 1977).

[b]Mass discrimination was calculated assuming atmospheric $^{40}Ar/^{36}Ar$ = 298.56±0.31 (Lee and others, 2006).

[c]Preferred age is the isochron age.

Table 4. ^{36}Cl cosmogenic surface-exposure ages of Quaternary volcanic rocks from northernmost Harrat Rahat.

[All ^{36}Cl cosmogenic surface-exposure ages were calculated using the CRONUScalc ^{36}Cl Exposure Age Calculator v2.0 (Marrero and others, 2016), and the Lal and Stone time-independent scaling model (Lal, 1991; Stone, 2000). Whole-rock Cl concentrations were measured by isotope dilution at the Purdue Rare Isotope Measurement (PRIME) Laboratory at Purdue University, West Lafayette, Indiana. Easting and northing coordinates are in the World Geodetic System of 1984 using the Universal Transverse Mercator zone 37 north system, and elevations are in meters above sea level (mASL). Abbreviations: cm, centimeter; g/cm^3, gram per cubic centimeter; ka, kilo-annum; SF, topographic shielding factor]

Easting	Northing	Elevation (mASL)	Thickness (cm)	Bulk density (g/cm^3)	SF	^{36}Cl/Cl (×10^{-15}) ±1σ	^{36}Cl atoms/g (×10^5)	^{35}Cl/^{37}Cl ±1σ	^{36}Cl ages ±1σ (ka)
Basalt of Al Labah, sample R14TS097									
577423	2696155	813	2	2.49	1	6.26±0.66	0.16 ±0.25	4.11±0.04	0.81±0.24
Basalt of Al Du'aythah, sample R14AC099									
550287	2700493	680	4	2.05	1	52.4±3.7	1.43±0.11	4.26±0.02	13.3±1.9
Hawaiite of Al Anahi 3, sample R15MS006									
578980	2682169	949	4	1.81	1	196.5±7.6	8.39±0.54	3.79±0.04	51.0±9.0

Early and Middle Pleistocene

The eruptive history of the northernmost part of Harrat Rahat shown in figure 4 starts in the early Pleistocene. The oldest dated Quaternary volcanic unit is a shield volcano that produced the basalt of Hill 892 at 1,014±14 ka (all uncertainties are at one sigma), located 20 km southeast of the city center. This is the only directly dated early Pleistocene eruptive unit within the area of interest for this chapter (fig. 9*A*). The next volcanic unit chronologically, and the oldest radiometrically dated within Al Madīnah itself, is the basalt of Al Ihn at 546.2±9.6 ka. This unit is mapped within the central part of the city, overlain and flanked by younger lava flows. These younger lavas lie to its east and west, forming a shallow valley that contains the center, and oldest part, of Al Madīnah.

The younger lava flows bordering this valley erupted over a period of 90 to 100 thousand years (k.y.), for which five radiometric dates provide age constraints. The oldest is the basalt of Rahat at 411.5±5.9 ka, which is present only as a limited exposure in the southwestern part of the city. Subsequently, the basalt of Al Urayd erupted at 401.8±6.3 ka and is exposed in the northeast part of the city. This was followed by eruption of the basalt of Al Harrah Al Gharbiyah at 382.5±5.8 ka and the basalt of Powerline Road at 378.8±10.0 ka. The former constitutes the western margin for the downtown area, whereas the latter is a kīpuka of small areal extent (0.4 km^2) surrounded by the 1256 C.E. basalt of Al Labah lava flow. The youngest dated unit within this time interval is the basalt of Al Mustarah at 344.7±4.8 ka, which is a lava flow that defines the northeast margin of the downtown area. Several other mapped units (basalts of Quraydah, Al Iskan, and Quba) may fall into this time interval based on their stratigraphic superpositions (among age constrained units) but heavy urbanization precluded obtaining samples suitable for radiometric dating. The basalt of Hathm potentially falls within this time interval as well but it could be much older as it underlies the basalt of Al Urayd at 401.8±6.3 ka and no underlying unit is exposed. As such, the basalt of Hathm could be considerably older than surrounding units but no suitable sample for radiometric dating has been identified.

Only two units have radiometric ages between 300 and 200 ka. The first is the low-lying shield volcano and associated lava flows that compose the basalt of Al Huzaym at 285.1±6.6 ka. Based on a general observation of erosional rills on weakly alkalic and transitional basalt shield volcanoes, Camp and Roobol (1991) previously interpreted this shield volcano to be the oldest volcanic unit in the Al Madīnah area and assigned it to the Hammah basalts, which were proposed to have erupted between 2.5 and 1.7 Ma. However, the basalt of Al Huzaym has been observed overlying the basalt of Al Harrah Al Gharbiyah at 382.5±5.8 ka and underlying the basalt of Shuran at 191.5±4.2 ka (weighted mean of three groundmass ages in table 3), which supports its ^{40}Ar/^{39}Ar age. The basalt of Al Huzaym was followed by eruption of the basalt of Banthane Dam at 223.4±8.6 ka, which is exposed near the south-central part of Al Madīnah. The basalt of Banthane Dam provides a minimum age constraint on the underlying, and undated, basalt of Quraydah and a maximum age constraint on all remaining overlying middle and late Pleistocene eruptive products within the south-central part of Al Madīnah.

The end of the middle Pleistocene was a time of intense volcanic activity with at least nine eruptions emplacing lava flows within the vicinity of present-day Al Madīnah, of which five have been dated. The basalt of Shuran erupted at 191.5±4.2 ka, which provides a maximum age constraint on the overlying, and undated, basalt of Al Jassah. Along the eastern to central part of figure 4 are three basalts with overlapping eruption ages. These are the hawaiite of Al Anahi 1 at 139.0±5.4 ka, basalt of Mahd Adh Thahab Road at 136.7±7.6 ka, and basalt of Nubala at 131.2±8.3 ka. Despite overlapping age uncertainties, they fall within the correct stratigraphic order from oldest to youngest. Additionally, the basalt of Mahd Adh Thahab Road (136.7±7.6 ka) provides minimum age constraints on three underlying and undated units, which share an indirect maximum age constraint from the overlying basalt of Banthane Dam (223.4±8.6 ka). These are the basalts of Al Muzayyin, Ar Rummanah, and Al Rafi'ah. Based on age uncertainties, several of these units may have erupted within the late Pleistocene.

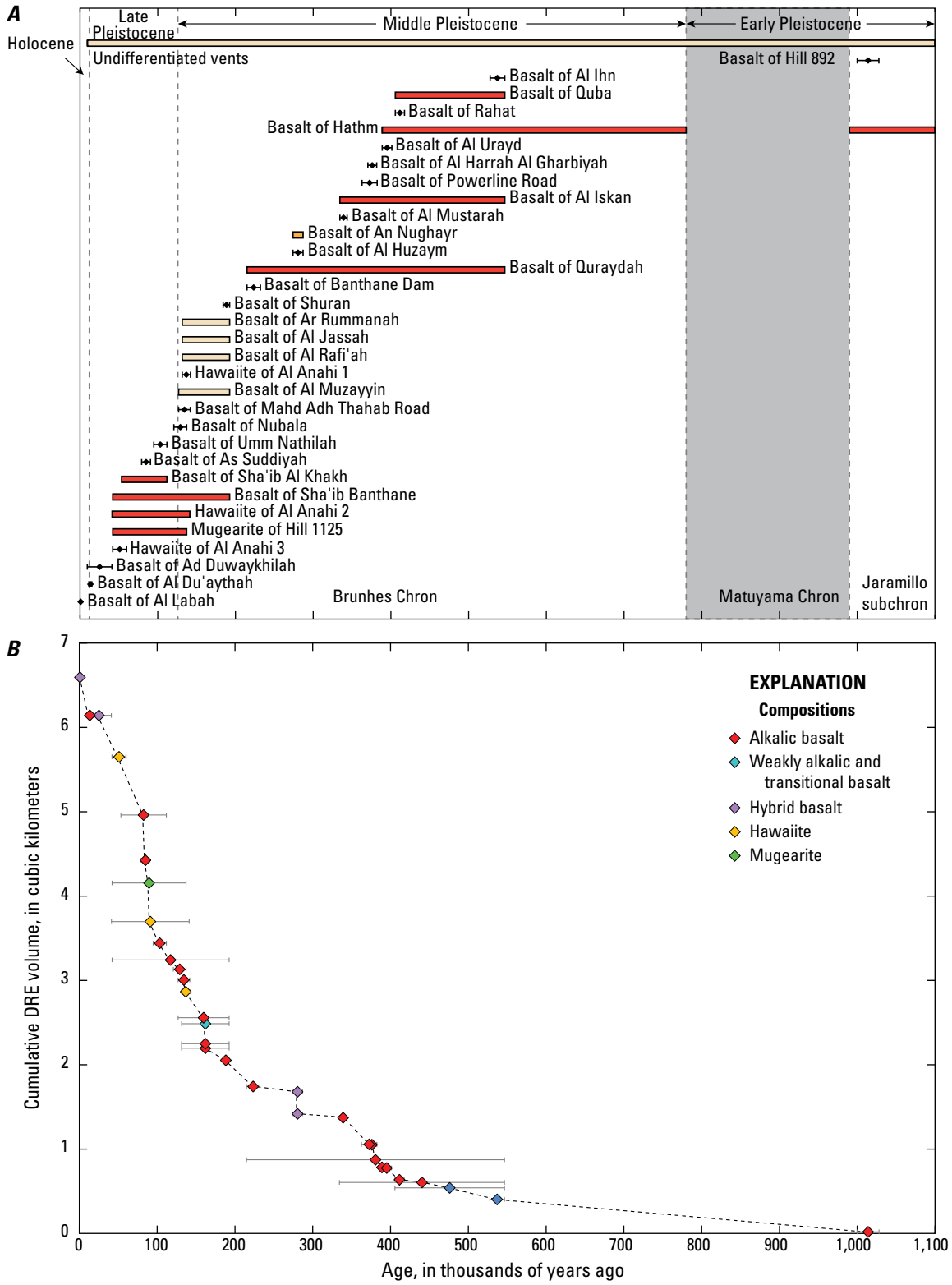

Figure 9. Graphs showing the ages and volume of exposed mafic volcanic units in the northernmost Harrat Rahat. *A*, Black diamonds with solid black error bars show ages and one-sigma analytical uncertainties for units. Units designated with a red bar are stratigraphically constrained, those with a tan bar are both stratigraphically and paleomagnetically constrained, and the one with an orange bar (basalt of An Nughayr) is only paleomagnetically constrained. White areas are normal polarity and gray areas are reverse polarity time intervals. *B*, Eruption ages plotted by cumulative dense rock equivalent (DRE) volumes with symbols denoting compositions and solid gray bars showing analytical uncertainties.

Late Pleistocene

The oldest definitively identified late Pleistocene eruptions produced the basalt of Umm Nathilah at 105.0±8.6 ka, which erupted near the southwestern limits of Al Madīnah. This was followed by an eruption near the eastern city limits of the basalt of As Suddiyah at 85.7±5.7 ka (weighted mean of two groundmass ages in table 3).

The ^{36}Cl cosmogenic surface-exposure dating technique yielded an age of 51.0±9.0 ka on the young-looking, uneroded and rough morphology of the hawaiite of Al Anahi 3 lava flow (table 4). This is significantly younger than the age of 270±60 ka presented by Moufti and others (2013) from a ^{40}Ar/^{39}Ar experiment on a sample from the hawaiite of Al Anahi 3. The young morphology and 51.0±9.0 ka age agree with the stratigraphic position of the hawaiite of Al Anahi 3 overlying the basalt of Nubala (131.2±8.3 ka) and other similar-aged mafic lava flows. This result is further supported by age constraints on surrounding lava flows presented by Downs and others (2019) and Stelten and others (2020). The 51.0±9.0 ka age from the hawaiite of Al Anahi 3 also provides a minimum age constraint on several underlying and undated, but young-looking units. These include the mugearite of Hill 1125, hawaiite of Al Anahi 2, and basalts of Sha'ib Banthane and Sha'ib Al Khakh, which have maximum age constraints from other dated middle and late Pleistocene units. It can be inferred that these undated units all erupted after 100 ka based on their young morphologies and stratigraphic positions.

Younger still, the basalt of Ad Duwaykhilah erupted at 25.6±16.2 ka from a vent near the eastern limit of Al Madīnah. This unit overlies the basalt of As Suddiyah (85.7±5.7 ka) and is overlain by the historical 1256 C.E. basalt of Al Labah lava flow. The large uncertainty allows for a possible Holocene eruption age, however, achieving a more precise age on such a young, low-K_2O sample would be difficult by current ^{40}Ar/^{39}Ar techniques.

During the end of the late Pleistocene four north-northwest aligned scoria cones of the basalt of Al Du'aythah, of which the northern two contain short 115 to 200 m long lava flows, erupted within what is now a western suburb of Al Madīnah. There has been uncertainty over the age of the basalt of Al Du'aythah in the literature. An eruption was suggested for either the year 640 or 641 C.E. based on an unconfirmed historical account from western Saudi Arabia. A brief description in Wafā' Al-Wafā' Bi Akhbār Dār Al-Muṣṭafā by Al-Samhūdī (1488) states that during the reign of the second Rashidi Caliphate of Omar Bin al-Khattab, a small fire rose from Harrat Al Madīnah and soon died out. This prompted Camp and Roobol (1989) to propose that the scoria cones and short lava flows now designated as the basalt of Al Du'aythah were products of the eruption that inspired this historical account. However, these same historical accounts seem to present conflicting locations. Accounts indicate that an earthquake destroyed homes in Al Madīnah in 641 C.E. (Ambraseys and others, 2005) and as a result an eruption was linked to this event. Yet, Ambraseys and others (2005) also suggested that this same earthquake may have been related to either one or two eruptions that occurred in 640 C.E. within Harrat Uwayrid, which is at least 300 km north of Al Madīnah (fig. 1*B*). Adding to the uncertainty is that these accounts were written centuries after the proposed eruption. Therefore, a sample of the basalt of Al Du'aythah was collected for ^{36}Cl cosmogenic surface-exposure dating, which yielded an age of 13.3±1.9 ka (table 4). This unit could have erupted during the late Pleistocene or early Holocene given its analytical uncertainty.

Holocene

The only two confirmed Holocene eruptions of Harrat Rahat were the 1256 C.E. basalt of Al Labah that lies along the present east-southeast city limit of Al Madīnah and the trachyte lava dome and pyroclastic flows of Um Rgaibah at 6.6±2.9 ka (weighted mean of ^{40}Ar/^{39}Ar and ^{36}Cl determinations) situated 55 km south-southeast of Al Madīnah's center (Stelten and others, 2023). The Al Labah eruption produced the best-studied eruptive products anywhere within the volcanic field (Camp and others, 1987; Kawabata and others, 2015; Dietterich and others, 2018). This unit was dated using the ^{36}Cl cosmogenic surface-exposure technique as a test of the method's robustness and an age of 0.8±0.2 ka was calculated (table 4), which matches well with the historically documented age of 0.76 ka.

As summarized by Camp and others (1987), eruption of the basalt of Al Labah initiated after 5 days of increasingly stronger earthquakes felt by the residents of Al Madīnah, on Monday, June 26, 1256 C.E., when a basaltic fissure began erupting 20 km southeast of the city center. In total, this eruption lasted 52 days, ending on Sunday, August 20, 1256 C.E. It formed seven scoria cones along a 2.25 km long fissure vent, which dispersed 0.0077 km^3 of air-fall-tephra deposits as far as 5 km from the vent (Kawabata and others, 2015), and emplaced 0.45 km^3 of lava that flowed as far as 23 km from the vent; it reached to within 8 km of the city center. Historical accounts have been recorded in Wafā' Al-Wafā' Bi Akhbār Dār Al-Muṣṭafā by Al-Samhūdī (1488) and recapitulated by Burton (1893).

Another historical eruption (not including the previously discussed 640 or 641 C.E. eruption) has been proposed at 1292 or 1293 C.E. and continues to be propagated throughout the literature as either possible or certain (Ambraseys and others, 2005; Siebert and others, 2010; Moufti and others, 2013; Murcia and others, 2015, 2017), despite no eruptive products being identified. Vents for three young appearing, minimally eroded lava flows are situated 93 to 115 km south-southeast of Al Madīnah's center (Camp and Roobol, 1991). These flows are undated, lying outside the study area of the joint Saudi Geological Survey and U.S. Geological Survey effort. One or more of these central Harrat Rahat lava flows may have erupted in the Holocene, but the absence of historical accounts, despite common travel between Makkah al Mukarramah and Al Madīnah, casts doubt that any of these eruptions were as recent as 1292 or 1293 C.E. In comparison, the basalt of Al Labah from 1256 C.E. is present

as a distinctively young, vitric, black scoria cone complex, air-fall-tephra deposit, and lava flow with well-preserved textures, which are corroborated by well-documented historical records. An eruption close to Al Madīnah only 37 years after 1256 C.E. would be just as obvious in the field, in aerial and satellite imagery, and documented by the presented geochronology of all young lava flows, particularly since young volcanism was concentrated near the northernmost end of Harrat Rahat, proximal to Al Madīnah, which was already a major regional city at the time.

Paleomagnetic Interpretation

Paleomagnetic directions were used for correlation purposes, with the assumption that each eruptive unit records a single, consistent direction of remanent magnetization acquired during a geologically instantaneous time interval (days, months, or years). This assumption is based on consistencies in petrographic and geochemical characteristics combined with mapped stratigraphic superposition of individual units, and documentation that the basalt of Al Labah erupted over 52 days. Similar integration of geochemical, petrographic, and paleomagnetic studies from other volcanic fields have yielded results consistent with brief eruption durations (Muffler and others, 2011; Deligne and others, 2016). Therefore, it is inferred that none of northern Harrat Rahat's eruptions spanned protracted periods of multiple years to decades.

Most paleomagnetic results from individual units exhibit a single, uniform direction of magnetization. For example, the 1256 C.E. basalt of Al Labah eruption provides an ideal paleomagnetic case study. Three sites were drilled for analysis and all yielded inclination and declination pairs that overlap at 95-percent confidence limits (fig. 10). Similar tight groupings are present for most units in table 2 with the average for each unit displayed in bold. Additionally, a handful of these units are interpreted to have undergone magma mixing prior to eruption, which is shown by their heterogeneous whole-rock compositions, hindering simple chemical correlations among exposures. For example, the basalt of Al Huzaym (285.1±6.6 ka) was previously assigned to two separate age categories by Camp and Roobol (1991). The shield volcano was assigned to the Hammah basalts between 2.5 and 1.7 Ma and the lava flow that forms the northern part of the unit to age category Qm_2 between 1.2 and 0.9 Ma. The shield volcano and lava flow differ in chemical composition and texture, including whole-rock compositions of transitional and alkalic basalts, respectively. Such significant differences would normally impede simple correlations, particularly in an urban environment where constructional morphology of volcanic deposits is largely destroyed and exposures are discontinuous. However, paleomagnetic secular variation from two sites encompassed by the shield volcano and three sites within the lava flows yield the same unique average inclination of 45° and declination of 24° (table 2, fig. 11*A*). Therefore, it is statistically unlikely that these represent two temporally separate eruptions. Moreover, recent demolition of the cone in the middle of the shield volcano has uncovered alkalic basalt similar in composition to the lava flows north of the shield volcano. Thus, paleomagnetic data demonstrate this to have been a single, geologically instantaneous eruption in which an alkalic basalt erupted with lavas flowing north, followed by eruption of a transitional basalt from the same vent, creating the shield volcano, with mixing between disparate magmas pre- and (or) syneruptively.

Integrating field relations, geochemistry, and paleomagnetism can provide insights into geologic mapping but it is also useful to combine paleomagnetic results with geochronology. This permits further age constraints by resolving (1) if an age falls within the broad-scale of a normal or reverse geomagnetic interval, (2) whether an age with its uncertainties fits into a short-duration (typically 2 k.y. or less) excursional time interval, (3) if an undated eruptive unit (or units that are ideally stratigraphically constrained) has an identical or unique mean remanent magnetization direction compared to a unit with an established eruption age, or (4) if a group of stratigraphically constrained eruptive units contain paleomagnetic secular variations defining a path that could plausibly be interpreted as following the usual rates of geomagnetic secular variation on decade to century timescales.

The paleomagnetic results also help to constrain estimates of eruption ages. Several volcanic units have paleomagnetic secular variations considered excursional, which is taken here as any virtual geomagnetic pole with a colatitude greater than 23°. The oldest of these is the basalt of Hill 892 (1,014±14 ka), which is both reverse polarity and excursional. This unit may have been emplaced during the termination of the Jaramillo subchron from 1 Ma to 990 ka (fig. 9*A*). Similarly, a single scoria cone (site R16DC003 in table 2), geographically located between the basalts of Banthane Dam and Al Ihn (fig. 4), is also reverse polarity, indicating that it

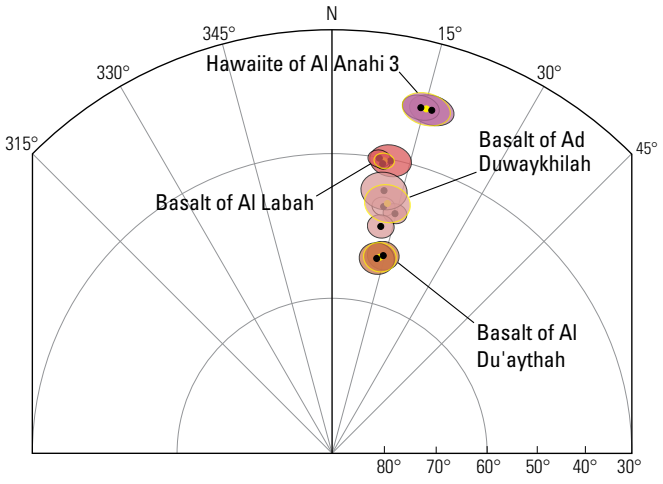

Figure 10. Part of a lower hemisphere equal-area stereographic projection displaying site (black dots and ovals) and unit (yellow dots and ovals) mean directions of remanent magnetization. Ovals display 95 percent confidence of paleomagnetic directions measured on the youngest (50 thousand years ago or younger) units from the northernmost part of Harrat Rahat.

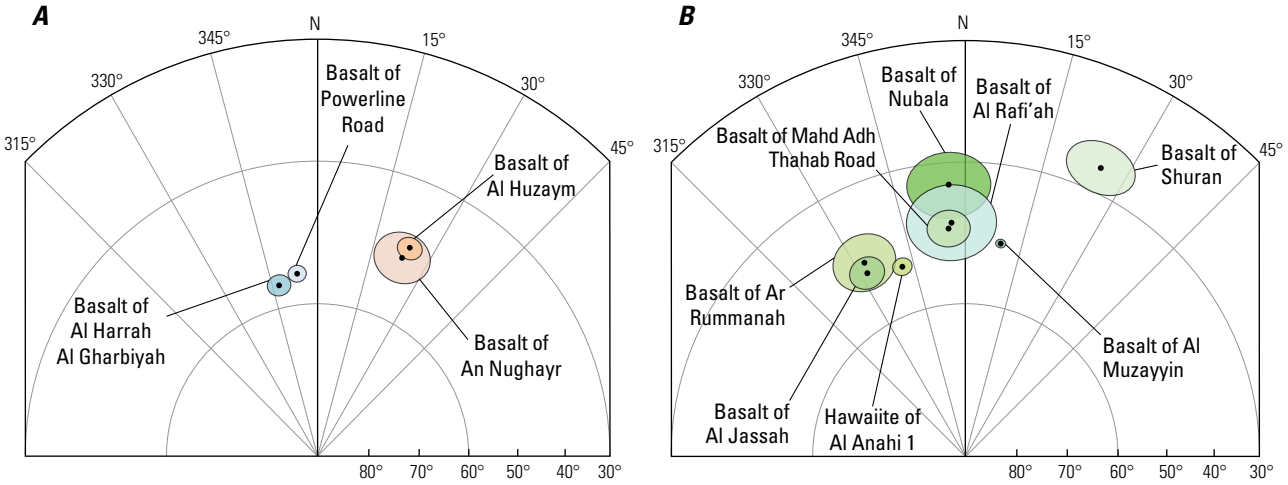

Figure 11. Part of a lower-hemisphere equal-area stereographic projection displaying average unit mean directions of remanent magnetization and ovals at 95 percent confidence of paleomagnetic directions measured. *A,* Basalt of Al Huzaym (285.1±6.6 kilo-annums [ka]) and age equivalent basalt of An Nughayr, and basalt of Al Harrah Al Gharbiyah (382.5±5.8 ka) and temporally similar basalt of Powerline Road (378.8±10.0 ka). *B*, Basalt of Shuran (191.5±4.2 ka), undated basalts of Ar Rummanah and Al Jassah, hawaiite of Al Anahi 1 (139.0±5.4 ka), basalt of Mahd Adh Thahab Road (136.7±7.6 ka), undated basalts of Al Rafi'ah and Al Muzayyin, and basalt of Nubala (131.2±8.3 ka).

likely erupted sometime between 990 and 780 ka during the Matuyama Chron (fig. 9*A*). These are the only reverse polarity volcanic rocks identified within the map area in figure 4 and they are also the oldest. Although normal and reverse time intervals can last for longer than 100 k.y., excursional time intervals typically exist over short durations of 2 k.y. or less and coincide with increased rates of geomagnetic secular variation (Champion and Shoemaker, 1977). Several eruptive units, apart from the basalt of Hill 892, have larger values of paleomagnetic secular variation indicating that they effused during excursional time intervals. Two sites drilled in the basalt of Rahat (411.5±5.9 ka) yield inclinations of −13.8° and 1.1° and declinations of 56.7° and 351.4° (table 2), which is at an appropriate time to coincide with an excursion during the mid-Brunhes Chron (Oda, 2005).

Some mapped eruptive products are separated geographically and are chemically distinct, but cluster together temporally. The basalts of Al Harrah Al Gharbiyah (382.5±5.8 ka) and Powerline Road (378.8±10.0 ka) have overlapping age uncertainties at one sigma, suggesting they share an eruptive time interval on the order of no more than 10 to 20 k.y. Remanent magnetic mean directions for each of these units also overlap and are separated by only 4°, with the basalt of Al Harrah Al Gharbiyah yielding an average inclination of 55° and declination of 347° and the basalt of Powerline Road having an average inclination of 54° and declination of 354° (fig. 11*A*). Based on usual rates of geomagnetic secular variation (Champion and Shoemaker, 1977) these eruptions are interpreted to have been separated by at most a few centuries. Similarly, the basalt of Al Huzaym (285.1±6.6 ka) has a paleomagnetic secular variation with implications for the geochronology of the undated basalt of An Nughayr. The basalt of Al Huzaym has unique paleomagnetic secular variation values that resemble those of the nearby basalt of An Nughayr with an inclination of 47.0° and declination of 23.2° (figs. 9*A*, 11*A*). Therefore, it is inferred that both basalt units erupted within a few decades to centuries of each other at 285.1±6.6 ka.

Multiple eruptions were spatiotemporally clustered as well. One of the most voluminous (1.4 km^3) and well-exposed (138 km^2) groups consists of eight lava flows that are bracketed between the basalt of Shuran at 191.5±4.2 ka and the basalt of Nubala at 131.2±8.3 ka (fig. 11*B*). Half of these eight eruptive units have radiometric ages, which helps to estimate the ages of the remaining undated units. The basalt of Shuran (191.5±4.2 ka) provides a maximum age constraint for the overlying basalt of Al Jassah. Neither of these lava flows is in direct contact with the other six in this time interval. Of the remaining six units, the undated basalt of Ar Rummanah is the stratigraphically lowest, with a maximum age constraint provided by the underlying basalt of Banthane Dam (223.4±8.6 ka). The basalt of Ar Rummanah is overlain by the undated basalt of Al Rafi'ah, which is overlain by the hawaiite of Al Anahi 1 at 139.0±5.4 ka and the undated basalt of Al Muzayyin, both of which are overlain by the basalt of Mahd Adh Thahab Road at 136.7±7.6 ka. The basalt of Nubala (131.2±8.3 ka) directly overlies the basalts of Ar Rummanah, Al Rafi'ah, and Al Muzayyin. Three of the eight units fall within an excursional time interval. These are the basalt of Shuran (191.5±4.2 ka), and the undated basalts of Ar Rummanah and Al Jassah. The basalt of Shuran falls into a time interval commonly referred to as the Iceland Basin excursion (Oda, 2005), whereas the undated basalts of Ar Rummanah and Al Jassah have similar paleomagnetic directions (inclinations of 46.3° and 48.5°, declinations of 332.4° and 331.8°, respectively), indicating that they were also erupted during an excursional time interval (fig. 11*B*). The excursional nature of these two units narrows the time

interval during which the basalts of Ar Rummanah and Al Jassah erupted (1) during the Iceland Basin excursion but after eruption of the basalt of Shuran (191.5±4.2 ka) when the geomagnetic field had sufficient time to move to a different direction or (2) a subsequent excursion younger than the Iceland Basin event but older than 139 ka, as constrained by the overlying hawaiite of Al Anahi 3 at 139.0±5.4 ka. Of the remaining five lava units, the hawaiite of Al Anahi 1 (139.0±5.4 ka) does not match the remanent magnetization of any other, which indicates that it does not cluster temporally with the rest of the group (fig. 11*B*). However, the basalts of Mahd Adh Thahab Road at 136.7±7.6 ka and Nubala at 131.2±8.3 ka, and the undated basalts of Al Rafi'ah and Al Muzayyin, form a closely spaced array using their average paleomagnetic remanent directions (fig. 11*B*). It is therefore suggested that these basaltic lava flows erupted over a relatively narrow time interval of 200 to 500 years based on usual rates of geomagnetic secular variation (Champion and Shoemaker, 1977).

Discussion

Eruption ages indicate that volcanism near the present-day site of Al Madīnah spanned from at least 1,014±14 ka to the historical eruption at 1256 C.E., based on exposed volcanic rocks. Products of any earlier volcanism, if present, are concealed in the subsurface beneath younger lava flows. Only a few exposed units are older than 500 ka, which include the basalt of Hill 892 (1,014±14 ka), a reverse polarity scoria cone with no exposed lava flow, the basalt of Al Ihn (546.2±9.6 ka), and potentially the undated basalt of Hathm lava flow (figs. 4, 9*A*). Near complete coverage of the study area by volcanic rocks younger than 500 ka precludes estimates of changes in eruption rate and volcanic flux prior to that time (fig. 9*B*). Ten scoria cones are shown in figure 4 that lack correlative lava flows and a similar number of lava flows lack identified scoria cones. Additionally, the thickness of volcanic strata throughout this small map area has yet to be determined. Aeromagnetic data collected at greater than 1 km resolution (Blank and Sadek, 1983) was used to create an isopach map of Harrat Rahat by Camp and Roobol (1989), which suggests that most of the area around Al Madīnah is covered by a pile of lavas less than 100 m thick, although parts may attain thicknesses as much as 200 m. Langenheim and others (2019, 2023) also calculate the depth to Precambrian basement in the area surrounding central Al Madīnah as less than 100 m based on a high-resolution gravity survey. Low-density materials above the basement consist of Harrat Rahat volcanic rocks and possible underlying sediments, which thicken to the south where there is greater constructional volcanic relief. The thickness of lavas at the far northern edge of Harrat Rahat are regarded as relatively thin (presumably only a single flow at 10 to 15 m thickness) compared to farther south (potentially thicker than 300 m in areas; Langenheim and others, 2019, 2023). Since most of the individual mafic lava flows are relatively thin (10 m thick, typically), there could be a significant thickness of older lava flows buried beneath parts of the map area creating a thick lava pile. This is particularly relevant along the southern and eastern limits of figure 4, where most units erupted from the main vent axis (fig. 2). The number of eruptions from northernmost Harrat Rahat could be 30 percent greater than quantified by mapping and dating exposed volcanic rocks. Any older, concealed eruptive products would likely have vented before 500 ka and consist mainly of alkalic or transitional basalts based on a general lack of more evolved hawaiite or mugearite compositions before that time (fig. 9*B*). Runge and others (2014) suggest that only a third of vents currently remain exposed within Harrat Rahat but this number seems unlikely within the smaller map area of figure 4 as it is the young leading edge of the volcanic field where much of the volcanic strata is a single lava flow thick and it is predominantly away from the main volcanic axis.

Integrated paleomagnetic data and geochronology demonstrate that some of these eruptions were temporally clustered. Ages of the basalts of Al Harrah Al Gharbiyah (382.5±5.8 ka) and Powerline Road (378.8±10.0 ka) coincide within analytical uncertainty and their mean remanent magnetic directions indicate that they erupted no more than a few centuries apart. Although these units crop out only 14 km apart, their aerial distributions along the east (basalt of Powerline Road) and west (basalt of Al Harrah Al Gharbiyah) flanks of the map area of figure 4 make it impossible for them to have vented from the same location. Furthermore, differences in major-oxide and trace-element abundances and petrography indicate that these were separate, distinct magma batches that erupted within a brief time. Additionally, some eruptions are spatiotemporally clustered. The basalts of Al Huzaym and An Nughayr are both interpreted to have erupted over a short duration at 285.1±6.6 ka, based on nearly identical and unique paleomagnetic variations and chemical similarities. These attributes are interpreted to represent derivation from the same mixed magma batch, of which a small volume that formed the basalt of An Nughayr is inferred to have split off from the larger volume basalt of Al Huzaym magmatic dike during ascent and erupted from a scoria cone 2 km away.

Mafic volcanic fields are generally constructed from multiple adjacent and (or) overlapping monogenetic eruptions, wherein a single magma batch erupts once from each vent (Wood, 1979), albeit in many cases closely spaced. Although each vent within the map area is interpreted to have erupted only once, some of their products encompass a variety of petrographic and geochemical characteristics that indicate multiple magma sources having mixed pre- and (or) syneruptively. In addition to the basalts of Al Huzaym and An Nughayr, the basalts of Al Labah and Ad Duwaykhilah also consist of lava flows and scoria cones with diverse petrographic and geochemical traits. The basalts of Al Labah and Ad Duwaykhilah are more chemically heterogeneous than other mafic eruptive products. Each unit for which magma mixing is inferred has two clear end-member compositions and typically a third hybrid composition between these end members (Camp and others, 1987; Murcia and others,

2017). End members are typically alkalic and weakly alkalic, or in some cases transitional, basalts. Besides significant geochemical diversity, compositions from both Camp and others (1987) and Downs and others (2018) yield linear trends for incompatible-element ratios that indicate mixing and contain heterogeneous phenocryst assemblages of olivine ± plagioclase with disequilibrium textures.

Other researchers reject magma mixing and attribute geochemical and petrographic differences to tapping of a vertically differentiating magma column (Murcia and others, 2017). However, Moufti and others (2012) showed that trace element plots (Nd/Sm versus Nd and La/Yb versus La) have convex trends that indicate magmas came from different source regions and (or) have undergone variable degrees of fractionation and mixing. If crystal fractionation were the exclusive process occurring, these trace-element plots would display linear trends (Hofmann and Feigenson, 1983; Weinstein and others, 2006). Magma mixing has been implicated at small-volume mafic volcanic fields within western Saudi Arabia and around the world using geochemical and petrographic data (for example, Camp and others, 1987, 1991, 1992; Camp and Roobol, 1989; Shaw and others, 2003; McGee and others, 2012, 2013; Moufti and others, 2012).

Vent Alignments and Magma Ascent

Volcanic eruptions are a manifestation of magma ascent through the crust, within the upper crust mainly, and in some cases though the entire crust, as dikes. Eruptions may occur as single or clustered events, but the role of tectonism in diking events remains enigmatic. Eruptive vents are aligned in many volcanic fields, which is typically inferred to be related to coupled magmatic, volcanic, and tectonic processes (Connor and Conway, 2000; Valentine and Krogh, 2006; Gaffney and others, 2007; Muffler and others, 2011; Runge and others, 2016). Tectonic extension has been invoked for Harrat Rahat (Camp and Roobol, 1989, 1992) but only one fault (trending N. 10° W.) with 10 m or less displacement has been mapped in the northern third of the volcanic field, and several 1- to 3-m-wide ground cracks with similar orientations cut some basalts (Downs and others, 2019; Robinson and Downs, 2023). High-resolution lidar topography shows no offsets in Quaternary alluvium adjacent to the volcanic field. The absence of young faults contrasts remarkably with Camp and Roobol (1989, 1991) and their depiction of faults and (or) fractures cutting volcanic rocks in a large range of orientations. Upon closer inspection, both in the field and using lidar, aerial, and satellite imagery, almost all the proposed faults and (or) fractures mapped by Camp and Roobol (1989, 1991) coincide with natural drainage channels within and at the margins of lava flows.

Most notable within the central part of northern Harrat Rahat is the high-standing alignment of vents (scoria cones, domes, and craters) of the main vent axis (fig. 2). Scoria cones in the map area of figure 4, as well as throughout Harrat Rahat, are broadly aligned with both the main vent axis and Red Sea rift with orientations of about N. 30° W. Figure 4 encompasses both elongate scoria cones, along with aligned craters and (or) cones from individual eruptions, which are the result of fissure eruptions that can have surface manifestations greater than 2 km long. These vents are oriented between N. 16° W. and N. 33° W., with an average alignment of N. 20° W., including the seven cones and craters of the 1256 C.E. basalt of Al Labah eruption that stretch 2.25 km and have an orientation of N. 30° W. These vent alignments are used to infer the presence and orientation of subsurface structures that dikes used to transect the crust and are interpreted as local strain markers. This is supported by vent alignments for individual eruptions and the overall main vent axis being broadly parallel to faulting within surrounding Tertiary volcanic rocks and Proterozoic rocks (Pellaton, 1981). Camp and Roobol (1992) invoke left-lateral movement across the Makkah-Madīnah-Nafud volcanic line to explain the right stepping en echelon pattern of main vent axes throughout Harrat Rahat. Such an explanation could be invoked on a small-scale for individual vents themselves throughout Harrats Rahat, Khaybar, Ithnayn, and Kurá (fig. 1).

Transporting small-volume magmas through the crust by development and propagation of fractures is necessary, but the state of stress in the crust is important in influencing propagation and dike ascent (Shaw, 1980; Lister, 1990; Lister and Kerr, 1991). Rapid transport would be required to prevent stalling and solidification within the thick (40 km) Proterozoic crust beneath Harrat Rahat. Buoyancy-driven magmatic fracturing in an extensional stress field would assist magma ascent to the surface without stalling (Takada, 1989; Spence and Turcotte, 1990). Volatile assisted eruption is shown for explosive components of the 1256 C.E. basalt of Al Labah eruption that included fire fountaining to heights of 500 to 1,000 m (Kawabata and others, 2015). In some instances, boiling and incorporation of groundwater dominated eruption explosivity, as some units include phreatomagmatic eruption products (for example, the basalt of Al Du'aythah in Murcia and others, 2015). Episodes of volcanic activity could have been tied to stress changes in the crust, including periods of elevated extension and (or) a lithostatic response caused by Afar-plume-related erosion at the base of the lithosphere (Elkins-Tanton, 2007; Wang and others, 2015; Konrad and others, 2016). An alternative cause would be forced dike injection resulting from accumulation of magma in the deep crust or upper mantle leading to high overpressures (Rubin, 1995; Traversa and others, 2010). This would account for the lack of regional northward-trending Cenozoic crustal stress indicators beyond the limits of the volcanic fields associated with the Makkah-Madīnah-Nafud volcanic line.

Conclusions

The northernmost part of the Harrat Rahat volcanic field consists of small-volume mafic lava flows and their source vents with compositions ranging from alkalic and transitional basalt to hawaiite and mugearite. In total, 33 distinct, mafic eruptive units have been mapped underlying and surrounding the city of Al Madīnah based on integrated field relations,

geochemistry, paleomagnetism, eruption ages, digital topography, and aerial and satellite imagery. Both geochemical and paleomagnetic analyses confirm the validity of the contacts for the 33 mapped units. Although mapped lava flows range from smaller than 1 to 23 km long, typical lava flows are approximately 10 to 15 km long (average of 13.5 km), 1 to 3 km wide, and 10 m thick. Geochemical variations indicate fractionation, predominantly of clinopyroxene, olivine (± chromian spinel), and plagioclase. Measured eruption ages accord with observed stratigraphic superposition, with eruptive products ranging in age from at least 1 Ma to the most recent eruption in 1256 C.E. Contrary to prior investigations, the only confirmed Holocene eruption near Al Madīnah produced the vent complex and lava flow of the basalt of Al Labah, with the next youngest proximal unit being the four scoria cones in the southwestern suburbs that erupted at 13.3±1.9 ka (basalt of Al Du'aythah). Major times of lava flow emplacement close to, or within, the present-day site of Al Madīnah were between 400 and 340 ka and 180 and 100 ka. Radiometric ages coupled with paleomagnetic directions indicate that several eruptions were clustered over relatively short intervals. The basalts of Al Harrah Al Gharbiyah at 382.5±5.8 ka and Powerline Road at 378.8±10.0 ka are interpreted to have erupted only a few hundred years apart, whereas the basalts of Al Huzaym and An Nughayr are both interpreted to have erupted at 285.1±6.6 ka from the same magma batch. Similarly, four units (basalts of Al Rafi'ah, Al Muzayyin, Mahd Adh Thahab Road, and Nubala) are proposed to have erupted over at most a few centuries based on stratigraphic superposition, overlapping eruption ages, and similarities in paleomagnetic analyses that can be explained through normal rates of geomagnetic secular variation. The relatively primitive nature of these erupted magmas argues against appreciable assimilation of crustal rocks or the existence of a sizeable, long-lived crustal magma reservoir; however, the mixing of magmas pre- and (or) syneruptively occasionally occurs. These magmas are inferred to follow middle to upper crustal structures during ascent to the surface, as shown by northwest to north-trending alignments of scoria cones, craters, and fissure vents. This is consistent with an extensional system along the Makkah-Madīnah-Nafud volcanic line caused by far-field plate motions or by flexure of the lithosphere (Calvert and Sisson, 2023) uplifted by loss of its deep lithospheric root related to the Afar plume. Accumulation of magma near the base of the crust, leading to high magma overpressures, may account for periods of greater eruption frequency and flux.

Acknowledgments

This research was funded by the Saudi Geological Survey through a technical cooperative agreement between the Saudi Geological Survey and the U.S. Geological Survey. David Sherrod, Thomas Sisson, Andrew Calvert, Joel Robinson, and Tim Orr of the U.S. Geological Survey, and Fawaz Muquyyim, Mahmod Ashur, and many other Saudi Geological Survey employees are thanked for help with field work. Support for the $^{40}Ar/^{39}Ar$ dating was provided by the hard work of James Saburomaru, Dean Miller, Katie Sullivan, and Brandon Swanson of the U.S. Geological Survey. Reviews by David Damby and Joel Robinson that helped improve this chapter are appreciated.

References Cited

Abdelwahed, M.F., El-Masry, N., Moufti, M.R., Kenedi, C.L., Zhao, D., Zahran, H., and Shawali, J., 2016, Imaging of magma intrusions beneath Harrat Al-Madinah in Saudi Arabia: Journal of Asian Earth Sciences, v. 120, p. 17–28, https://doi.org/10.1016/j.jseaes.2016.01.023.

Al-Samhūdī, A.B.A.A., 1488 [edited and reprinted in 2001], Wafā' Al-Wafā' Bi Akhbār Dār Al-Muṣṭafā: London, Al-Furqān Islamic Heritage Foundation, 2,615 p.

Ambraseys, N.N., Melville, C.P., and Adams, R.D., 2005, The seismicity of Egypt, Arabia and the Red Sea—A historical review: Cambridge, United Kingdom, Cambridge University Press, 204 p., https://doi.org/10.1017/CBO9780511524912.

Blank, H.R., and Sadek, H.S., 1983, Spectral analysis of the 1976 aeromagnetic survey of Harrat Rahat, Kingdom of Saudi Arabia: U.S. Geological Survey Open-File Report 83–640, 29 p., https://doi.org/10.3133/ofr83640.

Burton, R.F., 1893, Personal narrative of a pilgrimage to Al Madinah and Maccah: New York City, New York, Dover Publications, 959 p.

Cabanis, B., and Lecolle, M., 1989, Le diagramme La/10-Y/15-Nb/8—Un outil pour la discrimination des series volcaniques et lamise en evidence des processus demelange et/ou de contamination crustale: Compte Rendus de I'Académie des Sciences Series II, v. 309, p. 2023–2029.

Calvert, A.T., and Sisson, T.W., 2023, Cenozoic tectonics of the western Arabia Plate related to harrat magmatism near Al Madīnah, Kingdom of Saudi Arabia, chap. B *of* Sisson, T.W., Calvert, A.T., and Mooney, W.D., eds., Active volcanism on the Arabian Shield—Geology, volcanology, and geophysics of northern Harrat Rahat and vicinity, Kingdom of Saudi Arabia: U.S. Geological Survey Professional Paper 1862 [also released as Saudi Geological Survey Special Report SGS–SP–2021–1], 28 p., https://doi.org/10.3133/pp1862B.

Camp, V.E., Hooper, P.R., Roobol, M.J., and White, D.L., 1987, The Madinah eruption, Saudi Arabia—Magma mixing and simultaneous extrusion of three basaltic chemical types: Bulletin of Volcanology, v. 49, p. 498–508, https://doi.org/10.1007/BF01245475.

Camp, V.E., and Roobol, M.J., 1989, The Arabian continental alkali basalt province—Part I. Evolution of Harrat Rahat, Kingdom of Saudi Arabia: Geological Society of America Bulletin, v. 101, p. 71–95, https://doi.org/10.1130/0016-7606(1989)101%3C0071:TACABP%3E2.3.CO;2.

Camp, V.E., and Roobol, M.J., 1991, Geologic map of the Cenozoic lava field of Harrat Rahat, Kingdom of Saudi Arabia: Saudi Arabian Deputy Ministry for Mineral Resources Geoscience Map GM-123, scale 1:250,000, 37 p.

Camp, V.E., and Roobol, M.J., 1992, Upwelling asthenosphere beneath western Arabia and its regional implications: Journal of Geophysical Research, v. 97, p. 15255–15271, https://doi.org/10.1029/92JB00943.

Camp, V.E., Roobol, M.J., and Hooper, P.R., 1991, The Arabian continental alkali basalt province; Part II—Evolution of Harrats Khaybar, Ithnayn, and Kura, Kingdom of Saudi Arabia: Geological Society of America Bulletin, v. 103, p. 363–391, https://doi.org/10.1130/0016-7606(1991)103%3C0363:TACABP%3E2.3.CO;2.

Camp, V.E., Roobol, M.J., and Hooper, P.R., 1992, The Arabian continental alkali basalt province; Part III—Evolution of Harrat Kishb, Kingdom of Saudi Arabia: Geological Society of America Bulletin, v. 104, p. 379–396, https://doi.org/10.1130/0016-7606(1992)104%3C0379:TACABP%3E2.3.CO;2.

Champion, D.E., and Shoemaker, E.M., 1977, Paleomagnetic evidence for episodic volcanism on the Snake River Plain, *in* Greeley, R., and Black, D., eds., Planetary Geology Field Conference on the Snake River Plain, Idaho, October 1977: NASA Technical Memorandum 78436, p. 7–9.

Coleman, R.G., Gregory, R.T., and Brown, G.F., 1983, Cenozoic volcanic rocks of Saudi Arabia: U.S. Geological Survey Open-File Report 83–788, 82 p., https://doi.org/10.3133/ofr83788.

Condit, C.D., and Connor, C.B., 1996, Recurrence rates of volcanism in basaltic volcanic fields—An example from the Springerville volcanic field, Arizona: Geological Society of America Bulletin, v. 108, p. 1225–1241, https://doi.org/10.1130/0016-7606(1996)108%3C1225:RROVIB%3E2.3.CO;2.

Connor, C.B., and Conway, F.M., 2000, Basaltic volcanic fields, *in* Sigurdsson, H., Houghton, B., Rymer, H., Stix, J., and McNutt, S., eds., The Encyclopedia of Volcanoes (1st ed.): San Diego, California, Academic Press, p. 331–343.

Conway, F.M., Ferrill, D.A., Hall, C.M., Morris, A.P., Stamatakos, J.A., Connor, C.B., Halliday, A.N., and Condit, C., 1997, Timing of basaltic volcanism along the Mesa Butte fault in the San Francisco volcanic field, Arizona, from $^{40}Ar/^{39}Ar$ dates—Implications for longevity of cinder cone alignments: Journal of Geophysical Research, v. 102, p. 815–824, https://doi.org/10.1029/96JB02853.

Cox, K.G., Bell, J.D., and Pankhurst, R.J., 1979, The interpretation of igneous rocks: London, United Kingdom, George Allen and Unwin, 450 p.

Crosweller, H.S., Arora, B., Brown, S.K., Cottrell, E., Deligne, N.I., Guerrero, N.O., Hobbs, L., Kiyosugi, K., Loughlin, S.C., Lowndes, J., Nayembil, M., Siebert, L., Sparks, R.S.J., Takarada, S., and Venzke, E., 2012, Global database on large magnitude explosive volcanic eruptions (LaMEVE): Journal of Applied Volcanology, v. 1, p. 1–13, https://doi.org/10.1186/2191-5040-1-4.

Dalrymple, G.B., Alexander, E.C., Jr., Lanphere, M.A., and Kraker, G.P., 1981, Irradiation of samples for $^{40}Ar/^{39}Ar$ dating using the Geological Survey TRIGA reactor: U.S. Geological Survey Professional Paper 1176, 55 p., https://doi.org/10.3133/pp1176.

David, K., Schiano, P., and Allègre, C.J., 2000, Assessment of the Zr/Hf fractionation in oceanic basalts and continental materials during petrogenetic processes: Earth and Planetary Science Letters, v. 178, p. 285–301, https://doi.org/10.1016/S0012-821X(00)00088-1.

Deligne, N.I., Conrey, R.M., Cashman, K.V., Champion, D.E., and Amidon, W.H., 2016, Holocene volcanism of the upper McKenzie River catchment, central Oregon Cascades, USA: Geological Society of America Bulletin, v. 128, p. 1618–1635, https://doi.org/10.1130/B31405.1.

de Silva, S., and Lindsay, J.M., 2015, Primary volcanic landforms, *in* Sigurdsson, H., Houghton, B., McNutt, S., Rymer, H., and Stix, J., eds., The Encyclopedia of Volcanoes (2d ed.): San Diego, California, Academic Press, p. 273–297, https://doi.org/10.1016/B978-0-12-385938-9.00015-8.

Desilets, D., Zreda, M., Almasi, P.F., and Elmore, D., 2006, Determination of cosmogenic ^{36}Cl in rocks by isotope dilution—Innovations, validation and error propagation: Chemical Geology, v. 233, p. 185–195, https://doi.org/10.1016/j.chemgeo.2006.03.001.

Dietterich, H.R., Downs, D.T., Stelten, M.E., and Zahran, H., 2018, Reconstructing lava flow emplacement histories with rheological and morphological analyses—The Harrat Rahat volcanic field, Kingdom of Saudi Arabia: Bulletin of Volcanology, v. 80, no. 85, https://doi.org/10.1007/s00445-018-1259-4.

Downs, D.T., 2019, Major and trace-element chemical analyses of rocks from the northern Harrat Rahat volcanic field and surrounding area, Kingdom of Saudi Arabia: U.S. Geological Survey data release, https://doi.org/10.5066/P91HL91C.

Downs, D.T., Robinson, J.E., Stelten, M.E., Champion, D.E., Dietterich, H.R., Sisson, T.W., Zahran, H., Hassan, K., and Shawali, J., 2019, Geologic map of the northern Harrat Rahat volcanic field, Kingdom of Saudi Arabia: U.S. Geological Survey Scientific Investigations Map 3428 [also released as Saudi Geological Survey Special Report SGS–SP–2019–2], 65 p., 4 sheets, scales 1:75,000, 1:25,000, https://doi.org/10.3133/sim3428.

Downs, D.T., Stelten, M.E., Champion, D.E., Dietterich, H.R., Nawab, Z., Zahran, H., Hassan, K., and Shawali, J., 2018, Volcanic history of the northernmost part of the Harrat Rahat volcanic field, Saudi Arabia: Geosphere, v. 14, no. 3, p. 1253–1282, https://doi.org/10.1130/GES01625.1.

Downs, D.T., Stelten, M.E., Dietterich, H.R., Champion, D.E., Mahood, G.A., Sisson, T.W., Calvert, A.T., and Shawali, J., 2023, Explosive trachyte eruptions from the Al Efairia volcanic center in northern Harrat Rahat, Kingdom of Saudi Arabia, chap. G *of* Sisson, T.W., Calvert, A.T., and Mooney, W.D., eds., Active volcanism on the Arabian Shield—Geology, volcanology, and geophysics of northern Harrat Rahat and vicinity, Kingdom of Saudi Arabia: U.S. Geological Survey Professional Paper 1862 [also released as Saudi Geological Survey Special Report SGS–SP–2021–1], 14 p., https://doi.org/10.3133/pp1862G.

Duncan, R.A., and Al-Amri, A.M., 2013, Timing and composition of volcanic activity at Harrat Lunayyir, western Saudi Arabia: Journal of Volcanology and Geothermal Research, v. 260, p. 103–116, https://doi.org/10.1016/j.jvolgeores.2013.05.006.

Duncan, R.A., Kent, A.J.R., Thornber, C.R., Schlieder, T.D., and Al-Amri, A.M., 2016, Timing and composition of continental volcanism at Harrat Hutaymah, western Saudi Arabia: Journal of Volcanology and Geothermal Research, v. 313, p. 1–14, https://doi.org/10.1016/j.jvolgeores.2016.01.010.

Elkins-Tanton, L., 2007, Continental magmatism, volatile recycling and a heterogeneous mantle caused by lithospheric gravitational instabilities: Journal of Geophysical Research, v. 112, 13 p., https://doi.org/10.1029/2005JB004072.

Fleck, R.J., Calvert, A.T., Coble, M.A., Wooden, J.L., Hodges, K., Hayden, L.A., van Soest, M.C., du Bray, E.A., and John, D.A., 2019, Characterization of the rhyolite of Bodie Hills and $^{40}Ar/^{39}Ar$ intercalibration with Ar mineral standards: Chemical Geology, v. 525, p. 282–302, https://doi.org/10.1016/j.chemgeo.2019.07.022.

Gaffney, E.S., Damjanac, B., and Valentine, G.A., 2007, Localization of volcanic activity—2. Effects of preexisting structure: Earth and Planetary Science Letters, v. 263, p. 323–338, https://doi.org/10.1016/j.epsl.2007.09.002.

Gosse, J.C., and Phillips, F.M., 2001, Terrestrial in situ cosmogenic nuclides—Theory and application: Quaternary Science Reviews, v. 20, p. 1475–1560, https://doi.org/10.1016/S0277-3791(00)00171-2.

Hofmann, A.W., and Feigenson, M.D., 1983, Case studies on the origin of basalt—1. Theory and reassessment of Grenada basalts: Contributions to Mineralogy and Petrology, v. 84, p. 382–389, https://doi.org/10.1007/BF01160289.

Irvine, T.N., and Baragar, W.R.A., 1971, A guide to the chemical classification of the common volcanic rocks: Canadian Journal of Earth Sciences, v. 8, p. 523–548, https://doi.org/10.1139/e71-055.

Johnson, D.M., Hooper, P.R., and Conrey, R.M., 1999, XRF analysis of rocks and minerals for major and trace elements on a single low dilution Li-tetraborate fused bead: JCPDS-International Centre for Diffraction Data, p. 843–867.

Kawabata, E., Cronin, S.J., Bebbington, M.S., Moufti, M.R., El-Masry, N., and Wang, T., 2015, Identifying multiple eruption phases from a compound blanket—An example of the AD 1256 Al-Madinah eruption, Saudi Arabia: Bulletin of Volcanology, v. 77, no. 6, https://doi.org/10.1007/s00445-014-0890-y.

Knaack, C., Hooper, P.R., and Cornelius, S., 1994, Trace element analyses of rocks and minerals by ICP-MS: Pullman, Washington State University, Department of Geology Technical Notes, accessed on May 17, 2019, at https://environment.wsu.edu/facilities/geoanalytical-lab/technical-notes/icp-ms-method/.

Konrad, K., Graham, D.W., Thornber, C.R., Duncan, R.A., Kent, A.J.R., and Al-Amri, A.M., 2016, Asthenosphere-lithosphere interactions in western Saudi Arabia—Inferences from $^{3}He/^{4}He$ in xenoliths and lava flows from Harrat Hutaymah: Lithos, v. 248–251, p. 339–352, https://doi.org/10.1016/j.lithos.2016.01.031.

Kuntz, M.A., Champion, D.E., Spiker, E.C., and Lefebvre, R.H., 1986, Contrasting magma types and steady-state, volume-predictable, basaltic volcanism along the Great Idaho Rift, Idaho: Geological Society of America Bulletin, v. 97, p. 579–594, https://doi.org/10.1130/0016-7606(1986)97%3C579:CMTASV%3E2.0.CO;2.

Lal, D., 1991, Cosmic ray labeling of erosion surfaces—In situ nuclide production rates and erosions models: Earth and Planetary Science Letters, v. 104, p. 424–439, https://doi.org/10.1016/0012-821X(91)90220-C.

Langenheim, V.E., Ritzinger, B.T., Zahran, H., Shareef, A., and Al-dahri, M., 2019, Crustal structure of the northern Harrat Rahat volcanic field (Saudi Arabia) from gravity and aeromagnetic data: Tectonophysics, v. 750, p. 9–21.

Langenheim, V.E., Ritzinger, B.T., Zahran, H.M., Shareef, A., and Al-Dhahry, M.K., 2023, Depth to basement and crustal structure of the northern Harrat Rahat volcanic field, Kingdom of Saudi Arabia, from gravity and aeromagnetic data, chap. K *of* Sisson, T.W., Calvert, A.T., and Mooney, W.D., eds., Active volcanism on the Arabian Shield—Geology, volcanology, and geophysics of northern Harrat Rahat and vicinity, Kingdom of Saudi Arabia: U.S. Geological Survey Professional Paper 1862 [also released as Saudi Geological Survey Special Report SGS–SP–2021–1], 18 p., https://doi.org/10.3133/pp1862K.

Le Bas, M.J., Le Maitre, R.W., Streckeisen, A., and Zanettin, B., 1986, A chemical classification of volcanic rocks based on the total alkali-silica diagram: Journal of Petrology, v. 27, p. 745–750.

Le Corvec, N., Spörli, K.B., Rowland, J., and Lindsay, J.M., 2013, Spatial distribution and alignment of volcanic centers—Clues to the formation of monogenetic volcanic fields: Earth-Science Reviews, v. 124, p. 96–114, https://doi.org/10.1016/j.earscirev.2013.05.005.

Lee, J.-Y., Marti, K., Severinghaus, J.P., Kawamura, K., Yoo, H.-S., Lee, J.B., and Kim, J.S., 2006, A redetermination of the isotopic abundances of atmospheric Ar: Geochimica et Cosmochimica Acta, v. 70, p. 4507–4512, https://doi.org/10.1016/j.earscirev.2013.05.005.

Lister, J.R., 1990, Buoyancy-driven fluid fracture—Similarity solutions for the horizontal and vertical propagation of fluid-filled cracks: Journal of Fluid Mechanics, v. 217, p. 213–239, https://doi.org/10.1017/S0022112090000696.

Lister, J.R., and Kerr, R.C., 1991, Fluid-mechanical models of crack propagation and their application to magma transport in dykes: Journal of Geophysical Research, v. 96, p. 10049–10077, https://doi.org/10.1029/91JB00600.

Macdonald, G.A., and Katsura, T., 1964, Chemical composition of Hawaiian lavas: Journal of Petrology, v. 5, p. 82–133.

Marrero, S.M., Phillips, F.M., Borchers, B., Lifton, N., Aumer, R., and Balco, G., 2016, Cosmogenic nuclide systematics and the CRONUScalc program: Quaternary Geochronology, v. 31, p. 160–187, https://doi.org/10.1016/j.quageo.2015.09.005.

McElhinny, M.W., 1973, Paleomagnetism and Plate Tectonics: Cambridge, United Kingdom, University Press, 368 p.

McGee, L.E., Millet, M.-A., Smith, I.E.M., Németh, K., and Lindsay, J.M., 2012, The inception and progression of melting in a monogenetic eruption—Motukorea Volcano, the Auckland Volcanic Field, New Zealand: Lithos, v. 155, p. 360–374, https://doi.org/10.1016/j.lithos.2012.09.012.

McGee, L.E., Smith, I.E.M., Millet, M.-A., Handley, H.K., and Lindsay, J.M., 2013, Asthenospheric control of melting processes in a monogenetic basaltic system—A case study of the Auckland Volcanic Field, New Zealand: Journal of Petrology, v. 54, p. 2125–2153, https://doi.org/10.1093/petrology/egt043.

McGetchin, T.R., Settle, M., and Chouet, B.A., 1974, Cinder cone growth modeled after Northeast crater, Mount Etna, Sicily: Journal of Geophysical Research, v. 79, p. 3257–3272, https://doi.org/10.1029/JB079i023p03257.

Moufti, M.R., Moghazi, A.M., and Ali, K.A., 2012, Geochemistry and Sr–Nd–Pb isotopic compositions of the Harrat Al-Madinah Volcanic Field, Saudi Arabia: Gondwana Research, v. 21, p. 670–689, https://doi.org/10.1016/j.gr.2011.06.003.

Moufti, M.R., Moghazi, A.M., and Ali, K.A., 2013, $^{40}Ar/^{39}Ar$ geochronology of the Neogene-Quaternary Harrat Al-Madinah intercontinental volcanic field, Saudi Arabia—Implications for duration and migration of volcanic activity: Journal of Asian Earth Sciences, v. 62, p. 253–268, https://doi.org/10.1016/j.jseaes.2012.09.027.

Muffler, L.J.P., Clynne, M.A., Calvert, A.T., and Champion, D.E., 2011, Diverse, discrete, mantle-derived batches of basalt erupted along a short normal fault zone—The Poison Lake chain, southernmost Cascades: Geological Society of America Bulletin, v. 123, p. 2177–2200, https://doi.org/10.1130/B30370.1.

Murcia, H., Németh, K., El-Masry, N.N., Lindsay, J.M., Moufti, M.R.H., Wameyo, P., Cronin, S.J., Smith, I.E.M., and Kereszturi, G., 2015, The Al-Du'aythah volcanic cones, Al-Madinah City—Implications for volcanic hazards in northern Harrat Rahat, Kingdom of Saudi Arabia: Bulletin of Volcanology, v. 77, no. 54, 19 p., https://doi.org/10.1007/s00445-015-0936-9.

Murcia, H., Lindsay, J.M., Németh, K., Smith, I.E.M., Cronin, S.J., Moufti, M.R.H., El-Masry, N.N., and Niedermann, S., 2017, Geology and geochemistry of Late Quaternary volcanism in northern Harrat Rahat, Kingdom of Saudi Arabia—Implications for eruption dynamics, regional stratigraphy and magma evolution, *in* Németh, K., Carrasco-Núñez, G., Aranda-Gómez, J.J., and Smith, I.E.M., eds., Monogenetic Volcanism: Geological Society of London, Special Publications, v. 446, p. 173–204, https://doi.org/10.1144/SP446.2.

Oda, H., 2005, Recurrent geomagnetic excursions—A review for the Brunhes normal polarity chron: Journal of Geography, v. 114, p. 174–192, https://doi.org/10.5026/jgeography.114.2_174.

Pearce, J.A., and Norry, M.J., 1979, Petrogenetic implications of Ti, Zr, Y, and Nb variations in volcanic rocks: Contributions to Mineralogy and Petrology, v. 69, p. 33–47, https://doi.org/10.1007/BF00375192.

Pellaton, C., 1981, Geologic map of the Al Madinah quadrangle, sheet 24D, Kingdom of Saudi Arabia: Saudi Arabian Deputy Ministry for Mineral Resources Geoscience Map GM–52, scale 1:250,000, 19 p.

Robinson, J.E., and Downs, D.T., 2023, Overview of the Cenozoic geology of the northern Harrat Rahat volcanic field, Kingdom of Saudi Arabia, chap. R *of* Sisson, T.W., Calvert, A.T., and Mooney, W.D., eds., Active volcanism on the Arabian Shield—Geology, volcanology, and geophysics of northern Harrat Rahat and vicinity, Kingdom of Saudi Arabia: U.S. Geological Survey Professional Paper 1862 [also released as Saudi Geological Survey Special Report SGS–SP–2021–1], 20 p., scale 1:100,000, https://doi.org/10.3133/pp1862R.

Rubin, A.M., 1995, Propagation of magma-filled cracks: Annual Review of Earth and Planetary Sciences, v. 23, p. 287–336, https://doi.org/10.1146/annurev.ea.23.050195.001443.

Runge, M.G., Bebbington, M.S., Cronin, S.J., Lindsay, J.M., Kenedi, C.L., and Moufti, M.R.H., 2014, Vents to events—Determining an eruption event record from volcanic vent structures for the Harrat Rahat, Saudi Arabia: Bulletin of Volcanology, v. 76, no. 804, 16 p., https://doi.org/10.1007/s00445-014-0804-z.

Runge, M.G., Bebbington, M.S., Cronin, S.J., Lindsay, J.M., and Moufti, M.R., 2016, Integrating geological and geophysical data to improve probabilistic hazard forecasting of Arabian Shield volcanism: Journal of Volcanology and Geothermal Research, v. 311, p. 41–59, https://doi.org/10.1016/j.jvolgeores.2016.01.007.

Salters, V.J.M., Sachi-Kocher, A., Downs, D.T., Stelten, M.E., and Sisson, T.W., 2023, Isotopic and geochemical evidence for the sources of volcanism at Harrat Rahat, Kingdom of Saudi Arabia, chap. J *of* Sisson, T.W., Calvert, A.T., and Mooney, W.D., eds., Active volcanism on the Arabian Shield—Geology, volcanology, and geophysics of northern Harrat Rahat and vicinity, Kingdom of Saudi Arabia: U.S. Geological Survey Professional Paper 1862 [also released as Saudi Geological Survey Special Report SGS–SP–2021–1], 30 p., https://doi.org/10.3133/pp1862J.

Shaw, H.R., 1980, The fracture mechanisms of magma transport from the mantle to the surface, *in* Hargraves, R.B., ed., Physics of Magmatic Processes: Princeton, New Jersey, Princeton University Press, p. 201–264.

Shaw, J.E., Baker, J.A., Menzies, M.A., Thirlwall, M.F., and Ibrahim, K.M., 2003, Petrogenesis of the largest intraplate volcanic field on the Arabian Plate (Jordan)—A mixed lithosphere–asthenosphere source activated by lithospheric extension: Journal of Petrology, v. 44, p. 1657–1679, https://doi.org/10.1093/petrology/egg052.

Siebert, L., Simkin, T., and Kimberly, P., 2010, Volcanoes of the World [3rd ed.]: Berkeley, California, University of California Press, 568 p.

Sisson, T.W., Downs, D.T., Calvert, A.T., Dietterich, H.R., Mahood, G.A., Salters, V.J.M., Stelten, M.E., and Shawali, J., 2023, Mantle origin and crustal differentiation of basalts and hawaiites of northern Harrat Rahat, Kingdom of Saudi Arabia, chap. I *of* Sisson, T.W., Calvert, A.T., and Mooney, W.D., eds., Active volcanism on the Arabian Shield—Geology, volcanology, and geophysics of northern Harrat Rahat and vicinity, Kingdom of Saudi Arabia: U.S. Geological Survey Professional Paper 1862 [also released as Saudi Geological Survey Special Report SGS–SP–2021–1], 42 p., https://doi.org/10.3133/pp1862I.

Smith, I.E.M., Blake, S., Wilson, C.J.N., and Houghton, B.F., 2008, Deep seated fractionation during the rise of a small-volume basalt magma batch—Crater Hill, Auckland, New Zealand: Contributions to Mineralogy and Petrology, v. 155, p. 511–527, https://doi.org/10.1007/s00410-007-0255-z.

Spence, D.A., and Turcotte, D.L., 1990, Buoyancy-driven magma fracture—A mechanism for ascent through the lithosphere and the emplacement of diamonds: Journal of Geophysical Research, v. 95, p. 5133–5139, https://doi.org/10.1029/JB095iB04p05133.

Steiger, R.H., and Jäger, E., 1977, Subcommission on geochronology—Convention on the use of decay constants in the geo- and cosmochronology: Earth and Planetary Science Letters, v. 36, p. 359–362, https://doi.org/10.1016/0012-821X(77)90060-7.

Stelten, M.E., Downs, D.T., Dietterich, H.R., Mahood, G.A., Calvert, A.T., Sisson, T.W., Zahran, H., and Shawali, J., 2018, Timescales of magmatic differentiation from alkali basalt to trachyte within the Harrat Rahat volcanic field, Kingdom of Saudi Arabia: Contributions to Mineralogy and Petrology, v. 173, no. 68, 17 p., https://doi.org/10.1007/s00410-018-1495-9.

Stelten, M.E., Downs, D.T., Champion, D.E., Dietterich, H.R., Calvert, A.T., Sisson, T.W., Mahood, G.A., and Zahran, H., 2020, The timing and compositional evolution of volcanism within northern Harrat Rahat, Kingdom of Saudi Arabia: Geological Society of America Bulletin, v. 132, no. 7/8, p. 1381–1403, https://doi.org/10.1130/B35337.1.

Stelten, M.E., Downs, D.T., Champion, D.E., Dietterich, H.R., Calvert, A.T., Sisson, T.W., Mahood, G.A., and Zahran, H.M., 2023, Eruptive history of northern Harrat Rahat—Volume, timing, and composition of volcanism over the past 1.2 million years, chap. D *of* Sisson, T.W., Calvert, A.T., and Mooney, W.D., eds., Active volcanism on the Arabian shield—Geology, volcanology, and geophysics of northern Harrat Rahat and vicinity, Kingdom of Saudi Arabia: U.S. Geological Survey Professional Paper 1862 [also released as Saudi Geological Survey Special Report SGS–SP–2021–1], 46 p., https://doi.org/10.3133/pp1862D.

Stern, R.J., and Johnson, P., 2010, Continental lithosphere of the Arabian Plate—A geologic, petrologic, and geophysical synthesis: Earth-Science Reviews, v. 101, p. 29–67, https://doi.org/10.1016/j.earscirev.2010.01.002.

Stone, J., 2000, Air pressure and cosmogenic isotope production: Journal of Geophysical Research, v. 105, p. 23753–23760, https://doi.org/10.1029/2000JB900181.

Taggart, Jr., J.E., ed., 2002, Analytical methods for chemical analysis of geologic and other materials, U.S. Geological Survey: U.S. Geological Survey Open-File Report 02–223, 20 p., https://doi.org/10.3133/ofr02223.

Takada, A., 1989, Magma transport and reservoir formation by a system of propagating cracks: Bulletin of Volcanology, v. 52, p. 118–126, https://doi.org/10.1007/BF00301551.

Traversa, P., Pinel, V., and Grasso, J.R., 2010, A constant influx model for dike propagation—Implications for magma reservoir dynamics: Journal of Geophysical Research, v. 115, 18 p., https://doi.org/10.1029/2009JB006559.

Valentine, G.A., and Krogh, K.E.C., 2006, Emplacement of shallow dikes and sills beneath a small basaltic volcanic center—The role of pre-existing structure (Paiute Ridge, southern Nevada, USA): Earth and Planetary Science Letters, v. 246, p. 217–230, https://doi.org/10.1016/j.epsl.2006.04.031.

Valentine, G.A., and Perry, F.M., 2007, Tectonically controlled, time-predictable basaltic volcanism from a lithospheric mantle source [central Basin and Range Province, USA]: Earth and Planetary Science Letters, v. 261, p. 201–216, https://doi.org/10.1016/j.epsl.2007.06.029.

Valentine, G.A., and Connor, C.B., 2015, Basaltic volcanic fields, *in* Sigurdsson, H., Houghton, B., McNutt, S., Rymer, H., and Stix, J., eds., The Encyclopedia of Volcanoes [2d ed.]: San Diego, California, Academic Press, p. 423–439, https://doi.org/10.1016/B978-0-12-385938-9.00023-7.

Wang, H., van Hunen, J., and Pearson, D.G., 2015, The thinning of subcontinental lithosphere—The roles of plume impact and metasomatic weakening: Geochemistry, Geophysics, Geosystems, v. 16, p. 1156–1171, https://doi.org/10.1002/2015GC005784.

Weinstein, Y., Navon, O., Altherr, R., and Stein, M., 2006, The role of lithospheric mantle heterogeneity in the generation of Plio-Pleistocene alkali basaltic suites from NW Harrat Ash Shaam (Israel): Journal of Petrology, v. 47, p. 1017–1050, https://doi.org/10.1093/petrology/egl003.

Wood, C., 1979, Monogenetic volcanoes of the terrestrial planets, *in* Proceedings of the 10th Lunar and Planetary Science Conference, Houston, Texas, Lunar and Planetary Institute: New York, Pergamon Press, p. 2815–2840.

Appendix 1. Selected $^{40}Ar/^{39}Ar$ Age-Spectra Diagrams

$^{40}Ar/^{39}Ar$ age-spectra diagrams from units displayed on figure 4 of the main text. WMPA is the weighted mean plateau age and MSWD is the mean square of weighted deviates. The gray boxes were used to calculate the ages of samples, whereas red boxes were excluded when calculating the ages of samples. Numbers next to the gray and red boxes correspond to the temperature (in degrees Celsius) at which the gas was extracted. See table 3 of the main text for experiment details. $^{40}Ar/^{36}Ar_i$, $^{40}Ar/^{36}Ar$ isochron intercept; ka, kilo-annum.

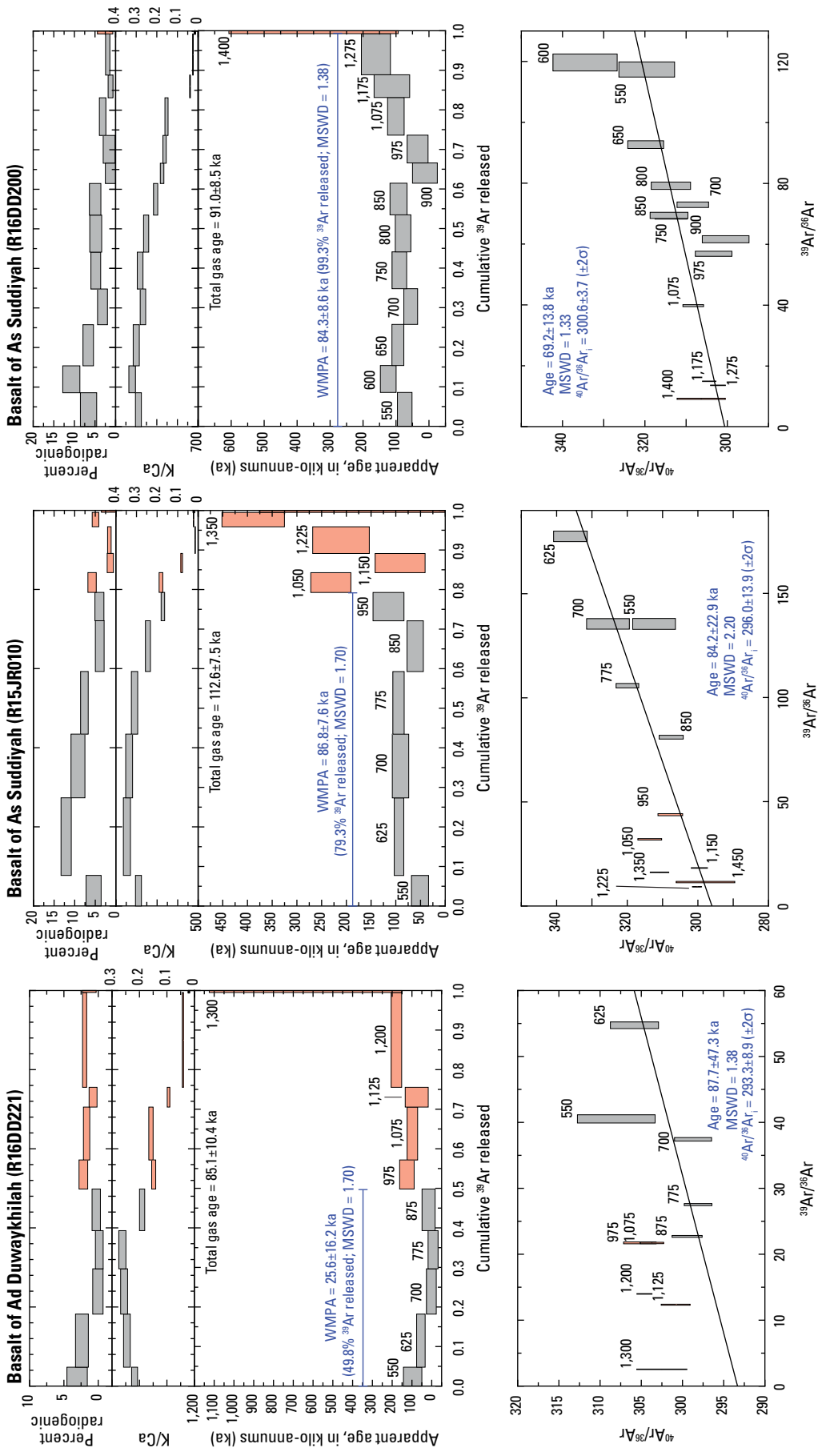
Basalt of Ad Duwaykhilah (R16DD221)
Basalt of As Suddiyah (R15JR010)
Basalt of As Suddiyah (R16DD200)
Percent radiogenic
K/Ca
Apparent age, in kilo-annums (ka)
Total gas age = 85.1±10.4 ka
WMPA = 25.6±16.2 ka
(49.8% 39Ar released; MSWD = 1.70)
Total gas age = 112.6±7.5 ka
WMPA = 86.8±7.6 ka
(79.3% 39Ar released; MSWD = 1.70)
Total gas age = 91.0±8.5 ka
WMPA = 84.3±8.6 ka (99.3% 39Ar released; MSWD = 1.38)
Cumulative 39Ar released
40Ar/36Ar
39Ar/36Ar
Age = 87.7±47.3 ka
MSWD = 1.38
40Ar/36Ari = 293.3±8.9 (±2σ)
Age = 84.2±22.9 ka
MSWD = 2.20
40Ar/36Ari = 296.0±13.9 (±2σ)
Age = 69.2±13.8 ka
MSWD = 1.33
40Ar/36Ari = 300.6±3.7 (±2σ)

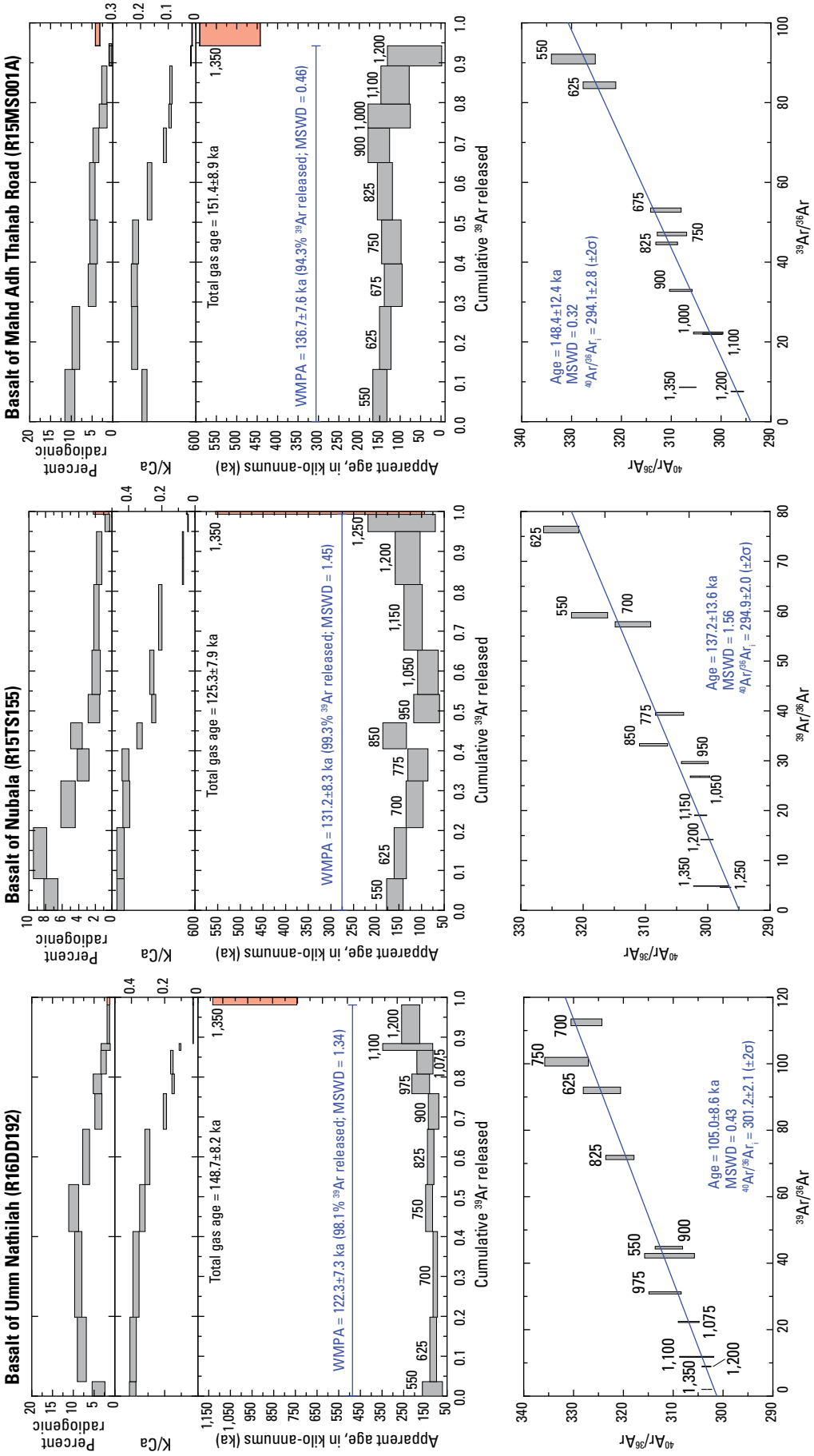
Basalt of Umm Nathilah (R16DD192)
Basalt of Nubala (R15TS155)
Basalt of Mahd Adh Thahab Road (R15MS001A)
Percent radiogenic
K/Ca
Apparent age, in kilo-annums (ka)
Total gas age = 148.7±8.2 ka
WMPA = 122.3±7.3 ka (98.1% 39Ar released; MSWD = 1.34)
Total gas age = 125.3±7.9 ka
WMPA = 131.2±8.3 ka (99.3% 39Ar released; MSWD = 1.45)
Total gas age = 151.4±8.9 ka
WMPA = 136.7±7.6 ka (94.3% 39Ar released; MSWD = 0.46)
Cumulative 39Ar released
40Ar/36Ar
39Ar/36Ar
Age = 105.0±8.6 ka
MSWD = 0.43
40Ar/36Ari = 301.2±2.1 (±2σ)
Age = 137.2±13.6 ka
MSWD = 1.56
40Ar/36Ari = 294.9±2.0 (±2σ)
Age = 148.4±12.4 ka
MSWD = 0.32
40Ar/36Ari = 294.1±2.8 (±2σ)

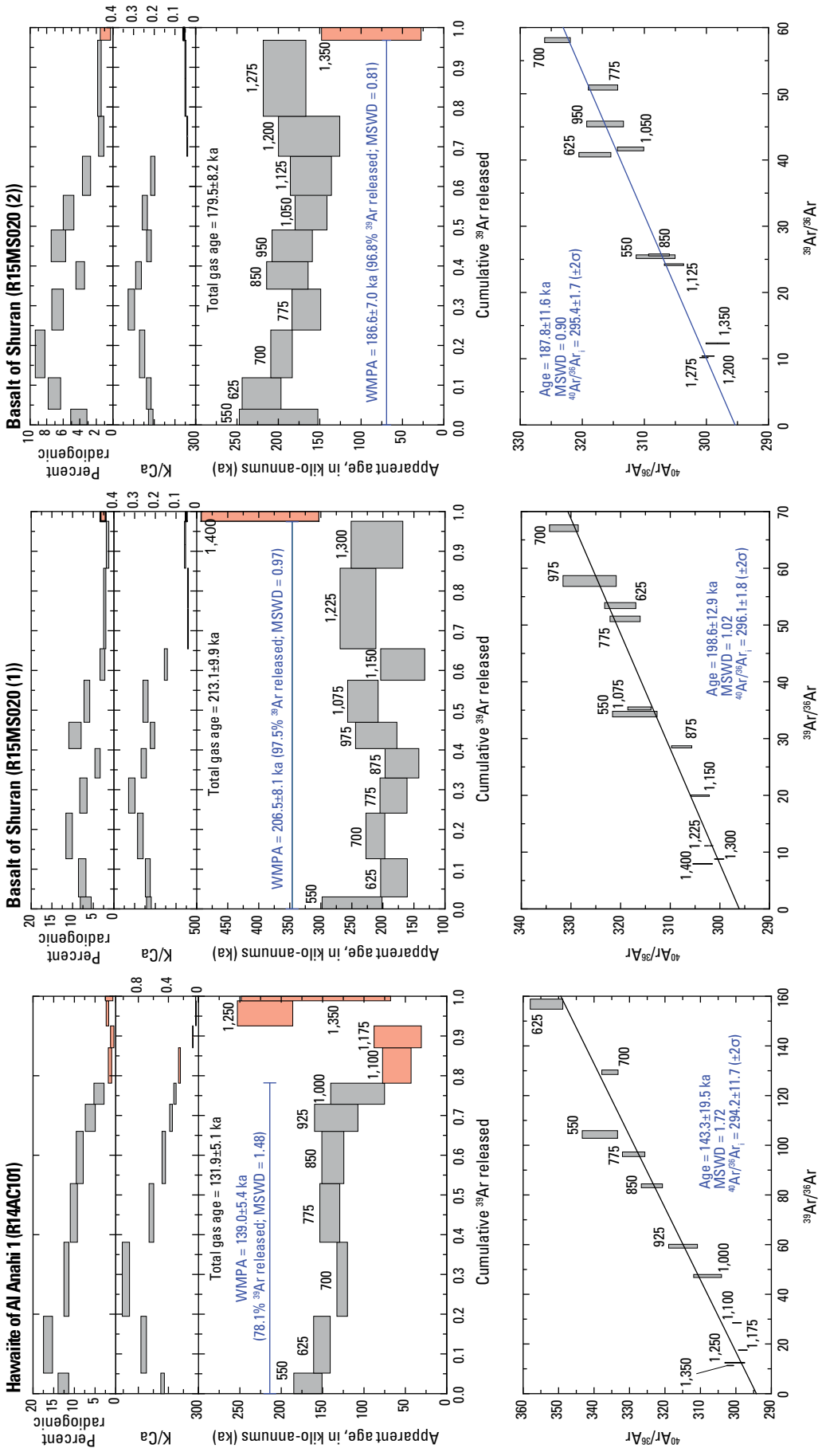
Hawaiite of Al Anahi 1 (R14AC101)
Basalt of Shuran (R15MS020 (1))
Basalt of Shuran (R15MS020 (2))
Percent radiogenic
K/Ca
Apparent age, in kilo-annums (ka)
Cumulative ^{39}Ar released
Total gas age = 131.9±5.1 ka
WMPA = 139.0±5.4 ka
(78.1% ^{39}Ar released; MSWD = 1.48)
Total gas age = 213.1±9.9 ka
WMPA = 206.5±8.1 ka (97.5% ^{39}Ar released; MSWD = 0.97)
Total gas age = 179.5±8.2 ka
WMPA = 186.6±7.0 ka (96.8% ^{39}Ar released; MSWD = 0.81)
^{40}Ar/^{36}Ar
^{39}Ar/^{36}Ar
Age = 143.3±19.5 ka
MSWD = 1.72
^{40}Ar/^{36}Ar$_i$ = 294.2±11.7 (±2σ)
Age = 198.6±12.9 ka
MSWD = 1.02
^{40}Ar/^{36}Ar$_i$ = 296.1±1.8 (±2σ)
Age = 187.8±11.6 ka
MSWD = 0.90
^{40}Ar/^{36}Ar$_i$ = 295.4±1.7 (±2σ)

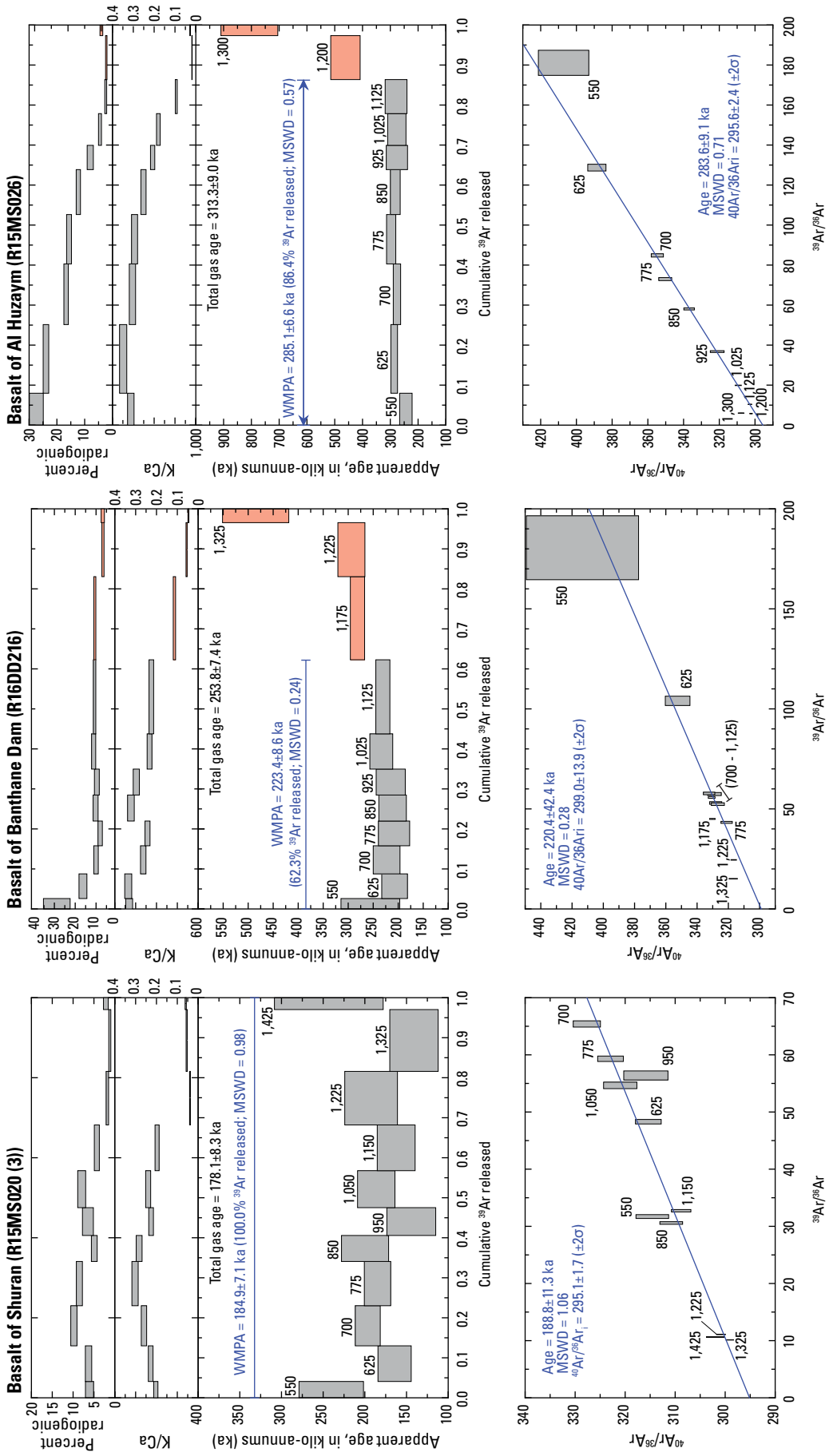
Basalt of Shuran (R15MS020 (3))
Basalt of Banthane Dam (R16DD216)
Basalt of Al Huzaym (R15MS026)
Percent radiogenic
K/Ca
Apparent age, in kilo-annums (ka)
Cumulative 39Ar released
Total gas age = 178.1±8.3 ka
WMPA = 184.9±7.1 ka (100.0% 39Ar released; MSWD = 0.98)
Total gas age = 253.8±7.4 ka
WMPA = 223.4±8.6 ka
(62.3% 39Ar released; MSWD = 0.24)
Total gas age = 313.3±9.0 ka
WMPA = 285.1±6.6 ka (86.4% 39Ar released; MSWD = 0.57)
40Ar/36Ar
39Ar/36Ar
Age = 188.8±11.3 ka
MSWD = 1.06
40Ar/36Ari = 295.1±1.7 (±2σ)
Age = 220.4±42.4 ka
MSWD = 0.28
40Ar/36Ari = 299.0±13.9 (±2σ)
Age = 283.6±9.1 ka
MSWD = 0.71
40Ar/36Ari = 295.6±2.4 (±2σ)

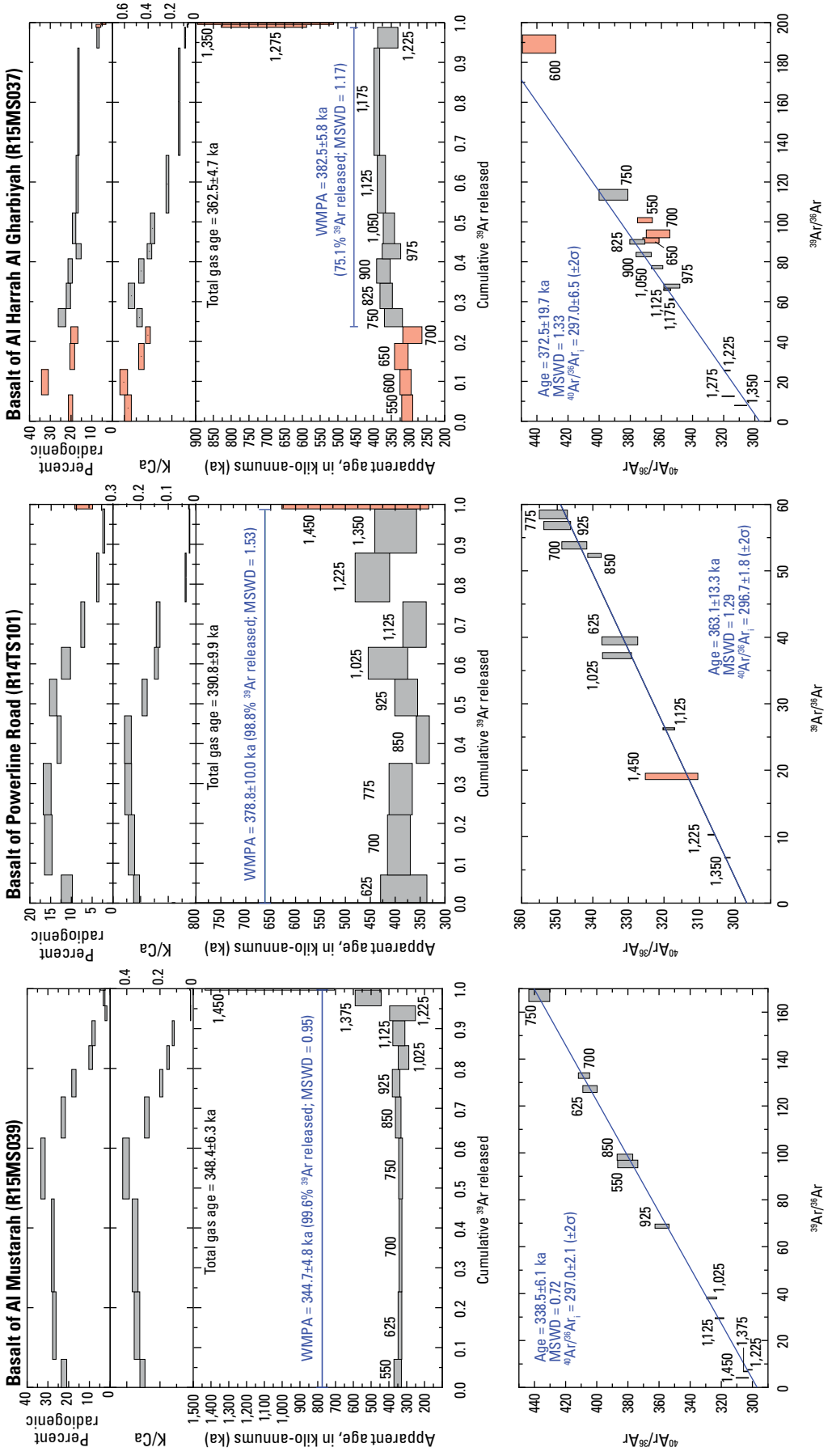
Basalt of Al Mustarah (R15MS039)
Basalt of Powerline Road (R14TS101)
Basalt of Al Harrah Al Gharbiyah (R15MS037)
Percent radiogenic
K/Ca
Apparent age, in kilo-annums (ka)
Total gas age = 348.4±6.3 ka
WMPA = 344.7±4.8 ka (99.6% 39Ar released; MSWD = 0.95)
Total gas age = 390.8±9.9 ka
WMPA = 378.8±10.0 ka (98.8% 39Ar released; MSWD = 1.53)
Total gas age = 362.5±4.7 ka
WMPA = 382.5±5.8 ka
(75.1% 39Ar released; MSWD = 1.17)
Cumulative 39Ar released
40Ar/36Ar
39Ar/36Ar
Age = 338.5±6.1 ka
MSWD = 0.72
40Ar/36Ari = 297.0±2.1 (±2σ)
Age = 363.1±13.3 ka
MSWD = 1.29
40Ar/36Ari = 296.7±1.8 (±2σ)
Age = 372.5±19.7 ka
MSWD = 1.33
40Ar/36Ari = 297.0±6.5 (±2σ)

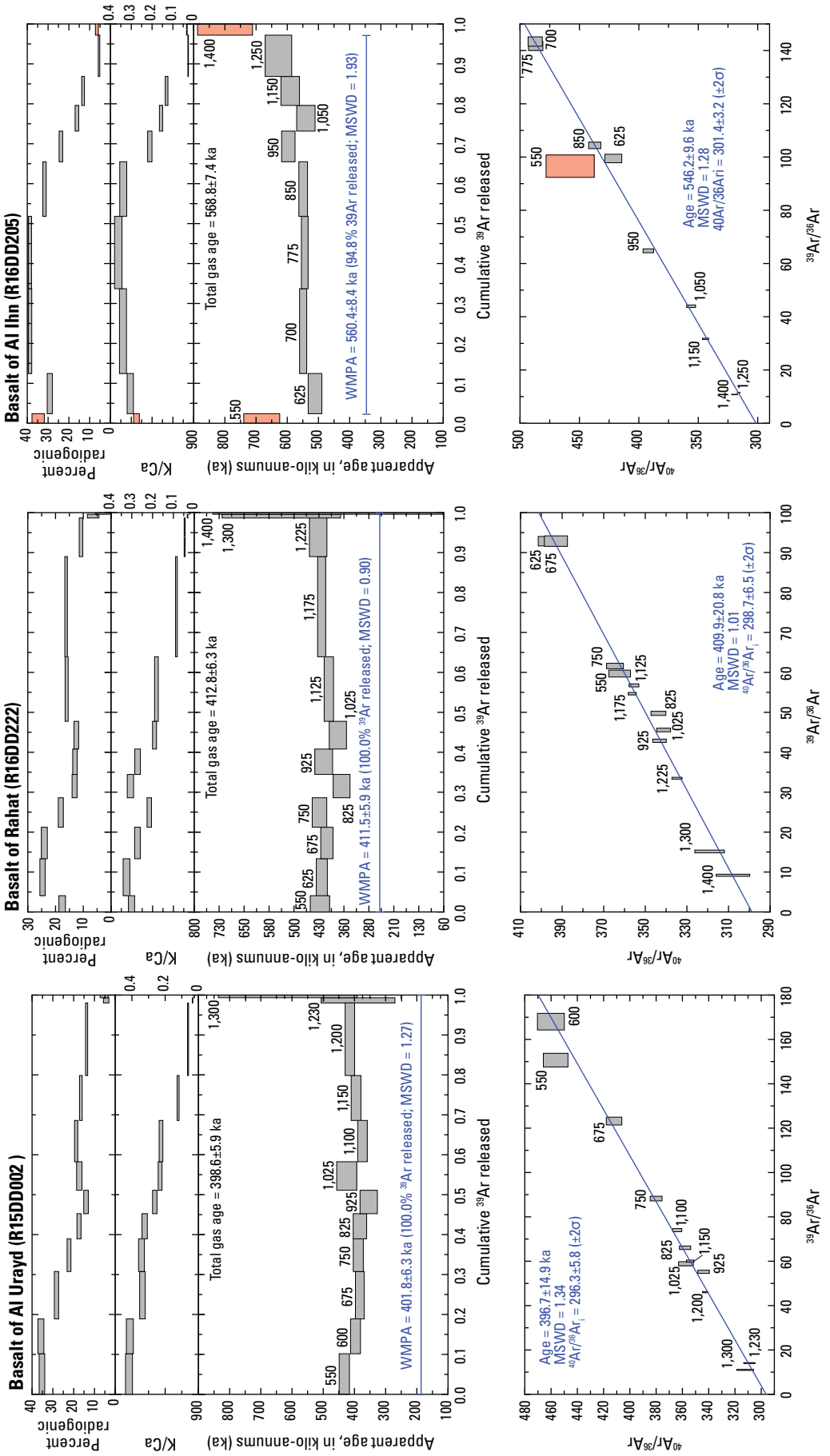
Basalt of Al Urayd (R15DD002)
Total gas age = 398.6±5.9 ka
WMPA = 401.8±6.3 ka (100.0% 39Ar released; MSWD = 1.27)
Age = 396.7±14.9 ka
MSWD = 1.34
40Ar/36Ari = 296.3±5.8 (±2σ)
Basalt of Rahat (R16DD222)
Total gas age = 412.8±6.3 ka
WMPA = 411.5±5.9 ka (100.0% 39Ar released; MSWD = 0.90)
Age = 409.9±20.8 ka
MSWD = 1.01
40Ar/36Ari = 298.7±6.5 (±2σ)
Basalt of Al Ihn (R16DD205)
Total gas age = 568.8±7.4 ka
WMPA = 560.4±8.4 ka (94.8% 39Ar released; MSWD = 1.93)
Age = 546.2±9.6 ka
MSWD = 1.28
40Ar/36Ari = 301.4±3.2 (±2σ)
Percent radiogenic
K/Ca
Apparent age, in kilo-annums (ka)
Cumulative 39Ar released
40Ar/36Ar
39Ar/36Ar

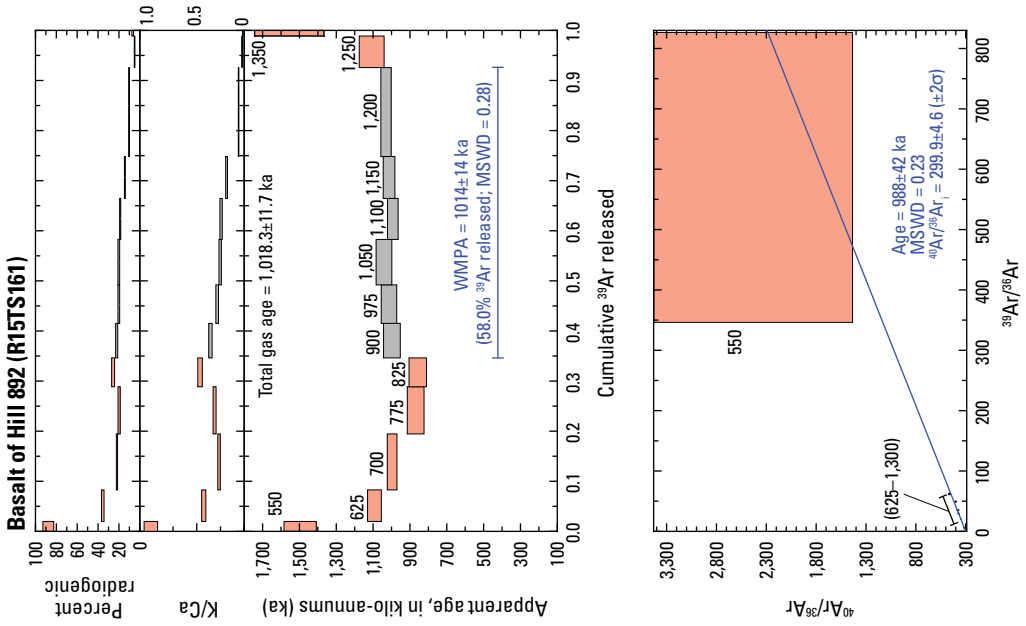

Moffett Field Publishing Service Center, California
Manuscript approved November 25, 2020
Edited by John Mark Brigham and Monica Erdman
Layout and design by Cory Hurd
Illustration support by Katie Sullivan

ISSN 1044-9612 (print)
ISSN 2330-7102 (online)
https://doi.org/10.3133/pp1862C